MOLECULAR AND BIOCHEMICAL CHARACTERIZATION OF HYDROCARBON PRODUCTION IN THE GREEN MICROALGA *Botryococcus braunii*

A Dissertation

by

TAYLOR LEIGH WEISS

Submitted to the Office of Graduate Studies of
Texas A&M University
in partial fulfillment of the requirements for the degree of

DOCTOR OF PHILOSOPHY

August 2012

Major Subject: Biochemistry

Molecular and Biochemical Characterization of Hydrocarbon

Production in the Green Microalga *Botryococcus braunii*

MOLECULAR AND BIOCHEMICAL CHARACTERIZATION OF HYDROCARBON PRODUCTION IN THE GREEN MICROALGA *Botryococcus braunii*

A Dissertation

by

TAYLOR LEIGH WEISS

Submitted to the Office of Graduate Studies of
Texas A&M University
in partial fulfillment of the requirements for the degree of

DOCTOR OF PHILOSOPHY

Approved by:

Chair of Committee,	Timothy P. Devarenne
Committee Members,	Pingwei Li
	Andreas Holzenburg
	Comer O. Patterson
Head of Department,	Gregory D. Reinhart

August 2012

Major Subject: Biochemistry

ABSTRACT

Molecular and Biochemical Characterization of Hydrocarbon Production in the Green Microalga *Botryococcus braunii*. (August 2012)

Taylor Leigh Weiss, B.S., Rochester University

Chair of Advisory Committee: Dr. Timothy P. Devarenne

Botryococcus braunii (Chlorophyta, Botryococcaceae) is a colony-forming green microalga that produces large amounts of liquid hydrocarbons, which can be converted into transportation fuels. While *B. braunii* has been well studied for the chemistry of the hydrocarbon production, very little is known about the molecular biology of *B. braunii*. As such, this study developed both apparatus and techniques to culture *B. braunii* for use in the genetic and biochemical characterization.

During genetic studies, the genome size was determined of a representative strain of each of the three races of *B. braunii*, A, B, and L, that are distinguished based on the type of hydrocarbon each produces. Flow cytometry analysis indicates that the A race, Yamanaka strain, of *B. braunii* has a genome size of 166.0 ± 0.4 Mb, which is similar to the B race, Berkeley strain, with a genome size of 166 ± 2.2 Mb, while the L race, Songkla Nakarin strain, has a substantially larger genome size at 211.3 ± 1.7 Mb. Phylogenetic analysis with the nuclear small subunit (18S) rRNA and actin genes were used to classify multiple strains of A, B, and L races. These analyses suggest that the

evolutionary relationship between *B. braunii* races is correlated with the type of liquid hydrocarbon they produce.

Biochemical studies of *B. braunii* primarily focused on the B race, because it uniquely produces large amounts of botryococcenes that can be used as a fuel for internal combustion engines. C_{30} botryococcene is metabolized by methylation to generate intermediates of C_{31}, C_{32}, C_{33}, and C_{34}. Raman spectroscopy was used to characterize the structure of botryococcenes. The spectral region from 1600–1700 cm^{-1} showed ν(C=C) stretching bands specific for botryococcenes. Distinct botryococcene Raman bands at 1640 and 1647 cm^{-1} were assigned to the stretching of the C=C bond in the botryococcene branch and the exomethylene C=C bonds produced by the methylations, respectively. A Raman band at 1670 cm^{-1} was assigned to the backbone C=C bond stretching. Finally, confocal Raman microspectroscopy was used to map the presence and location of methylated botryococcenes within a living colony of *B. braunii* cells.

DEDICATION

This work is dedicated to my grandmother. Though she did not live to see its completion, this work would not have been possible without her love and support.

ACKNOWLEDGEMENTS

I would foremost like to thank my advisor, Tim Devarenne. I came to him without a lab, a project, nor direction. He gave me all these things plus the freedom and confidence to pursue my most ambitious intellectual pursuits. I am forever grateful for his mentoring, guidance, and friendship.

I also thank our collaborator and good friend, Shigeru Okada. Without his aid, great patience, deep wisdom, and vast knowledge none of my studies would have been possible.

I would especially like to thank both Arum Han and Christian Hilty for allowing me to collaborate and work with my friends Hyun Soo Kim and Giridhar Sekar. I look forward to many years of friendship and science together.

I would like to thank all of the members of my committee, Andreas Holzenburg, Pingwei Li, James Manhart, C.O. Patterson, and Michael Polymenis, for all their service, suggestions, comments, and helpful conversations during the course of my studies. I would similarly like to thank Stanislav Vitha, Jaan Laane, Hye Jin Chun, Amanda Young, Margret Glasner, Wei-chuan Shih, Ji Qi, Larry Dangott, Eunah Lee, Patrick Killough, for all their collaborations, technical expertise, and fruitful conversation.

Finally, I would like to thank all the members of the Devarenne lab, past, present, temporary, transient, and otherwise honorary for their help and conversation. In particular, I am grateful to have both worked and laughed beside classmates Anna Nelson, Joel Gray, and Julian Avila.

TABLE OF CONTENTS

CHAPTER Page

CHAPTER Page

LIST OF FIGURES

FIGURE Page

FIGURE Page

LIST OF TABLES

CHAPTER I

INTRODUCTION*

Algae biofuels

In recent years, interest in the use of algae as a source of biofuels has increased due to the need to reduce greenhouse gas emissions and because of depletion of world petroleum reserves (Hu et al. 2008). Compared to current energy feedstocks, like corn and soybean, algae are especially attractive because they do not compete with food production and do not require the use of arable land (Chisti 2010). Algae are additionally capable of growing in non-potable, saline, and even waste water (Chisti 2007). This flexibility coupled with the ability to bioremediate waste water pollutants is especially important given growing world demand for freshwater (Chisti 2010). Similarly, since algae growth can be greatly increased by the addition of CO_2, algae may

---

This dissertation follows the style of the *Journal of Phycology*.

effectively scrub carbon-rich industrial emissions, such as flue gas from coal-fired power plants (Yoo et al. 2010). All of these environmentally-friendly traits are coupled with the ability to effectively convert CO_2 into an array of biofuels and bioproducts. While carbohydrates and triacylglycerides are the traditional biofuel feedstocks derived from plants, algae may also produce high amounts of isoprenoids suitable for both biofuel and bioproducts applications. Residual protein after oil extraction from algae may additionally be utilized as animal feed or further energy generation by anaerobic digestion (Chisti 2007).

For all these traits however, large scale algal biofuel production faces many hurdles. To meet demand, improvements will need to be made in many diverse aspects including culturing, harvesting, dewatering, product extraction, and product refinement (Chisti 2007). To be economically viable, production of alga derived biofuels will also need to be continuous and consistent, requiring improvements in both culture and product monitoring (Chisti 2007, 2008a; Radakovits et al. 2010). Besides engineering solutions, many of these impediments may be overcome through biological means such as selecting or genetically modifying algae strains that grow faster, produce more oil, are easier to harvest, and are generally more robust (Radakovits et al. 2010). A strong understanding of algal biology is needed however for such a deliberate and focused examination of desirable biofuel production traits.

Algae

Historically, the answer to even the simple question of "what is an alga?" has

been nebulous. This is in part because outdated definitions still persist colloquially despite redefinition over the years. For example, though prokaryotic cyanobacteria have been removed from the scientific definition of "algae," the prior label of "blue-green algae" continues to be the standard nomenclature to which cyanobacteria are commonly referred (Chapman 2005, 2009). This seems especially convenient when delineating heterotrophically derived "bacterial biofuels" from phototrophically derived "algae biofuels" though such products are identical. Even when excluding cyanobacteria as "algae", current biological standards attempt to unite "algae" as both a paraphyletic and polyphyletic group with mixed success (Cavalier-Smith 2004; Adl et al. 2005). Thus the currently accepted characterization of algae as small, aquatic, photoautotrophic eukaryotes still encompasses numerous exceptions like the brown macroalga *Macrocystis pyrifera* (Giant Kelp), terrestrial lichen symbiotes like the green alga *Dictyochloropsis reticulate*, and strict phagotrophic dinoflagellates like *Protoperidinium crassipes* (Guiry and Guiry 2012). Moreover, the database Algaebase currently distinguishes 30,227 eukaryotic algae species out of an estimated 39,000 to 140,500 species (Chapman 2005, 2009; Guiry and Guiry 2012). Certainly, an in-depth study of all algae to resolve this phylogeny represents an incredible task. However, except for a few strains of cyanobacteria and diatoms, biological studies focused on industrial algae production have been predominately focused on green microalgae alone.

Green algae belong to the kingdom Viridiplantae and are a paraphyletic group composed of two major phyla: Streptophyta, which includes Embryophytes (land plants), and Chlorophyta (green algae) (Lewis and McCourt 2004). It should be noted,

that organization under Viridiplantae is contentious because algae are not actually plants. Thus, in 2005 it was suggested that this kingdom be renamed "Chloroplastida" to reflect both this technicality and that the most common trait shared by all members is a primary green chloroplast, likely derived from a single common ancestor (Adl et al. 2005). This is why, unlike other types of algae, green algae research has notably benefitted from the large body of land plant research with respect to chloroplast studies, but somewhat less so with respect to nuclear genome encoded traits. Regardless, most green algae research focuses on Chlorophyta, which are further divided into four classes: Prasinophyceae, Ulvophyceae, Chlorophyceae, and Trebouxiophyceae. In general, the microalgae of the classes Chlorophyceae and Trebouxiophyceae, which include the relatively well-studied genera *Chlamydomonas* and *Chlorella*, respectively, are primary foci of algae biofuel research. The focus of this study, *Botryococcus braunii*, belongs to the class Trebouxiophyceae.

Botryococcus braunii

General biology

A trebouxiophyte of an undetermined order and of the family Botryococcaceae, *Botryococcus braunii* was first identified in 1849 by Friderico Kützing (Kützing 1849). Well into the 20th century, *B. braunii* morphology and classification were studied extensively by many European scientists culminating in a definitive review by Kathleen B. Blackburn in 1936 (Poulton 1930; Blackburn 1936). Though it would be at least another three decades before newer techniques would be used to address the many

unconventional biochemical traits of *B. braunii* (Maxwell et al. 1968; Knights et al. 1970), after more than a century and a half of research, a detailed view of *B. braunii* cell biology has remained elusive.

In general however, *B. braunii* is a colony-forming, green microalga with pyriform-shaped cells typically no more than 4 µm wide and 10 µm long (Fig. 1; Blackburn 1936). Colonies are essentially amorphous with each cell, typically clustered in groups of 2-4, embedded within an extracellular matrix with their broader ends protruding (Blackburn 1936). Reproduction appears autosporic with no zoosporic or sexual reproduction known (Senousy 2004). Cells are typically surrounded by a polysaccharidic cell wall and sometimes partially surrounded by a thick, lipophilic cuticle (Fig. 2; Wolf and Cox 1981). Each cell contains a single large "U-shaped" chloroplast which essentially envelope all cytoplasmic components of a cell—including a centrally located nucleus—except at the widest end where the Golgi apparatus is located (Fig. 2; Beakes and Cleary 1999). The exterior of *B. braunii* colonies are wrapped in a pectic layer that extends from the broad end of the cell wall out in all directions (Wolf and Cox 1981). As a likely result of this layering, most *B. braunii* synthesize exceptional amounts of exopolysaccharides (Allard and Casadevall 1990; Lupi et al. 1991, 1994). Internally, colonies are held together by an extracellular matrix (ECM) composed of a cross-linked aldehyde polymer core (Fig. 2; Maxwell et al. 1968; Knights et al. 1970; Metzger et al. 1993, 2008). *B. braunii* is a prodigious producer of liquid hydrocarbon oils, which are mainly (90–95%) stored in the ECM with the remainder found inside the cells as lipid bodies (Banerjee et al. 2002; Knights et al.

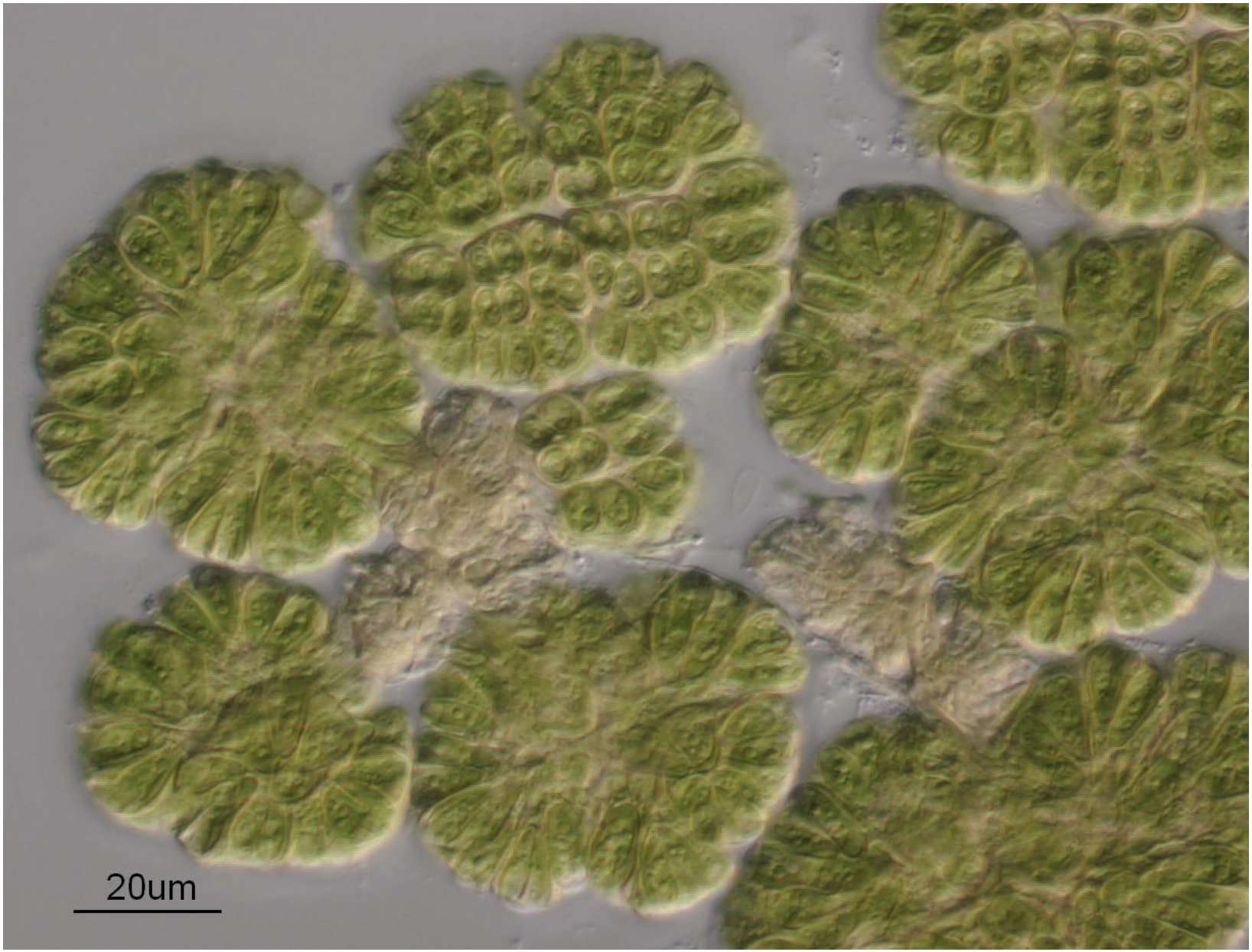

FIGURE 1. Colonies of *Botryococcus braunii, B race,* Berkeley strain. A transmitted light microscope image of several old colonies which include regions of dead cells.

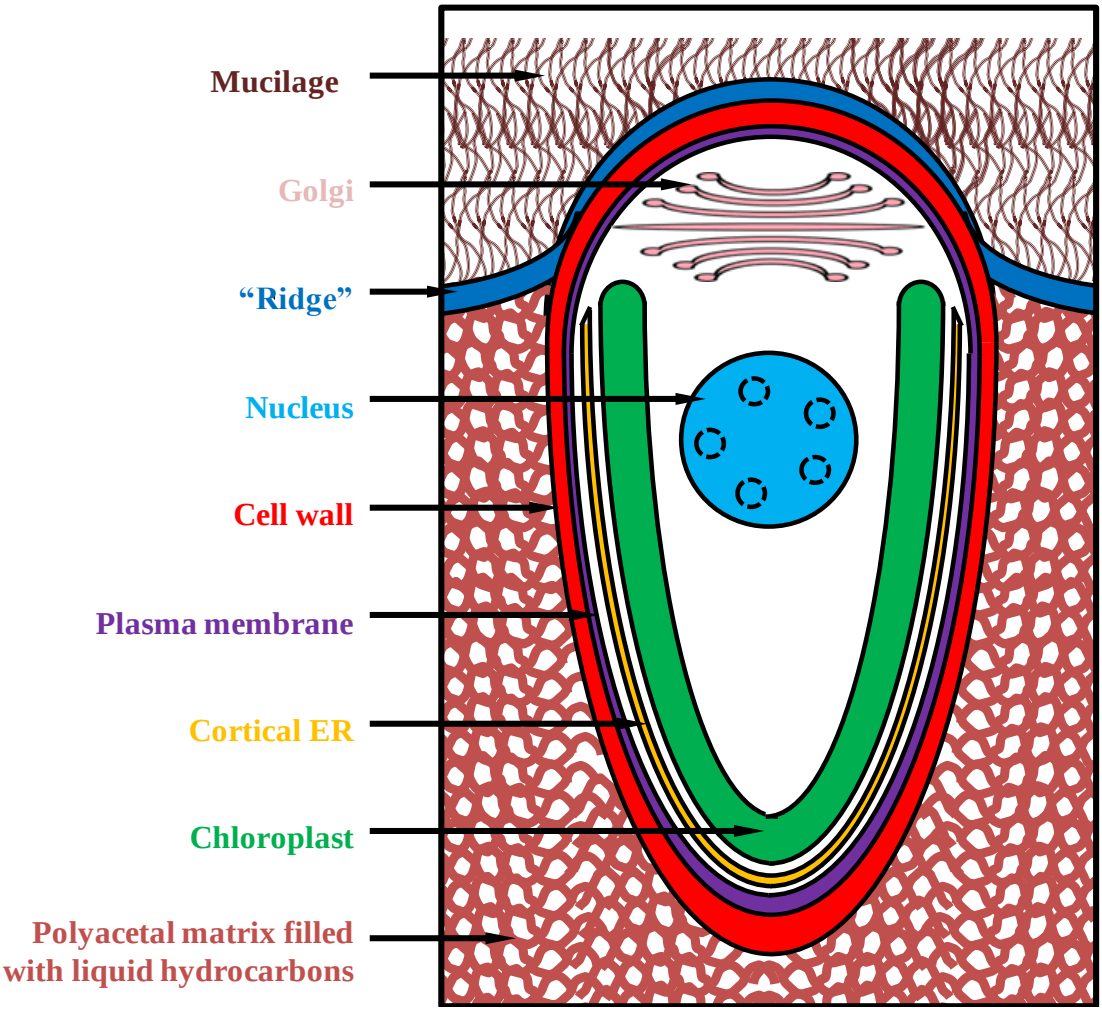

FIGURE 2. General *B. braunii* cellular organization.

1970; Maxwell et al. 1968; Metzger et. al 1987; Wolf et al. 1985).

Like most algae, variants of *B. braunii* are often identified as isolate, strains, or holotype by the location or country they were found (e.g. Berkeley, Bolivia) or researcher who first identified it (e.g. Showa, Kützing) (Weiss et al. 2010b, 2011). Additionally however, there are three races of *B. braunii*, which are classified based on the type of hydrocarbons they produce. The A race produces fatty acid-derived alkadienes and alkatrienes (Metzger et al. 1985, 1986; Templier et al. 1984, 1991), the L race produces the tetraterpene lycopadiene (Metzger 1987, 1990), and the B race produces triterpenes known as botryococcenes (Metzger 1985, 1987, 1988). The maximum dry-weight oil contents of each race also varies, with the A and B races topping out at 61% and 86%, respectively, but the L race with much less at 8% (Banerjee et al. 2002). While all races are ubiquitous in fresh to brackish, slow-moving, lake, and ephemeral bodies of water, the A and B races of *B. braunii* are distributed world-wide, except possibly for Antarctica, while the L race has only been found in tropical regions (Metzger and Largeau 1999). The three races have been found to coexist and, though they typically occupy oligotrophic or mesotrophic waters, large numbers may bloom in eutrophic waters (Smittenberg et al. 2005; Zhang et al. 2007). Because *B. braunii* are slow growing however, they do not rapidly proliferate into algal blooms in a competitive environment (Smittenberg et al. 2005). When blooms do occur, they may be large and prolonged or small and brief. The massive and extensively documented 1974 Darwin, Australia reservoir bloom lasted four years and was at one time estimated at 1500 tons of dry weight (Hillen et al. 1982; Wolf et al. 1983). By

contrast, Lake Kinneret, Israel, algae populations have been periodically dominated by *B. braunii* for thousands of years (Pollingher 1986) and its seasonal blooms can last as little as a few days (Zohary 2004).

Biofuel potential

Hydrocarbons from all three races of *B. braunii* can be converted into fuels suitable for combustion engines and have been found as major constituents of currently used petroleum and coal deposits (Cane 1977; Moldowan and Seifert 1980; Brassell et al. 1986; McKirdy et al. 1986; Glikson et al. 1989; Mastalerz and Hower 1996; Stasiuk 1999; Testa et al. 2001; Audino et al. 2002; Banerjee et al. 2002; Summons et al. 2002; Adam et al. 2006). This makes *B. braunii* an attractive source of renewable biofuels, especially the B race because botryococcenes can be efficiently converted (up to 97%) into high octane gasoline, kerosene, and diesel fuels using standard petroleum hydrocracking and distillation procedures (Fig. 3; Banerjee et al. 2002). *B. braunii* fuels are also notable as they contain virtually no sulfur or nitrogen which may poison catalysts—a credit to the relatively "pure" feedstock of crude extracted hydrocarbons (Banerjee et al. 2002). Given that *B. braunii* hydrocarbons already constitute a significant portion of current world energy production, this strongly suggests that the millions of years of fossilization and carbon emissions required to utilize these molecules from crude oil could be supplanted by simply growing *B. braunii*—a process that takes up carbon dioxide—and extracting its hydrocarbons directly for use in existing world infrastructure. *B. braunii* biofuel production, however, is hindered by

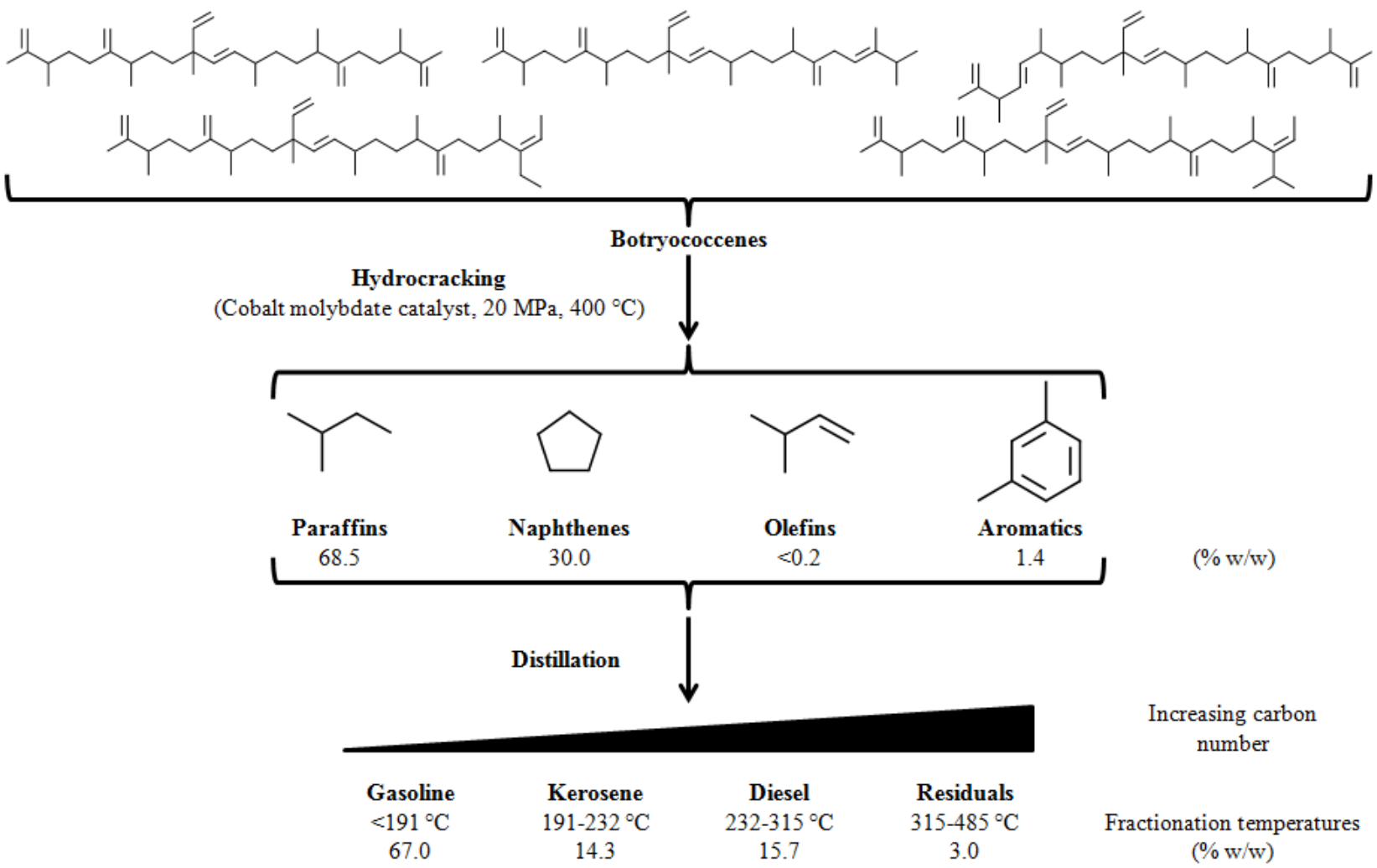

FIGURE 3. Botryococcene hydrocracking. *B. braunii* crude oil extracted from a wild-harvested B race, represented here by the five identified botryococcenes (collectively, 78% of the total crude oil contents), may be hydrocracked into a mixture of paraffins, naphthenes, olefins, and aromatics. The single greatest product quantified is illustrated for each category except for olefins (represented by isopentene), which were so sparse individual identification was not possible. When submitted to distillation, this mixture of compounds yields fractions suitable for gasoline, kerosene, and diesel. (Hillen et al. 1982; Niehaus et al. 2011).

slow growth with cells doubling every 6 days when bubbled with air and every 40 hours with at least 0.3% CO_2 (Wolf et al. 1985a). Strangely, though studies of petroleum deposits have generated information about the hydrocarbons synthesized by the ancestors of *B. braunii*, little is known about the molecular biology directing such synthesis in the organism living today.

Hydrocarbon synthesis

Isoprenoids

The hydrocarbons synthesized by the B and L races of *B. braunii* are terpenoids or, as will hereafter be referred to, isoprenoids. Isoprenoids are a diverse group of lipids that differ from fatty acids, which are also lipids. All organisms synthesize a wide array of isoprenoids to fulfill many critical functions of life indicating that the isoprenoid pathway is very ancient in origin (Phillips et al. 2008). These compounds and functions include, but are not limited to, ubiquinones for mitochondrial electron transport, sterols such as cholesterol for modifying membrane fluidity, and hormones for cellular communication (Phillips et al. 2008). Isoprenoids are derived from repeating, five-carbon isoprene (2-methyl-1,3-butadiene) units. Though all organisms ultimately synthesize isoprenoids from isopentenyl pyrophosphate (IPP), there are two biosynthetic pathways which generate IPP: the mevalonate (MVA) pathway and the non-mevalonate pathway (also called the mevalonate-independent pathway or, for short, the MEP, DOXP, or MEP/DOXP pathway after two of the intermediates) (Schwender et al. 2001;

Rodríguez-Concepción and Boronat 2002; Eisenreich et al. 2004; Phillips et al. 2008; Miziorko 2011).

MVA pathway reactions occur in the cytosol, but several enzymes are localized to the exterior of the endoplasmic reticulum (ER) (Fig. 4; Miziorko 2011). It begins with the catalysis of two molecules of acetyl-CoA by thiolase to form acetoacetyl-CoA (Miziorko 2011). The second step, the first dedicated step toward isoprenoid synthesis, condenses acetoacetyl-CoA with a third molecule of acetyl-CoA to form 3-hydroxy-3-methylglutaryl-CoA (HMG-CoA), a process catalyzed by HMG-CoA synthase (Miziorko 2011). Only in the third step is the namesake of the pathway, mevalonate, synthesized by the reduction of HMG-CoA by HMG-CoA Reductase (Miziorko 2011). As this is the rate limiting step of the mevalonate pathway, HMG-CoA Reductase is the target of an entire class of inhibitors called statins, which are widely prescribed to lower cholesterol synthesis in humans (Miziorko 2011). The remainder of the mevalonate pathway requires two kinases and two ATP to generate 5-pyrophosphatemevalonate (Miziorko 2011). 5-pyrophosphatemevalonate is then decarboxylated to form either IPP or dimethylallyl pyrophosphate (DMAPP), which can be interconverted by isomerization (Miziorko 2011).

By contrast, the MEP/DOXP pathway occurs in bacteria and in the stroma of plastids and begins with the condensation of pyruvate with D-Glyceraldyhyde-3-phosphate (GA3P) to form 1-deoxy-D-xylulose-5-phosphate (DOXP) (Fig. 5; Phillips et al. 2008). This reaction is catalyzed by DOXP Synthase (DXS). The second step is the reduction of DOXP by DOXP reductase (DXR) to form 2C-methyl-D-erythritol-4-

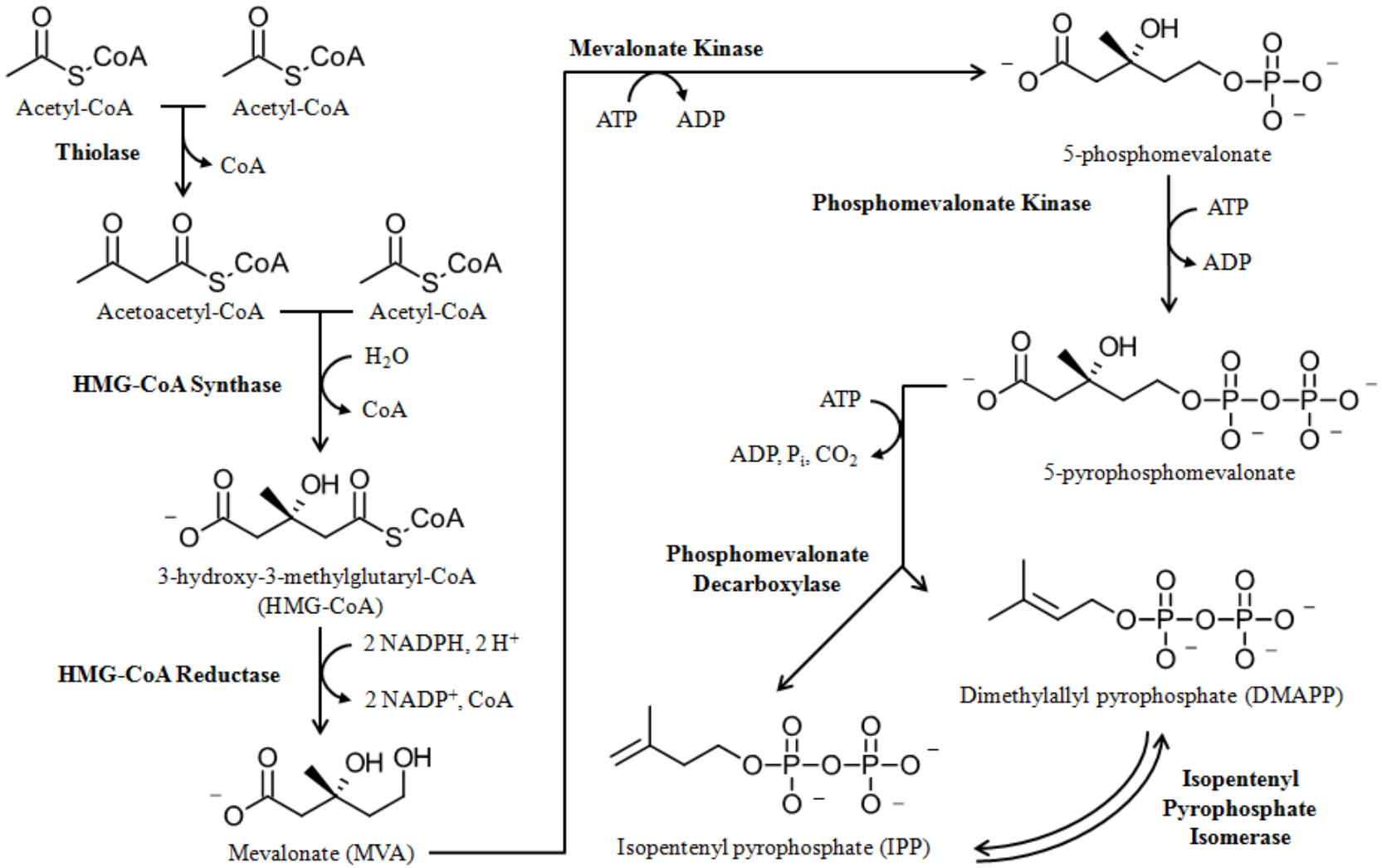

FIGURE 4. General scheme of the mevalonate (MVA) pathway. The MVA pathway is carried out in the cytosol. Enzymes are in bold. Note that Phosphomevalonate Decarboxylase catalyzes the formation of either IPP or DMAPP at a 5:1 ratio, respectively (Rohdich et al. 2002, 2003).

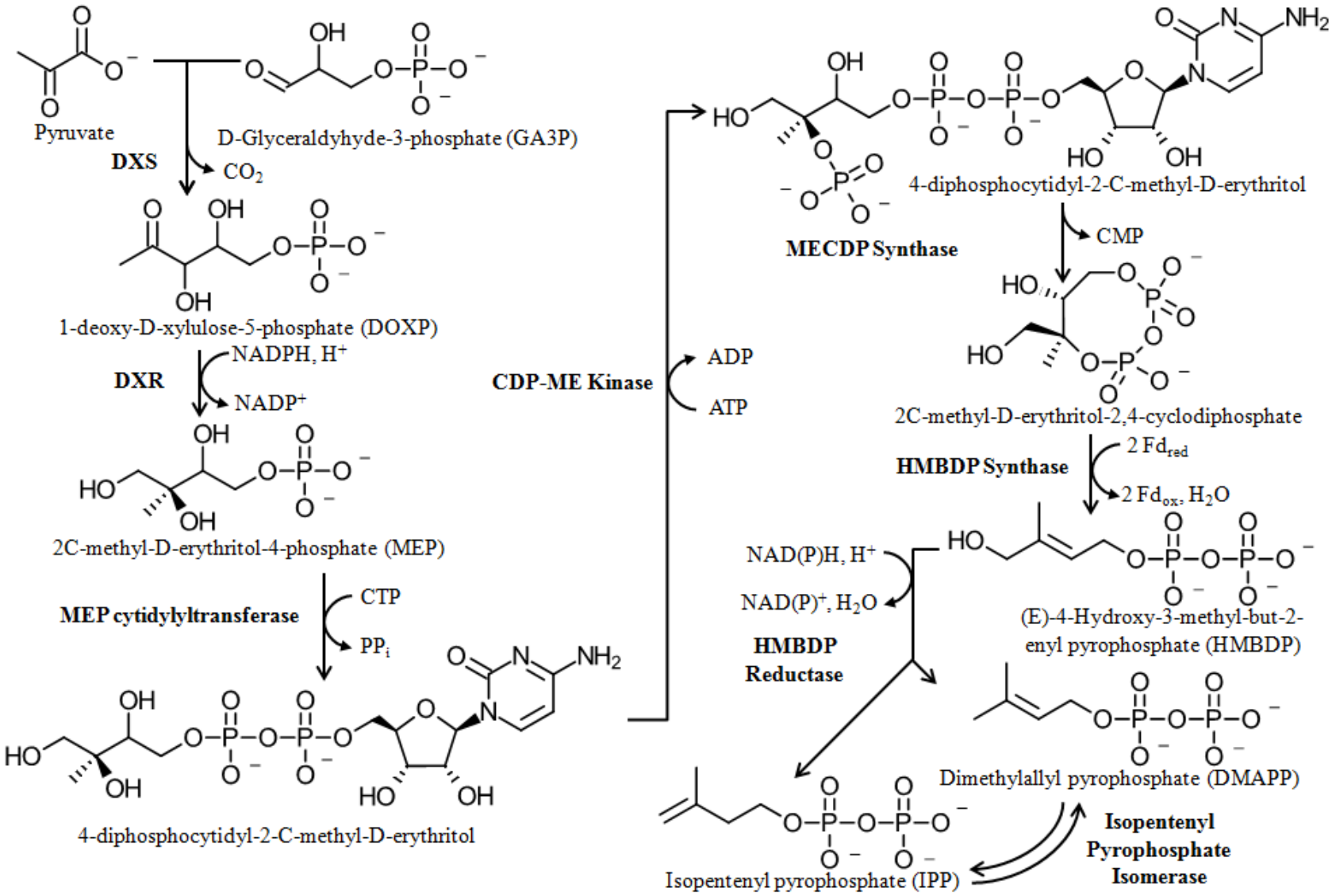

FIGURE 5. General scheme of the non-mevalonate (DOXP/MEP) pathway. The DOXP/MEP pathway is carried out in plastids. Enzymes are in bold. Note that HMBDP Reductase catalyzes the formation of either IPP or DMAPP at a 5:1 ratio, respectively (Rohdich et al. 2002, 2003).

phosphate (MEP) (Phillips et al. 2008). It requires a further four steps before (E)-4-Hydroxy-3-methyl-but-2-enyl pyrophosphate (HMBDP) reductase finally yields IPP or DMAPP that may be interconverted by isomerization (Phillips et al. 2008). Unlike the MVA pathway, the rate-limiting step of the MEP/DOXP pathway is not well elucidated, but plant studies suggest both DXS and DXR have rate-limiting roles (Cordoba 2009). Recent research has shown that the *B. braunii*, B race expresses three DXS paralogues simultaneously at times coinciding with increased isoprenoid production, suggesting DXS plays a significant rate-limiting role in the alga (Matsushima et al. 2012).

As the only organisms possessing both functional MVA and MEP/DOXP pathways however, plants are unusual. Generally speaking, animals, fungi, and archaea only utilize the MVA pathway (Miziorko 2011). Categorization is more difficult in bacteria however as each organism may utilize either pathway. There is currently insufficient information to categorize all algae definitively, but it appears at this time that green algae utilize the MEP/DOXP pathway only (Schwender et al. 2001; Lohr et al. 2012). Thus it is the MEP pathway which ultimately forms the basis for hydrocarbon synthesis in the *B. braunii* B and L races.

As previously stated, IPP production, through either pathway, only provides the foundation of further isoprenoid synthesis reactions shared by all organisms by synthesizing five-carbon isoprene units. These further processes require two enzymes, farnesyl pyrophosphate synthase (FPPS) and geranylgeranyl pyrophosphate synthase (GGPPS) (Fig. 6; Lohr et al. 2012). FPPS catalyzes two condensation reactions: first, the condensation of IPP and DMAPP to form C_{10} geranyl pyrophosphate (GPP) and

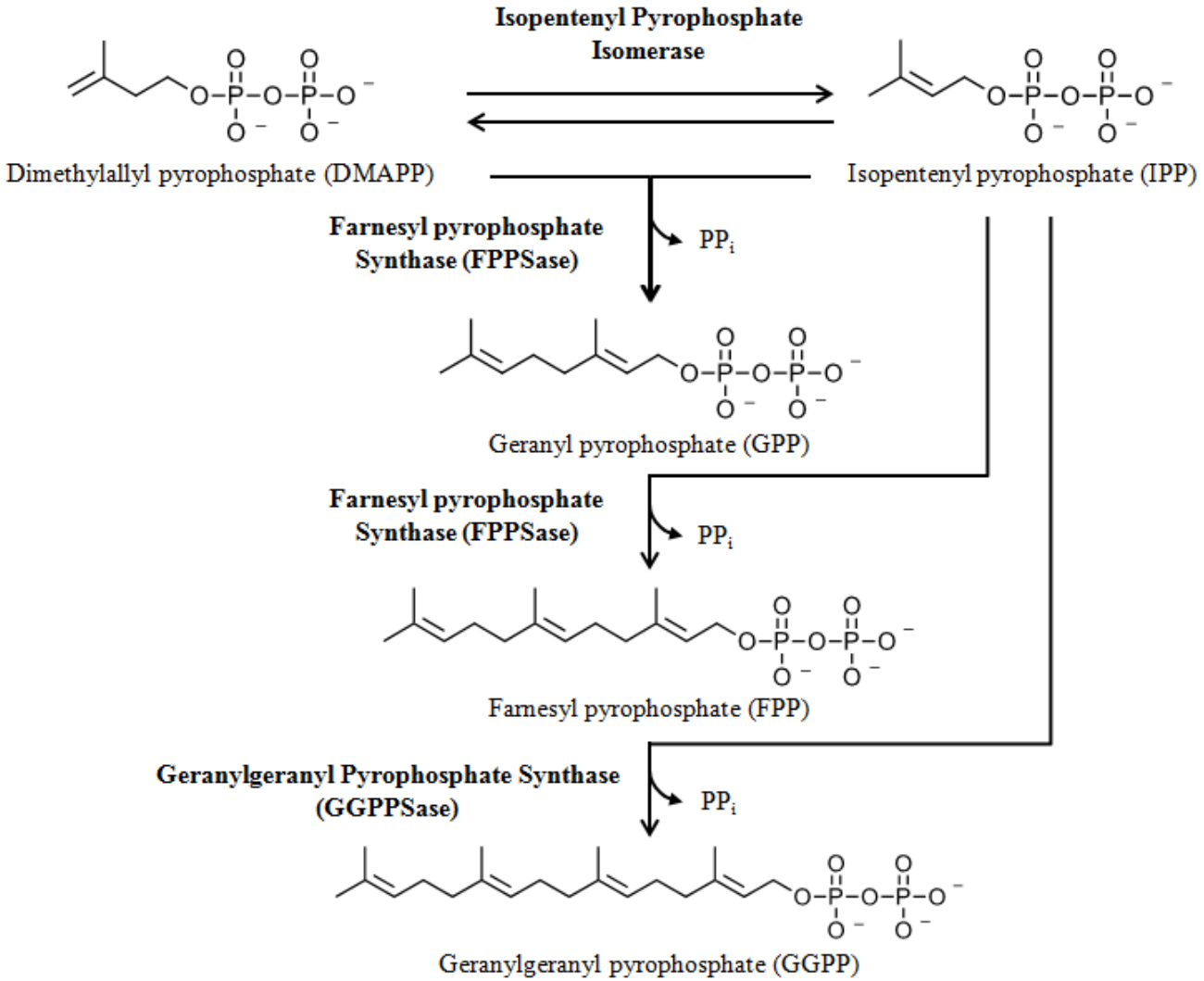

FIGURE 6. General scheme of isoprenoid precursor synthesis. Isoprenoid precursors are elongated by repeated head-to-tail condensations of IPP and the elimination of pyrophosphate. Note that due to common polyprenyl transferase activity among isoprenoid synthesis enzymes, GPP and FPP are often recognized as products of a single enzyme simply recognized as the FPP Synthase only (Chen and Poulter 1993; Lichtenthaler 2010).

second, the condensation of GPP and an additional IPP to form C_{15} farnesyl pyrophosphate (FPP) (Lohr et al. 2012). GGPPS catalyzes the further condensation of FPP and IPP to form C_{20} geranylgeranyl pyrophosphate (GGPP) (Lohr et al. 2012). The B and L races of *B. braunii* will specifically utilize FPP and GGPP substrates, respectively, to produce liquid hydrocarbons.

B Race

B race botryococcenes are triterpenes biosynthesized through the isoprenoid pathway and are similar in structure to another common triterpene, squalene (Sato et al. 2003; Okada et al. 2004). Both botryococcene and squalene are C_{30} compounds produced by the condensation of two molecules of FPP; however, they differ in how the farnesyl molecules are connected (Fig. 7). In *B. braunii*, squalene is synthesized by the enzyme *Botryococcus* Squalene Synthase (BSS) in the typical two-step process common to all squalene synthases. In the first step, two FPP molecules are condensed head-to-head, eliminating one pyrophosphate, and creating the stable cyclopropyl intermediate presqualene diphosphate (PSPP) (Niehaus et al. 2011). In the second step, PSPP is reduced by NADPH inducing a rearrangement that eliminates the second pyrophosphate and cleaves the cyclopropyl ring to yield a C1–C1′ bond between the parental FPP molecules (Figure; Niehaus et al. 2011). In contrast, C_{30} botryococcene has a C3–C1′ bond of the two farnesyl molecules which produces a central branch ending with a C=C bond (Figure; Huang and Poulter 1989; Okada et al. 2004). This unique branching is created via equally unique enzymes.

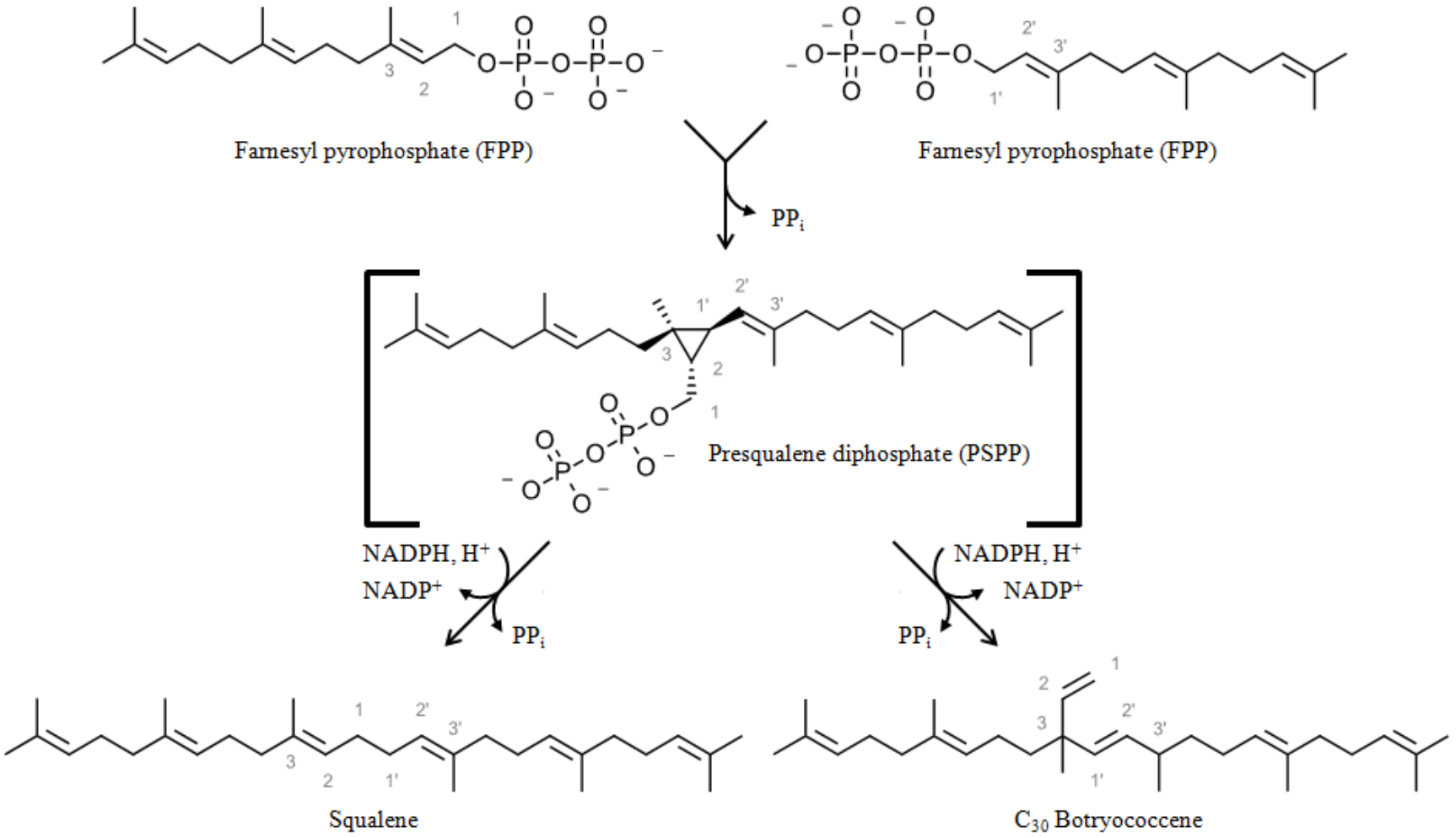

FIGURE 7. General scheme of *B. braunii* triterpene synthesis. The head-to-head condensation of two molecules of farnesyl diphosphate (FPP) proceeds through a cylcopropyl intermediate, presqualene diphosphate (PSPP), which may be differentially cleaved to yield a C1-C1′ bond (squalene) or a C3-1′ bond (C_{30} botryococcene) (Niehaus et al. 2011).

In the *B. braunii* B race, botryococcene synthesis is catalyzed by two enzymes: Squalene Synthase-Like 1 and 3 (SSL-1 and SSL-3) (Fig. 8; Niehaus et al. 2011). SSL-1 condenses two molecules of FPP to yield PSPP and a pyrophosphate, just like BSS. However, it does not catalyze the second step of opening the cyclopropyl ring of PSPP (Niehaus et al. 2011). Instead, SSL-3 then utilizes PSPP, reduced by NADPH, and induces a rearrangement to generate C_{30} botryococcene and its 3–1′ bond (Niehaus et al. 2011). Also unique to *B. braunii*, PSPP may be utilized with NADPH by the enzyme SSL-2 to produce squalene (Niehaus et al. 2011). The purpose of this second enzymatic pathway to squalene synthesis remains unknown, but it may produce squalene derivatives that are exported into the extracellular matrix, the same as botryococcenes (Niehaus et al. 2011).

Once created, C_{30} botryococcene is further metabolized by S-adenosyl methionine (SAM) methylation at carbons 3, 7, 16, and 20 to produce C_{31}, C_{32}, C_{33}, and C_{34} botryococcenes (Fig. 9; Casadevall et al. 1984; Wolf et al. 1985; Metzger et al. 1987), and even further methylated to $C_{35,}$ C_{36}, and C_{37} botryococcenes in some B race strains (Galbraith, M. N. et al. 1983; Metzger et al. 1985). In C_{34} botryococcene-producing strains such as the Berkeley (Showa) strain, the majority (~99%) of the C_{34} botryococcenes exist in the extracellular matrix whereas the intracellular oil comprises predominantly the lower carbon number botryococcenes (Metzger et al. 1985; Wolf et al. 1985). These botryococcenes are excreted to the extracellular matrix as they mature to C_{34} botryococcene, but may be methylated both inside and outside the cell (Wolf et al. 1985; Metzger et al. 1985, 1987b). The intracellular botryococcenes are presumed to be

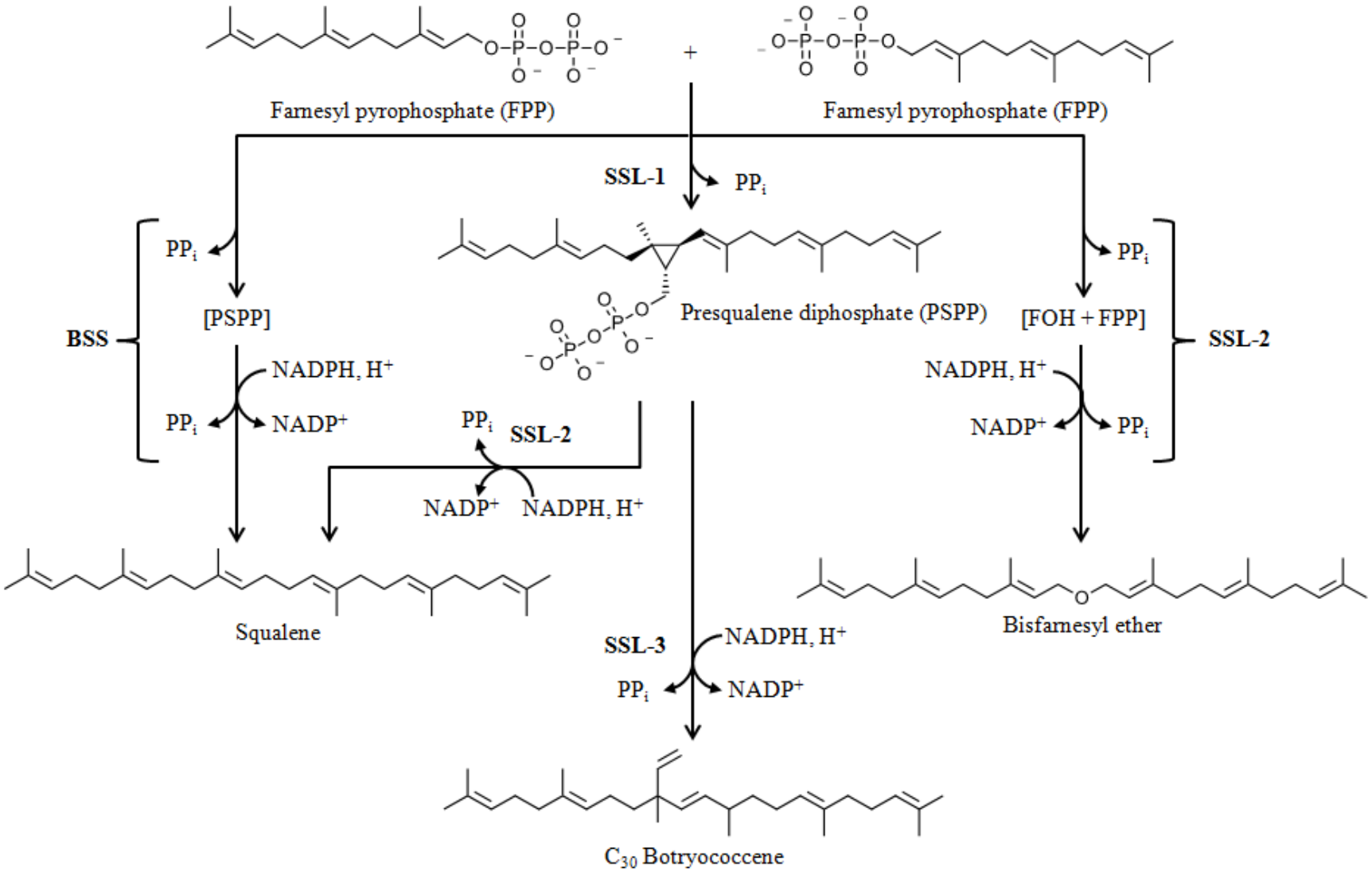

FIGURE 8. Enzymatic scheme of *B. braunii* triterpene synthesis. Botryococcus squalene synthase (BSS) catalyzes the formation of squalene from two molecules of farnesyl diphosphate (FPP) via an presqualene diphosphate (PSPP) intermediate. *B. braunii* may alternatively synthesize squalene through a combination of squalene synthethase like-1 (SSL-1), which catalyzes the formation of PSPP, and SSL-2, which catalyzes the formation of squalene. *In vitro*, SSL-2 may also catalyze FPP directly, produce a farnseol (FOH) intermediate, and yield the non-triterpene product, bisfarnesyl ether. Only SSL-3 catalyzing PSPP yields C_{30} botryococcene. (Niehaus et al. 2011)

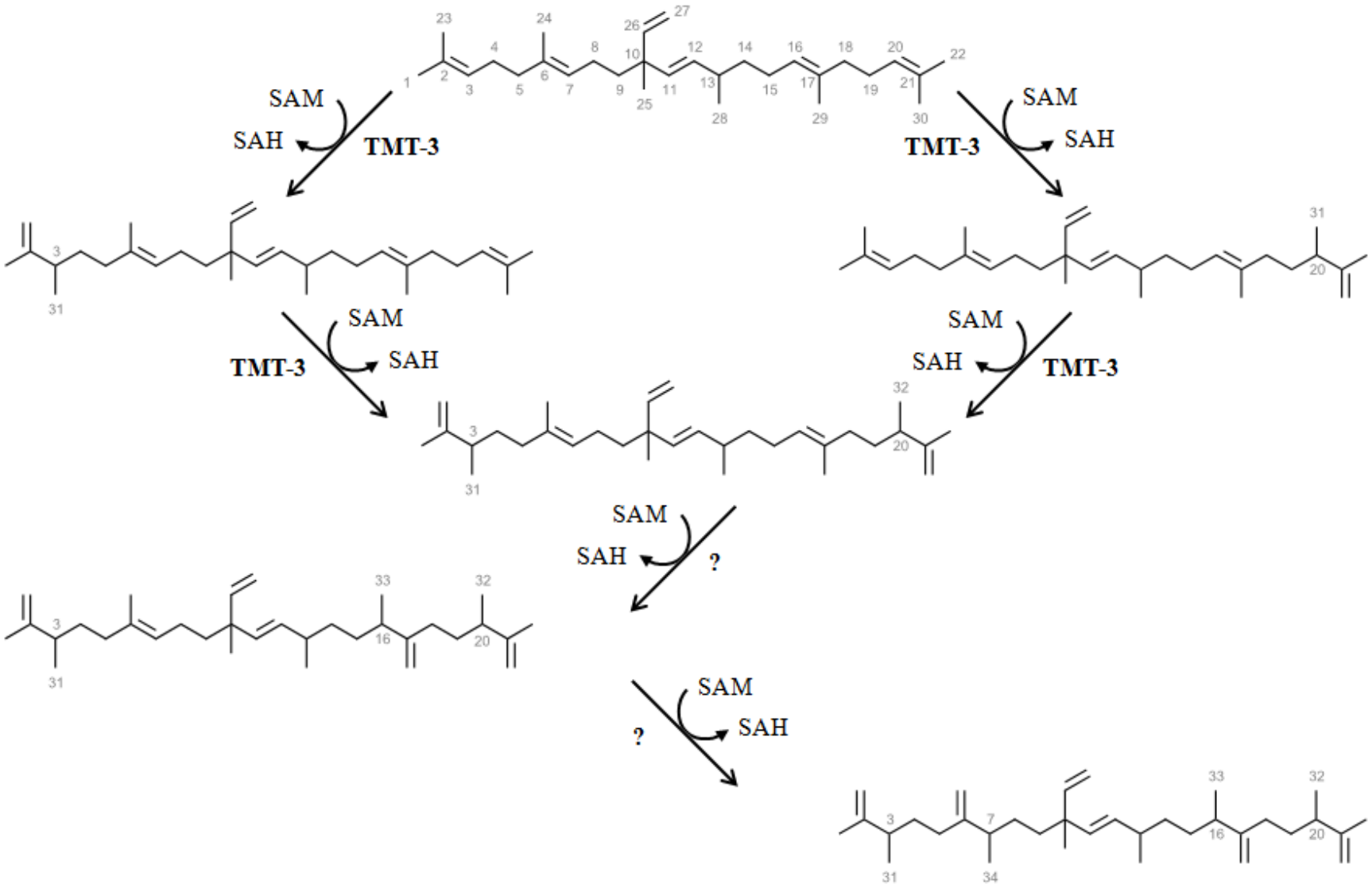

FIGURE 9. General scheme of *B. braunii* botryococcene methylation. C_{30} botryococcene is twice methylated at carbons 3 and 20 by triterpene methyltransferase 3 (TMT-3). The enzyme(s) which catalyze two further methylations first at carbon 15 and then at carbon 7 have not been identified. Each step uses the methyl donor S-adenosyl methionine (SAM) and generates S-adenosyl-L-homocysteine (SAH). (Niehaus et al. 2012)

located in the numerous intracellular oil bodies found within *B. braunii* cells (Maxwell et al. 1968; Knights et al. 1970; Banerjee et al. 2002).

Curiously, the B race may also synthesize tetramethylsqualene, though typically accumulating at much lower quantities than botryococcenes (Fig. 10; Achitouv et al. 2004). Due to the structural similarities of botryococcene, squalene, and the side-chains of sterols, it has been suggested that the triterpene methylating enzymes of B race hydrocarbons may be similar to sterol methyltransferases (SMTs) (Niehaus et al. 2012). This has been demonstrated both *in vitro* and *in vivo* by the identification of three SAM-dependent methyltransferases in *B. braunii* designated triterpene methyltransferases (TMTs) (Niehaus et al. 2012). TMT-1 and TMT-2 are both capable of catalyzing the methylation of squalene at carbons 3 and 22, while TMT-3 catalyzes the methylation of C_{30} botryococcene at carbons 3 and 20 (Niehaus et al. 2012). Enzymes which catalyze the further methylation of botryococcene or squalene above C_{32} have not yet been identified.

L Race

In contrast, the synthesis of the *B. braunii* L race liquid hydrocarbon remains virtually unknown. Despite this lack of attention, two slightly different models of lycopadiene synthesis have been proposed (Fig. 11; Metzger and Casadevall 1987; Metzger and Largeau 1999). One model, supported by biochemical observations in plants, suggests that two molecules of C_{20} geranylgeranyl pyrophosphate (GGPP) might first be reduced three times each yielding two phytyl diphosphates which then condense

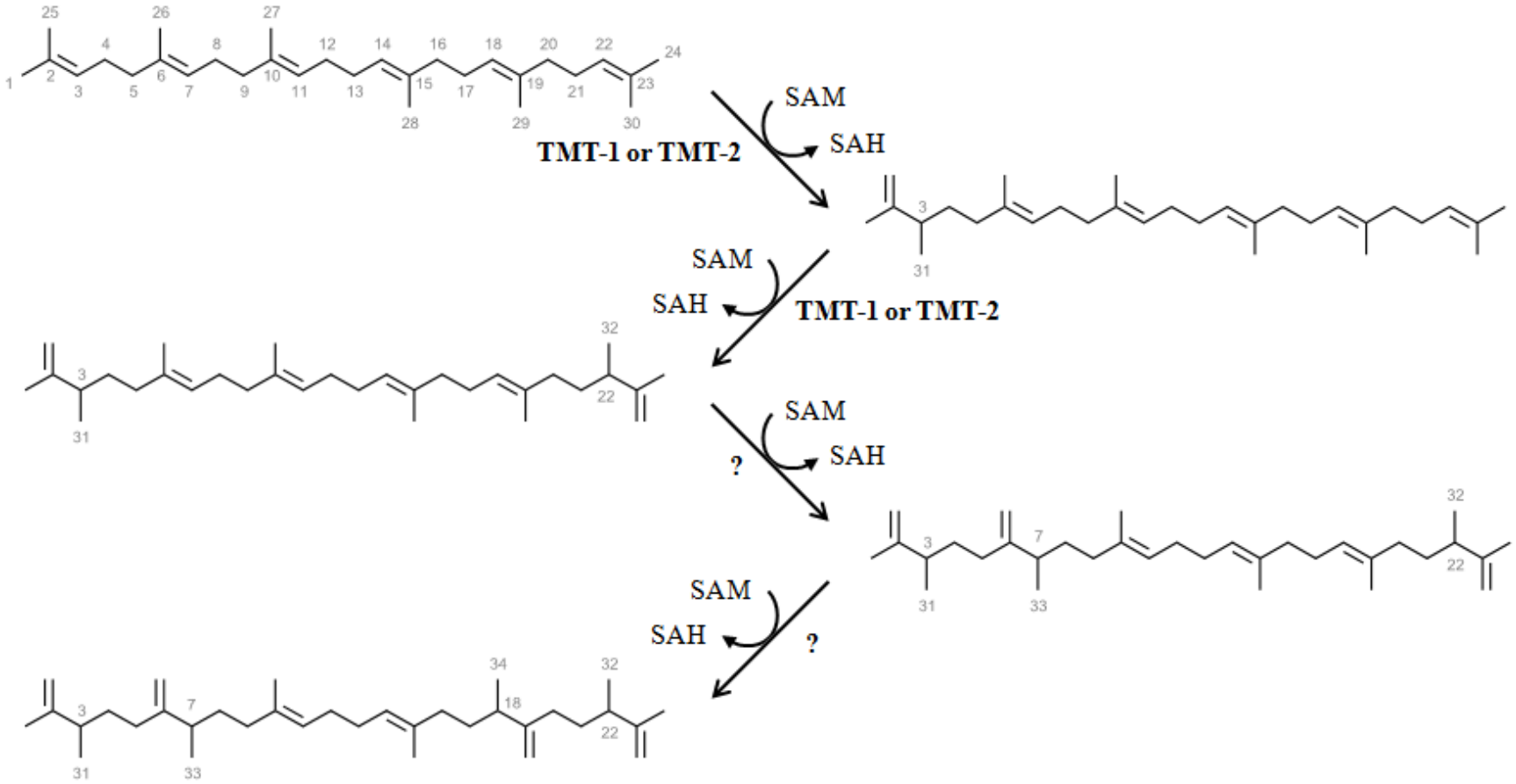

FIGURE 10. General scheme of *B. braunii* squalene methylation. Squalene is twice methylated at carbons 3 and 22 by triterpene methyltransferase 1 (TMT-1) and/or TMT-2. The enzyme(s) which catalyze two further methylations at carbons 7 and 18 have not been identified. Each step uses the methyl donor S-adenosyl methionine (SAM) and generate S-adenosyl-L-homocysteine (SAH). (Niehaus et al. 2012)

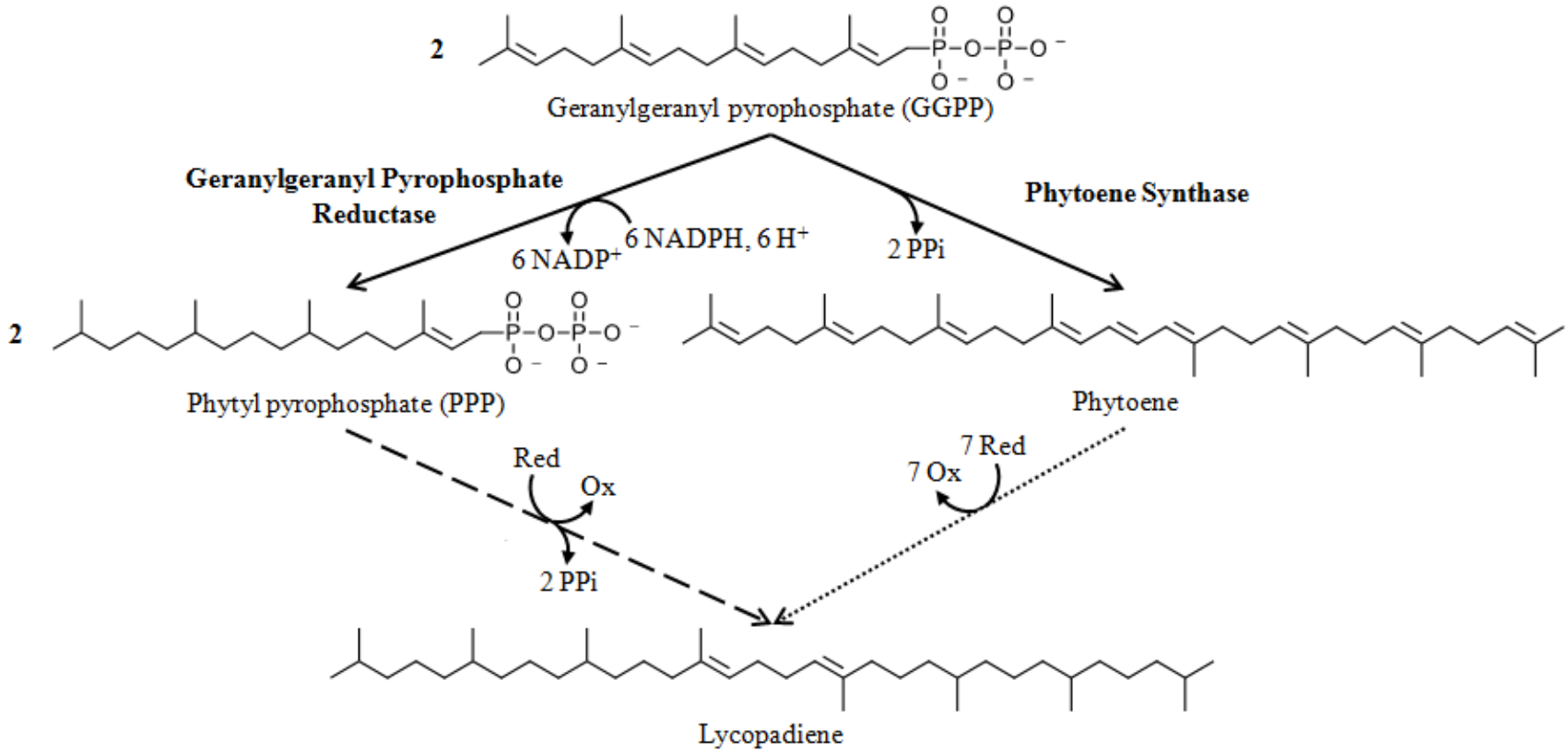

FIGURE 11. Two possible *B. braunii* lycopadiene synthetic pathways. In plants, geranylgeranyl pyrophosphate (GGPP) is reduced three times by geranyl pyrophosphate reductase to form phytyl pryophosphate (PPP) or may be condensed by phtyoene synthase to form phytoene (Metzger and Casadevall 1987; Metzger and Largeau 1999). These compounds, PPP and phytoene, in turn suggest two possible lycopadiene synthetic pathways. The first entails the reduction and condensation of two PPP (dashed line), while the second entails the reduction of phytoene seven times (dotted line).

head-to-head to form lycopadiene and two pyrophosphates (Metzger and Casadevall 1987). A second model suggests that two GGPP may condense head-to-head to form phytoene which must be saturated seven times to yield lycopadiene (Fig. 11; Metzger and Casadevall 1987). While some possible pathway precursors—lycopatriene and lycopadiene isomers—have been isolated from lake sediment layers, their molecular structures do not support one model over the other (Zhang et al. 2007). Explicit lycopadiene precursors have never been isolated from living *B. braunii*.

A Race

Unlike the *B. braunii* B and L races which synthesize isoprenoid hydrocarbons, A race hydrocarbons are fatty-acid derived (Fig. 12). These A race hydrocarbons predominately consist of long-chain, odd-numbered alkadienes and alkatrienes that possess a terminal carbon-carbon double-bond (Metzger and Largeau 1999). However, the variation in both the qualities and quantities of the hydrocarbons varies widely between strains. For instance, the total hydrocarbon content of the A race has been observed from 0.4% to 61% of dry biomass (Metzger and Largeau 1999). Hydrocarbon lengths in each strain may vary from C_{23} to C_{33}—though typically only over some portion of this range—and interior double bonds may be cis or trans (Metzger and Largeau 1999). Additionally, while strains like the Yamanaka are less variable, synthesizing only alkadienes, a Bolivian strain from Lake Overjuyo is extremely variable, synthesizing monoenes and tetraenes plus C_{26} and C_{28} even-numbered hydrocarbons (Metzger and Largeau 1999). Although this variability has generated

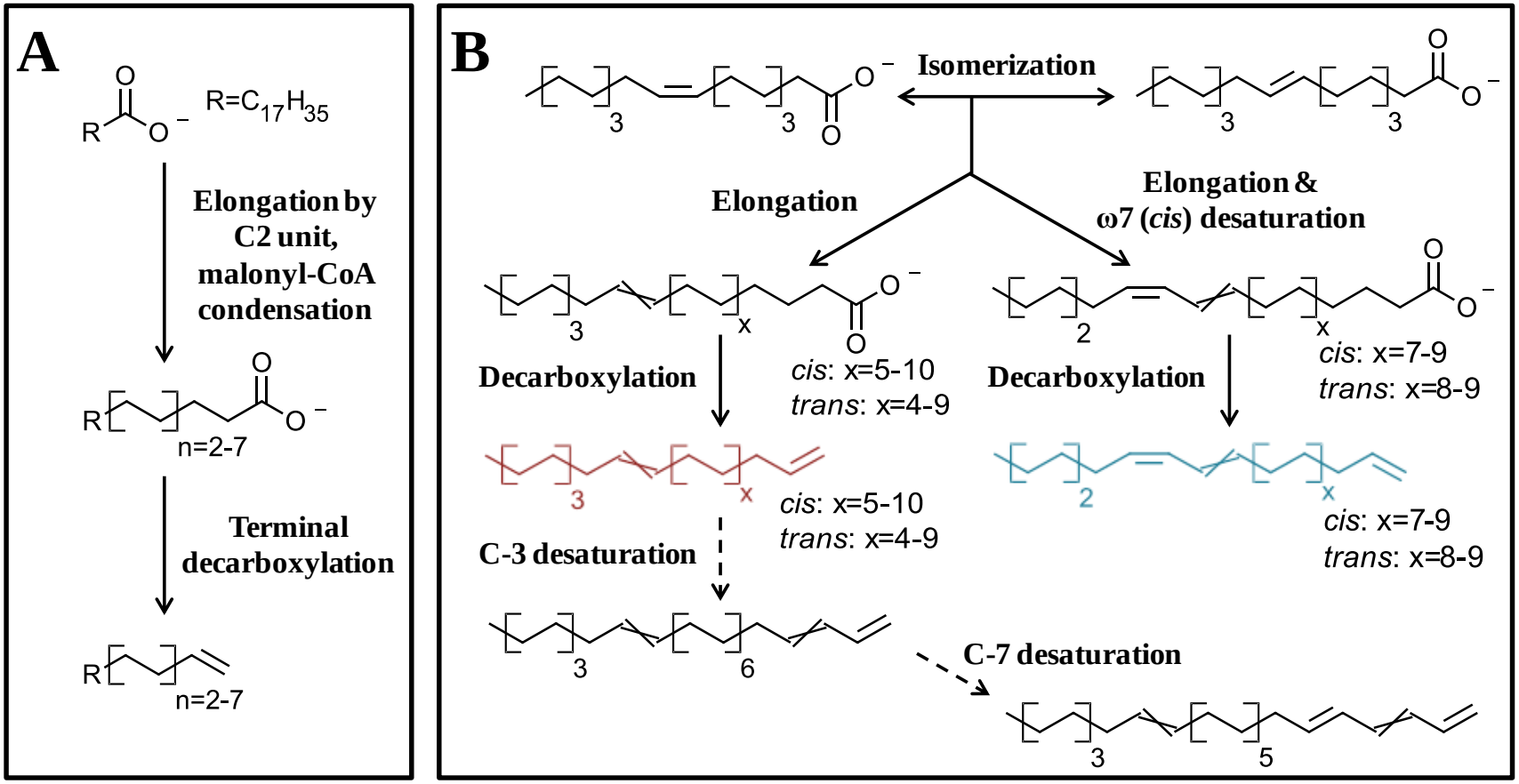

FIGURE 12. ***B. braunii,*** **A race *n*-long chain hydrocarbon synthesis.** Hydrocarbons of the A race are synthesized by repeated malonyl-CoA condensations with a fatty acid substrate followed by a terminal decarboxylation reaction. (a) Example synthesis beginning with a stearic acid substrate. Such alkamonoenes products are rare however, as the synthesis greatly favors a monounsaturated substrate. (b) The more common synthetic pathway begins with elongation of oleic and/or elaidic acid, which *B. braunii* may isomerize. Alkadienes are formed by the decarboxylation of the elongated products. In some strains, additional C-3 and then C-7 desaturatation may lead to alkatrienes and alkatetraenes, respectively (dashed arrows). Such putative syntheses are believed to be in series, but may occur via a parallel mechanism instead. Alkatrienes are most commonly formed by such a parallel pathway in which a fatty acid substrate is concurrently elongated and ω7 (*cis*) desaturated. The most commonly isolated *n*-long chain hydrocarbons are the alkadienes and alkatrienes highlighted in red and blue, respectively. (Templier et al. 1991; Metzger and Largeau 1999)

large amounts of chemical data, the exact biosynthetic pathway has not yet been identified.

Even without the isolation of biosynthetic enzymes, many years of radioisotope labeling studies suggest a model of alkadiene/alkatriene synthesis beginning with the fatty acid precursor oleic acid (18:1, cis-ω9), which is repeatedly elongated by malonyl-CoA derived C_2-unit incorporation until termination by decarboxylation (Metzger and Largeau 1999). Though oleic acid (18:1) is thought to be the primary precursor because of its rapid uptake and cellular depletion during hydrocarbon synthesis (Metzger and Largeau 1999), palmitic acid (16:0), stearic acid (18:0), and elaidic acid (18:1) may also be wholly incorporated into synthesized hydrocarbons (Metzger and Largeau 1999). The exchange of cis/trans conformations of all internal double bonds, particularly at the ω9 position, appears to be much slower than the rate of elongation and is controlled by an unidentified isomerase(s) (Metzger and Largeau 1999). The specification of this isomerization is not known, but is also unusual in that it does not allow the exchange of vinylic protons (Metzger and Largeau 1999).

Hydrocarbon accumulation

Though the specific mechanism of hydrocarbon synthesis varies, each race of *B. braunii* is able to deposit a majority of hydrocarbons in the extracellular matrix and a minority within cytoplasmic lipid bodies (Fig. 13; Banerjee et al. 2002; Knights et al. 1970; Maxwell et al. 1968; Metzger et. al 1987a,b; Wolf et al. 1985). The A and B races accumulate hydrocarbons in different ways however, and the L race remains unclear.

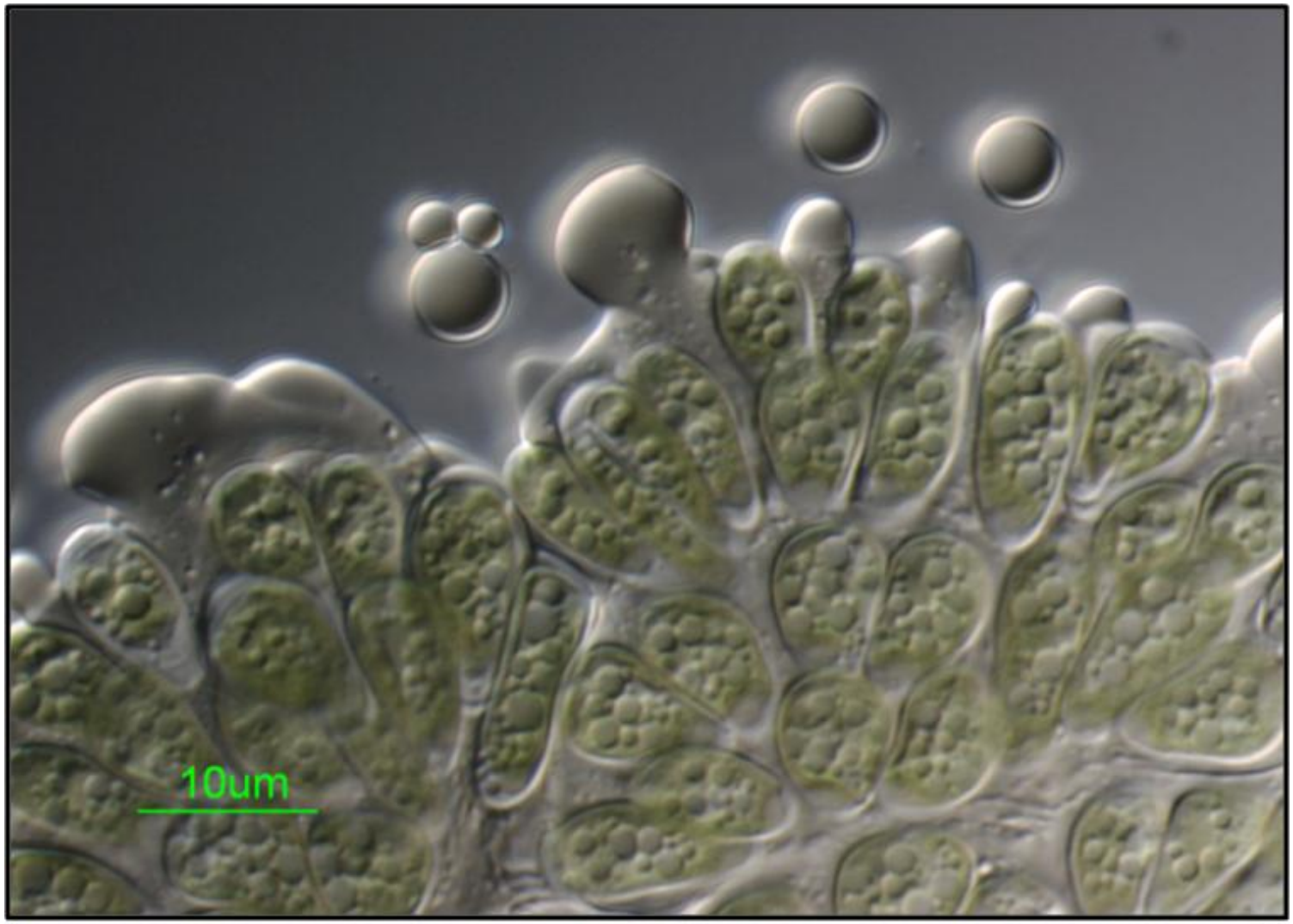

FIGURE 13. Microscopy imaging of *B. braunii* cells. A transmitted light microscope image of a partial *B. braunii* colony. Each cell contains numerous intracellular oil bodies. The pressure of flattening the colony for observation also causes the release of some extracellular oil.

Specifically, B race radiolabeling studies (hot-pulse/cold-chase using L-[Me-^{14}C]-methionine showed radioactive incorporation into hydrocarbons isolated from inside cells, before incorporation into hydrocarbons isolated from outside the cells (Metzger et al. 1987b). These data suggest that low-molecular weight botryococcenes are more rapidly methylated inside cells than outside the cells and possibly before being excreted into the extracellular matrix at higher-molecular weights (Metzger et al. 1987b). This also implies a unidirectional movement of botryococcenes from the internal hydrocarbon pool to the external hydrocarbon pool (Metzger et al. 1987b). In this regard, lipid bodies may essentially function as waypoints for botryococcenes prior to methylation which leads to excretion into the extracellular matrix. This is not true of the A race. Instead, hot pulse-cold chase radiolabeling studies using palmitic acid-[9,10-^{3}H] showed simultaneous radioactive incorporation into hydrocarbons isolated from both inside and outside cells (Largeau et al. 1980). This finding suggests that the hydrocarbons of the A race appear to be secreted and that no mixing of the intracellular and extracellular hydrocarbon pools occurs (Largeau et al. 1980). It also implies that alkadienes and alkatrienes are not synthesized within the cell, but rather at its periphery (plasma membrane, cell wall, etc.) and that a preference for long hydrocarbon chain export into the extracellular matrix somehow also generates lipid bodies primarily composed of shorter chains (Largeau et al. 1980). Though extraction and microscopic observations generally support these conclusions, resolving the underlying organization and function of lipid body formation has remained elusive.

Rationale

It is clear that *B. braunii* holds enormous potential for biofuel applications and the results of capturing its novel hydrocarbon synthetic genes is even more alluring: an alga, transformed by these biosynthetic genes, capable of both fast growth and copious production of hydrocarbons that can be processed into "drop-in" fuels compatible with existing petroleum-based infrastructure. However, it is also clear that while chemical and geochemical research has strongly supported this aim, *B. braunii* hydrocarbons will not be a viable source of alternative energy without a much greater understanding of the molecular biology of the organism and its biochemistry. At the time of these studies, B. braunii studies suffered three major impediments: one, the taxonomic classification of *B. braunii* was uncertain; two, few of the hydrocarbon synthetic enzymes had been identified, isolated, and purified; and three, slow and inefficient culturing and data collection was a serious impediment to experimentation. Therefore, with these specific challenges in mind, this study was undertaken to establish both a general foundation for *B. braunii* molecular analysis and to investigate its unique mechanisms of hydrocarbon biosynthesis while improving the tools and methods available to pursue both goals.

CHAPTER II

MATERIALS AND METHODS*

Growth apparatus design

Many algae strains studied in laboratories are grown very simply either autotrophically on sunny windowsills or heterotrophically in shaker flasks. Because of the slow growth rate of *B. braunii* however, a growth apparatus needed to be constructed which could reliably support algae cultures for up to six weeks without maintenance or condition variability, but with constant sterility and CO_2 gas enrichment. The apparatus was also designed to be both modular and condition-variable, so that the basic unit could supply expanded experimental needs while providing a platform that could also support the growth of additional algae strains besides *B. braunii*.

Mixed-gas system

To rapidly grow algae autotrophically, CO_2 must first be mixed and then

---

*Portions of the following articles have been reprinted with permission from: (1) Weiss, T. L., Chun, H. J., Okada, S., Vitha, S., Holzenburg, A., Laane, J., and Devarenne, T. P. 2010a. Raman spectroscopy analysis of botryococcene hydrocarbons from the green microalga *Botryococcus braunii*. *J. Biol. Chem.* 285:32458-66. Copyright 2010 © by The American Society for Biochemistry and Molecular Biology, Inc. (2) Weiss, T. L., Johnston, J. S., Fujisawa, K., Sumimoto, K., Okada, S., Chappell, J., and Devarenne, T. P. 2010b. Phylogenetic placement, genome size, and GC content of the liquid-hydrocarbon-producing green microalga *Botryococcus braunii* strain Berkeley (Showa) (Chlorophyta). *J. Phycol.* 46:534–540. Copyright 2010 © by Phycological Society of America (3) Weiss, T. L., Johnston, J. S., Fujisawa, K., Okada, S., and Devarenne, T. P. 2011. Genome size and phylogenetic analysis of the A and L races of *Botryococcus braunii*. *J. Appl. Phycol.* 23:833–839. Copyright 2010 © by Springer Science+Business Media B.V.

delivered to algae growth containers (Fig. 14). CO_2-enriched air was produced using a Witt Gas Mixer, KM 20-2 (Witt Gasetechnik GmbH & Co. KG, Witten, Germany). This special-order device is specifically designed to mix 0-5% CO_2 with a balancing percent air with an output flow rate of 0-20 L/min. Gas mixing is driven by maintaining minimum pressure inputs from a regulated cylinder of pure CO_2 and a building central air line. Also, when a CO_2 cylinder is completely consumed, air will continue to flow at the same constant rate as the mixed gas. This is unlike flow meter controlled mixing systems which control two mixing gas flow rates and are prone to imprecise gas mixing percentages and variable flow rates. An air line fed from a building-centralized compressor is also generally more reliable than small compressors.

To deliver and control the mixed gas output, gas flow was divided using vacuum/gas manifolds and water column (Fig. 14). While gas was originally distributed through a commercially available vacuum manifold (Chemglass, Vineland, NJ, USA), a superior manifold was later specially designed by the Texas A&M Glass Shop and integrated into the system. This new manifold possess a larger inner volume and two opposing gas inlet ports, both features which greatly simplify gas distribution at low pressures and volume. Because all samples are gas-fed in parallel, increasing or decreasing the flow rate on one sample can impact the flow rate on another. By utilizing a water column however, any fluctuations in gas flow can be redistributed to the water column without affecting every other sample.

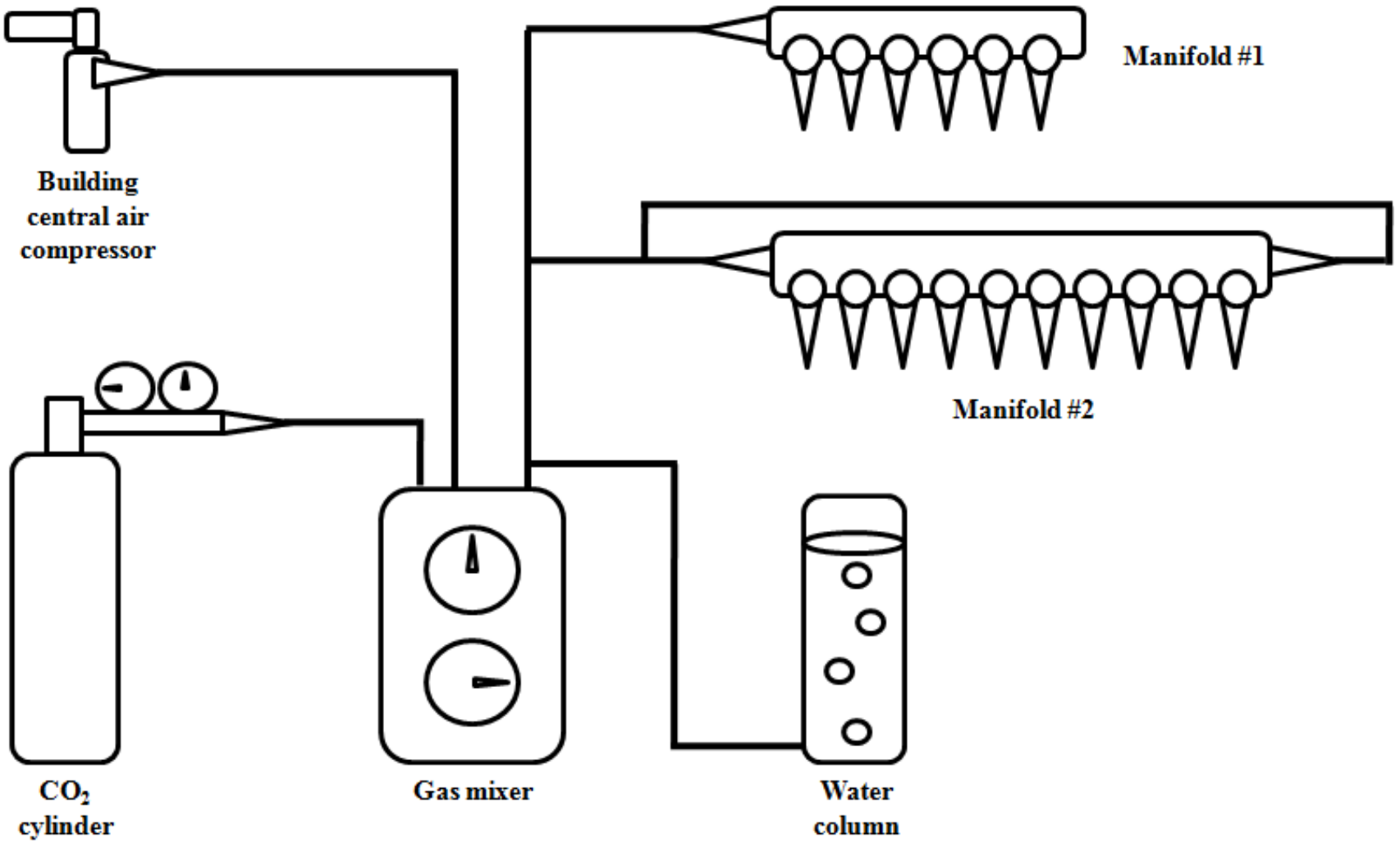

FIGURE 14. Mixed-gas system. Compressed air was combined with CO_2 via a mixer, which controls both % mixing and flow rate, before distribution to manifolds and a water column.

Lighting system

Illumination for algae autotrophic growth was generated via track lighting with multiple fixtures for compact fluorescent bulbs (Fig. 15). Typically, 13 W compact fluorescent bulbs of 65 K lighting at a distance of 7.62 cm from flasks were used, which produced a light intensity of 280 μmol photons · m^{-2} · s^{-1}. Power to each track was controlled through a digital timer (GE Lighting, Neela Park, OH, USA) to generate a typical lighting cycle of 12:12 light:dark (L:D). This yielded a temperature environment that varied between 24 °C in the light and 21 °C in the dark for a daily average of 22.5 °C.

Because each section of track operates from an independent power source that can be controlled by a digital timer, independent day-night cycles can be generated. Multiple compact fluorescent bulb fixtures also means that individualized light intensities can be generated by modifying the light bulb fixture position and utilizing light bulbs of varying wattage. This arrangement offers several experimental advantages and spatial options over traditional fluorescent tube lighting arrangements.

Liquid media growth

Flasks

Nearly all algae liquid cultures were carried out in 1 L Pyrex Roux flasks (Corning, Corning, NY, USA). To deliver mixed gas to the culture while maintaining sterility an autoclavable “headpiece” was designed (Fig. 16). This “headpiece” is primarily composed of a hollow silicone tapered stopper (EPSI, Franksville, WI, USA)

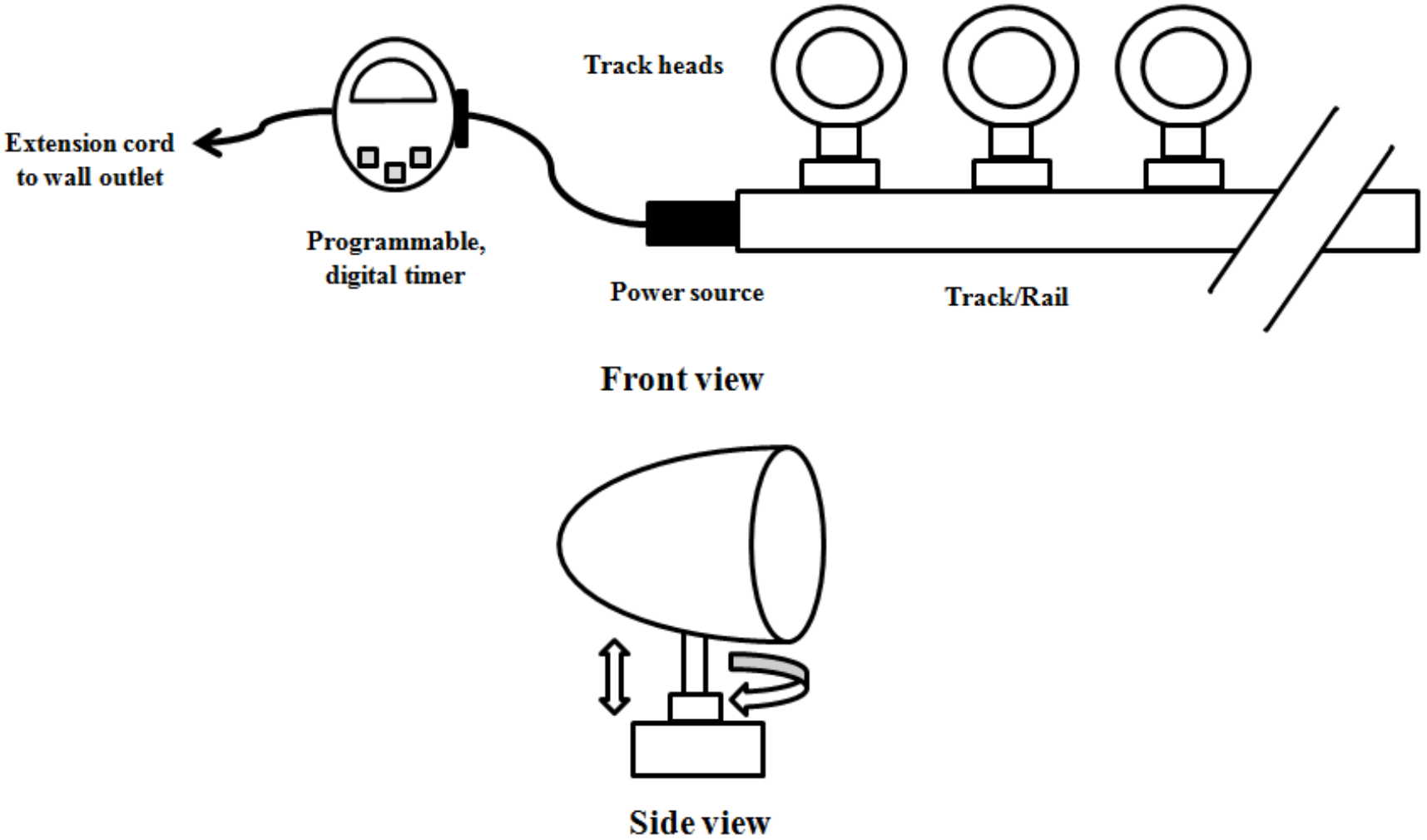

FIGURE 15. Lighting system. Power to track lighting was provided by one power source per rail. Tracks may be of any length and track head number, but were limited by the output of the power source. Day/night cycles of each rail was controlled by a programmable, digital timer. Track heads tilt and twist for optimized illumination.

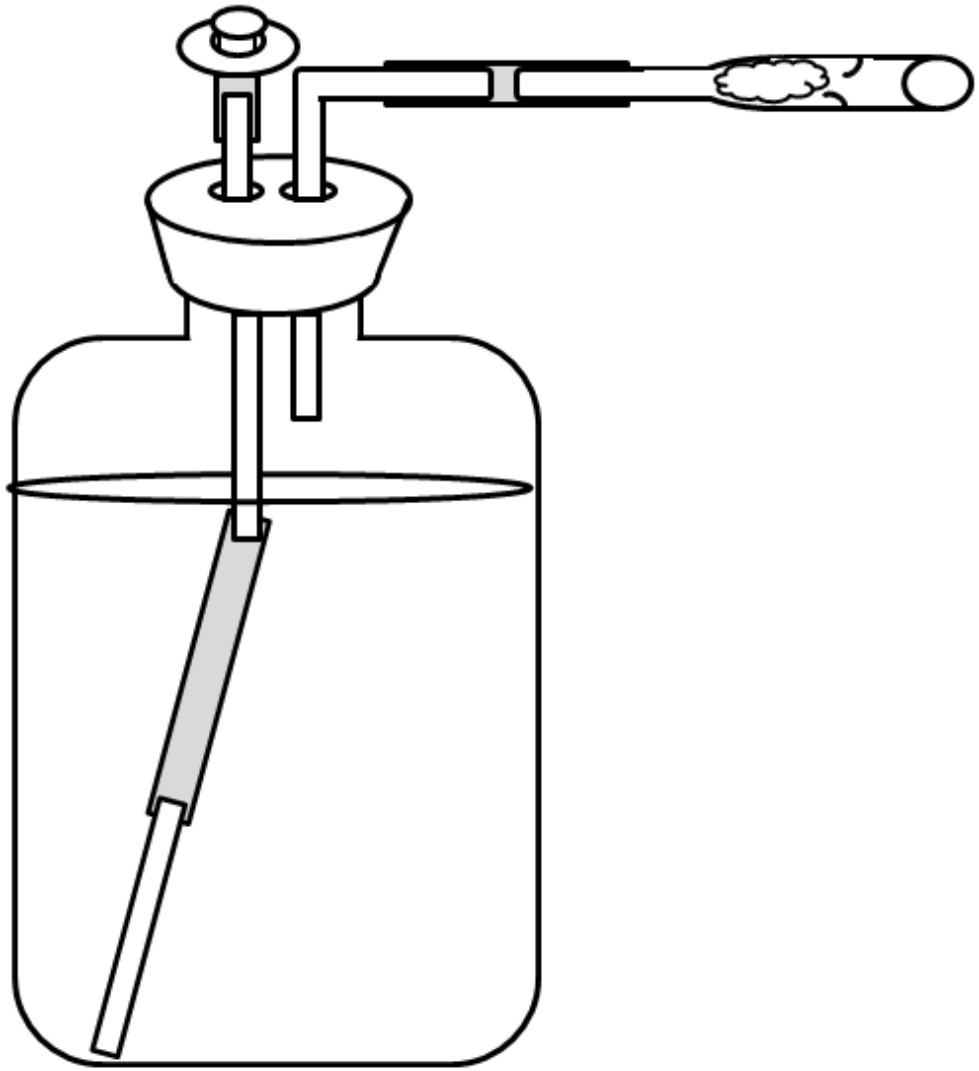

FIGURE 16. Culture flask design. A 1 L Roux flask topped with a silicone cap equipped with gas inlet and exhaust ports. Sterility is maintained by a filter disc on the inlet valve and cotton stuffing in the outlet port. Glass tubing is connected by silicone tubing which allows for flexibility.

that would cap the Roux flask shut. Two small holes are drilled in each cap to allow two pieces of glass tubing—one straight, one bent—to be inserted through the stopper with a snug fit. The straight piece of tubing serves as a gas inlet while the bent piece of glass tubing serves as a gas outlet. Mixed gas is delivered to the inlet via silicone tubing (GE Healthcare Life Sciences, Piscataway, NJ, USA) which is capped with 13 mm, 0.25 µm PTFE filter disc (Pall Corporation, Port Washington, NY, USA). Additional silicone tubing and glass tubing directs mixed gas to the bottom corner of the Roux flask culture for both aeration and mixing. The outlet port meanwhile is connected by silicone tubing to a cotton-stuffed exhaust port created by the Texas A&M Glass Shop. The additional length of the exhaust port and downward opening when in use helps to minimize contamination contact with the cotton plug and condensation, which is greatly reduced when the exhaust port is warmed by the lighting system. For maximum sterility, the three parts of the flask apparatus (flask with media, headpiece, and sterile filter) are autoclaved separately and reassembled in a sterile hood at the time of algae culturing.

Carboy

For occasions when a very large amount of biomass is required a glass carboy may be used. To facilitate such demands, a simple 5-gallon carboy apparatus was designed (Fig. 17). Briefly, lighting is supplied by fluorescent tubes placed on either side of the carboy to ensure irradiance of the total growth volume (14 L). Culture mixing and gas delivery is provided by four spatially-distributed sterilized 25-mL glass pipettes that are attached by vinyl tubing to a 9 L/min, four-way, aquarium air pump

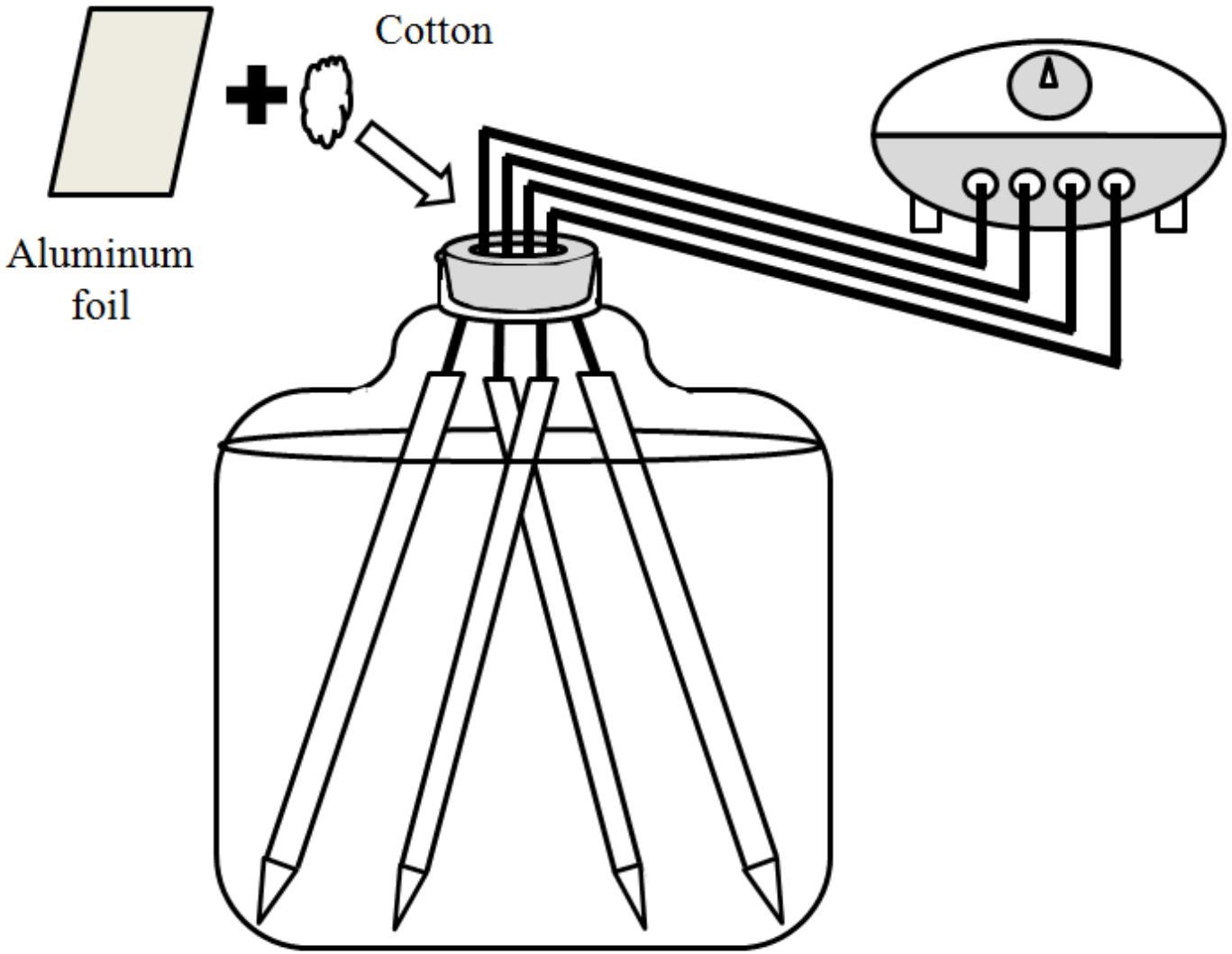

FIGURE 17. Culture carboy design. A four-valve aquarium air pump directed gas into the culture via four glass pipets. The lines passed through a hollowed-out stopper and the remaining gaps stuffed with cotton. Then entire opening was then wrapped in aluminum foil to maintain sterility.

with adjustable flow knob (PETCO, San Diego, CA, USA). The air lines are placed into the carboy through a rubber stopper with a single large hole, fixed with cotton stuffing, and covered in aluminum foil. 13 mm, 0.25 µm PTFE filter discs (Pall) are integrated into each air line and the air pump utilizes an integrated, fabric particulate filter. The carboy filled with media, air line assembly, and sterile filters may be autoclaved separately and assembled at the time of inoculation in a sterile hood. Autoclavable wire loops were also designed as "control arms" to assist pipette placement while maintaining sterility (Fig. 18). This system does not utilize CO_2-enriched air, but could easily be adapted to do so by placing the entire air pump into a CO_2-enriched air chamber similar to those used for solid media growth.

Solid media growth

All algae were routinely grown autotrophically on slant-tube solid media in the illumination of the lighting system. While this method is sufficient for long-term strain storage, without additional CO_2 for growth or moisture to prevent desiccation, the exceptionally slow growth of *B. braunii* made experimentation on solid media virtually impossible. To compensate, growth rates were substantially improved by employing CO_2-enriched 'chambers' that were designed from glass casserole dishes (Fig. 19). Mixed gas is supplied to these chambers via vacuum manifold and polyethylene tubing after bubbling through a 1 L vacuum Erlenmeyer flask filled with ddH_20. Bubbling through this volume of water provides back-pressure that does not disrupt the continuous flow of gas to liquid cultures while also adding a significant amount of evaporated

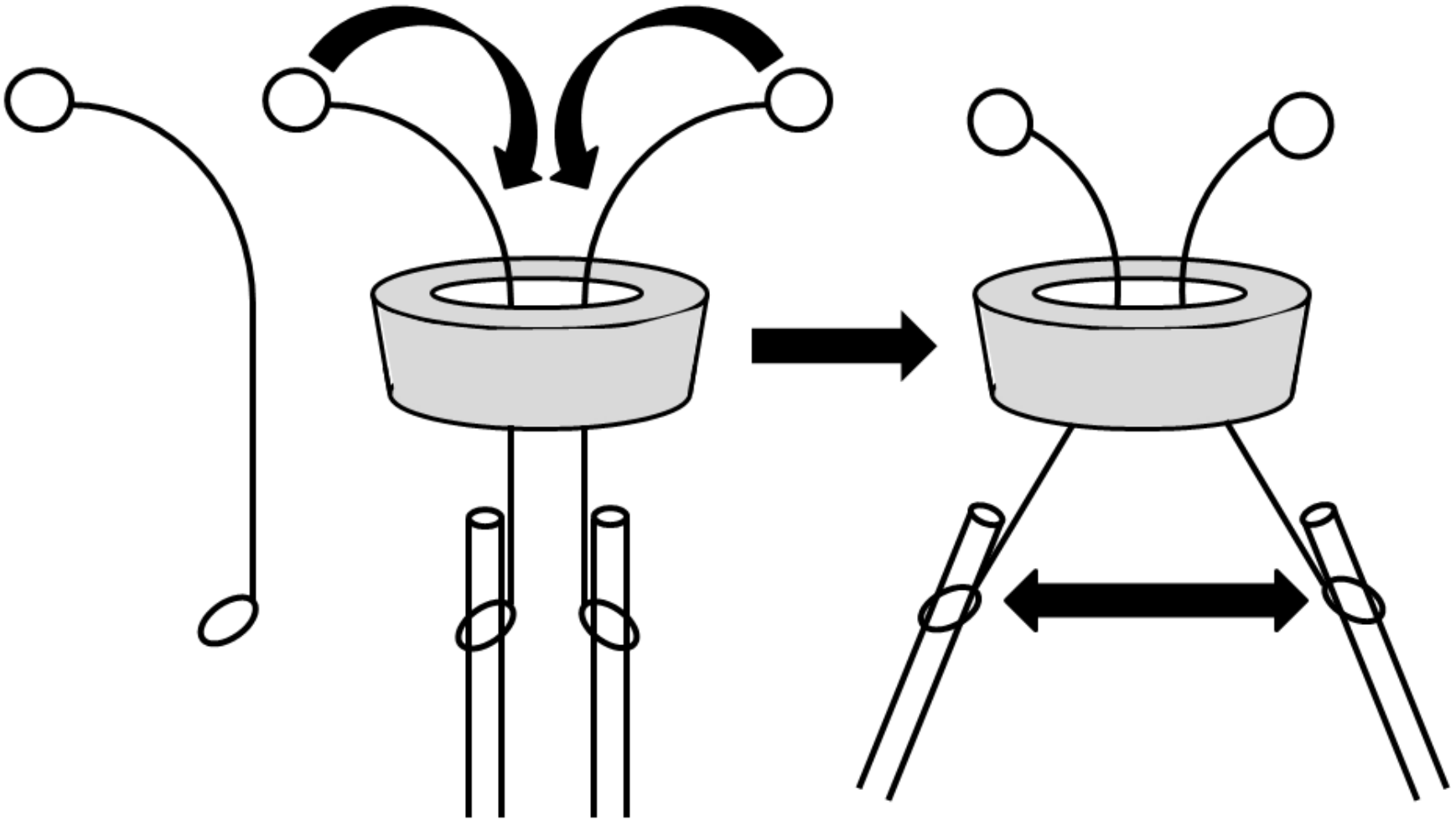

FIGURE 18. Carboy gas-line control arms. "Control arms" of heavy gauge wiring were constructed with a straight and curved length and two loops, one at each end, to fit over the glass pipet inside the carboy and facilitate hand control (left). By manipulating the control arms inward and downward (middle), the glass pipets would be forced apart (right). This allowed for precise gas-line positioning without compromising sterility. In practice, four control arms and gas-lines would be employed.

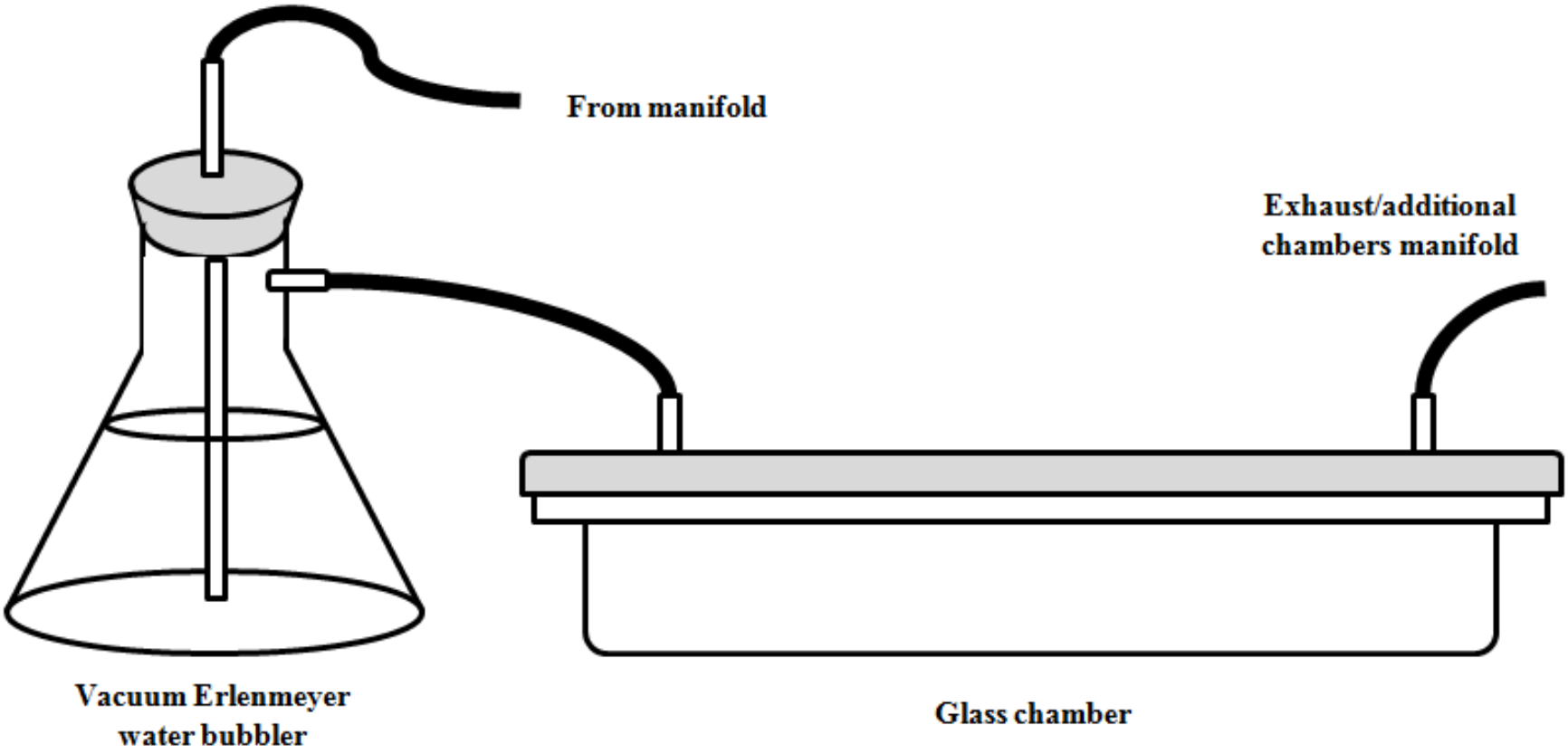

FIGURE 19. Solid media growth chamber. By providing a supply of CO_2, moisture, and attenuated lighting, this air-tight, glass chamber provides all the necessary elements for accelerating extended periods of photosynthetic growth. Lighting was directed through the bottom of the chamber from track light using angled mirrored tiles.

moisture to the gas, reducing solid media desiccation. The dishes are sealed snugly with lids and gas flows into the chambers at a sufficient rate to maintain both a CO_2 enriched atmosphere and positive pressure which helps maintain a semi-sterile environment. Additionally, because direct illumination can be too intense for *B. braunii* grown on solid media, illumination from the lighting apparatus is directed into the chambers using angled mirrors. Using these mirrors, up to 30% of the light intensity generated on a liquid media flask can be redirected onto chambered solid media plates.

Culturing of algae

A pure culture of *B. braunii* Berkeley (Showa), B race (Nonomura 1988) was obtained in the lab of Shigeru Okada, Tokyo University, through a combination of culture dilution with sterilized media and isolation of individual colonies under a microscope, which were transferred to fresh, sterile media for growth. Similar details on the isolation of the Yamanaka strain of *B. braunii*, A race, the Kawaguchi-1 and -2 and the Yayoi strains, B race, have been previously reported (Okada et al. 1995) and samples of these *B. braunii* strains were obtained from the lab of Shigeru Okada. The Songkla Nakarin strain of *B. braunii*, L race (Metzger and Casadevall 1987; Metzger et al. 1990), was obtained from the Algobank-Caen Microalgal Culture Collection, University of Caen Basse-Normandie, France (http://www.unicaen.fr/algobank/accueil/). *B. braunii* cultures were grown in modified Chu 13 media (Grung et al. 1989) using 13 W compact fluorescent 65 K lighting at a distance of 7.62 cm, which produced a light intensity of 280 µmol photons $\cdot$ m^{-2} $\cdot$ s^{-1}. Lighting was a cycle of 12:12 light:dark (L:D) at 22.5 °C.

The cultures were continuously aerated with filter sterilized, enriched air containing 2.5% CO_2 as described above. 50 mL of culture was used to inoculate 750 mL of subsequent subcultures every 4 weeks. The remaining culture volume was harvested by vacuum filtration using 35 µM nylon mesh (Aquatic Ecosystems Inc., Apopka, FL, USA). The accumulated colonies were rinsed with sterilized ddH_2O, frozen in liquid nitrogen, and stored at -80 °C.

Additionally, *Tetraselmis suecica*, although not the focus of these studies, was cultured and occasionally used as a negative control in a variety of experiments. *T. suecica* was obtained from the Culture Collection of Algae at the University of Texas (http://www.sbs.utexas.edu/utex/). *T. suecica* was grown in ASP-2-B_{12} Media (Provasoli et al. 1957), but otherwise using the same methods as *B. braunii* already described.

Cyrogenic storage

To generate an 8% DMSO solution of *B. braunii* culture suitable for cryogenic storage, 4 mL of DMSO was first aliquoted into 50 mL centrifugation tube (VWR, Suwanee, GA, USA) and cooled on ice until frozen. 46 mL of dense algal culture (typically, 20-30 days old) was then added to the frozen DMSO and gently mixed at room temperature until the DMSO is completely mixed and then quickly placed in a -80 °C freezer for storage. To culture cryopreserved algae, aliquots were thawed in a large, 30 °C water bath and then promptly diluted into fresh, sterile media to a final DMSO concentration of not greater than 1% (i.e. >350 mL media per 50 mL cryogenic aliquot).

Gene sequencing

Berkeley strain

18S rRNA

For phylogenetic analysis of the different *B. braunii* strains in an analysis similar to Sawayama et al. (1995), the *B. braunii* Berkeley 18S rRNA gene was amplified by reverse transcription–PCR (RT–PCR) using total RNA. This was carried out by the lab of Shigeru Okada. An algal sample from a pure Berkeley culture was ground in a mortar and pestle chilled with liquid nitrogen, and total RNA isolated by the SDS/LiCl method (López-Gómez and Gómez-Lim 1992; Okada et al. 2000). First-strand cDNA was synthesized from total RNA using Superscript II (Invitrogen, Carlsbad, CA, USA) and random hexamers. The first-strand cDNA was then used as a template to amplify the nuclear 18S rRNA gene by PCR in two overlapping sections using the same combinations of primers used by Sawayama et al. (1995)—primer combination 1, 5′-TACCTGGTTGATCCTGCCAGTAG and 5′-CCAATCCCTAGTCGGCATCGT; and primer combination 2, 5′-AGATACCGTCGTAGTCTCAACCA and 5′-ACCTTGTTACGACTTCTCCTTCCTC. PCR was carried out with 1 unit of KOD plus DNA polymerase (Toyobo Co., Ltd., Osaka, Japan) in the supplied 1×PCR buffer, 1 mM $MgSO_4$, 0.2 mM dNTPs, 0.3 µM of each primer, and 1 µL of first-strand cDNA in a final volume of 50 µL. PCR cycles were as follows: initial incubation at 94 °C for 2 min followed by 30 cycles of 94 °C for 15 s, 61 °C (for primer combination 1) or 59 °C (for primer combination 2) for 30 s, and 68 °C for 2 min. PCR products were isolated from agarose gels using MagExtractor (Toyobo), blunt ligated into the EcoRV site of

pBluescript II KS+ (Stratagene, La Jolla, CA, USA), transformed into Escherichia coli XL-1 Blue MRF′ strain (Stratagene) according to a standard $CaCl_2$ transformation procedure, and sequenced on both strands by the dideoxy-terminator method using a Thermo Sequenase Primer Cycle Sequencing kit (GE Healthcare) in a Shimadzu DQ2000 DNA Sequencer (Shimadzu, Kyoto, Japan). The isolated *B. braunii* Berkeley 18S rDNA sequence was submitted to GenBank, accession number FJ807044.

β-actin

The *B. braunii* Berkeley β-actin cDNA was also isolated by the lab of Shigeru Okada using the PCR techniques as described above with 1 µL of a 1:100 dilution of a *B. braunii* Berkeley cDNA library (Okada et al. 2000) as a template, degenerate primers based on plant actin sequences, and Taq polymerase (Toyobo). Degenerate primer sequences were as follows: forward primer, 5′-ATGACGCARATHATGTTYGAR; reverse primer, 5′-CCACATYTGYTGRAANGT. PCR cycles were as follows: initial incubation at 94 °C for 4 min followed by 30 cycles of 94 °C for 30 s, 43 °C for 30 s, and 72 °C for 1 min, and one final cycle of 72 °C for 7 min. The generated 699 bp PCR product was gel purified, blunt-end cloned, and sequenced as described above for the Berkeley 18S rRNA gene. The resulting *B. braunii* Berkeley β-actin sequence was submitted to GenBank, accession number GU049780.

Additional strains

18S rRNA

The *B. braunii* 18S rRNA genes from B race strains Kawaguchi-1, Kawaguchi-2, and Yayoi and A race strain Yamanaka were isolated by the lab of Shigeru Okada and amplified by polymerase chain reaction (PCR) from genomic DNA that was extracted with Nucleon Phytopure (GE Healthcare UK Ltd.) according to the manufacturers protocol. The genomic DNA was then used as a template to amplify the nuclear 18S rRNA gene by PCR in two overlapping sections again using the same combinations of primers used by Sawayama et al. (1995) described above. PCR was carried out with 1.25 units of Takara EX Taq polymerase (Takara Bio Inc., Japan) in the supplied 1×PCR buffer, 0.4 mM dNTPs, 2 μM of each primer, and 1 μL (10 ng) of genomic DNA in a final volume of 50 μL. PCR cycles were as follows: one cycle with initial incubation at 98 °C for 10 s, annealing at 62 °C for primer combination 1 or 59 °C for primer combination 2 for 1 min, extension at 72 °C for 2 min, followed by 34 cycles of 94 °C for 20 s, 62 °C (for primer combination 1) or 59 °C (for primer combination 2) for 1 min, 72 °C for 2 min, and a final incubation at 72 °C for 5 min. PCR products isolation, ligation, transformation, and sequencing were otherwise identical to those described above. The isolated *B. braunii* 18S rDNA sequences were deposited in GenBank: B race strains Yayoi (accession HM245351), Kawaguchi-1 (accession HM245349), and Kawaguchi-2 (accession HM245350) and A race strain Yamanaka (accession HM245352).

β-actin

The *B. braunii* β-actin genes from A race strain Yamanaka and L race strain Songkla Nakarin were amplified by RT-PCR using total RNA. Each algal sample from a pure culture was ground using a TissueLyser II (Qiagen, Valencia, CA, USA) with liquid nitrogen, and total RNA isolated by TRIzol (Sigma, St. Louis, MO, USA) and polysaccharide contamination removed by LiCl precipitation. First-strand cDNA was synthesized from total RNA using a Phusion RT-PCR Kit (New England Biolabs, Ipswich, MA, USA) and the previously utilized reverse degenerative primer sequence of sequence 5′-CCACATYTGYTGRAANGT. A 50 µL PCR reaction was then performed using 3 µL of the RT solution, Phusion Polymerase, the reverse degenerative primer (5′-CCACATYTGYTGRAANGT), and a forward degenerative primer (5′-ATGACGCARATHATGTTYGAR). PCR cycles were as follows: an initial incubation of 98 °C for 90 s followed by 35 cycles of 98 °C for 30 s, 55 °C for 30 s, and 72 °C for 30 s followed by a final incubation of 72 °C for 10 min. PCR products were isolated from agarose gels using a silica column (Engebrecht et al. 1991) and blunt ligated using a TOPO TA Cloning Kit (Invitrogen) following the manufacturers protocol. The ligation product was then transformed into *E. coli* DH5α strain according to a standard $CaCl_2$ transformation procedure (Seidman et al. 1997), and sequenced on both strands using M13 primers and BigDye Terminator cycle sequencing (Applied Biosystems, Foster City, CA, USA). The isolated *B. braunii* Yamanaka and Songkla Nakarin β-actin sequences were deposited into GenBank and given the accession numbers JN680814 and JN680815, respectively.

Phylogenetic analysis

The 18S rRNA gene sequences used for phylogenetic analysis were those produced here plus 58 obtained from GenBank based on accession numbers given in Senousy et al. (2004). The final 18S rRNA alignment used by Senousy et al. (2004) for phylogenetic analysis was obtained from TreeBASE (http://treebase.org/treebase/) under study #1156. New alignments that included the five newly isolated *B. braunii* strain 18S rRNA cDNA sequences were produced using MEGA 4.1 (Tamura et al. 2007). The β-actin gene sequences used for phylogenetic analysis are those produced here plus the following sequences obtained from GenBank: AB080314.1 (*Trebouxia erici*), AB046453.1 (*Nannochloris* sp. SAG 251-2), AB046457.1 (*Parachlorella kessleri*), AB046451.1 (*Marvania coccoides*), AB292587.1 (*Marvania geminate*), 3107918 (*Nannochloris bacillaris*), AB080313.1 (*Chlorella vulgaris*, actin-2), AB080312.1 (*Chlorella vulgaris*, actin-1), AB292588.1 (*Lobosphaeropsis lobophora*), AB080311.1 (*Chlorella sorokiniana*), AB053215.1 (*Pseudochlorella* sp. CCAP 211 / 1A), 915193 (*Chlamydomonas reinhardtii*), 14719361 (*Dunaliella salina*), 170648 (*Volvox carteri*), 34581635 (*Chlamydomonas moewusii*), AF061018.1 (*Scherffelia dubia*), and 50355608 (*Ulva pertusa*). Organism synonyms reflect current species taxonomies as identified by DNA Data Bank of Japan (DDBJ)/European Molecular Biology Laboratory (EMBL)/GenBank accession numbers at the time of publishing.

Trees were constructed using MEGA 4.1 (Tamura et al. 2007), MrBayes (Hall 2001; Huelsenbeck and Ronquist 2001), and PhyMl 3.0 (Guindon and Gascuel 2003). Trees were drawn with MEGA 4.1 (Tamura et al. 2007) and TreeView (Page 1996).

Data analysis methods included distance (neighbor joining [NJ] and minimum evolution [ME]), maximum parsimony (MP), and likelihood (maximum likelihood [ML] and Bayesian inference [BI]). For rRNA phylogeny, sequences of *Nephroselmis olivacea* and *Pseudoscourfieldia marina* remained the rooted outgroup (Senousy et al. 2004), and for β-actin phylogeny, sequences of *Scherffelia dubia* and *Ulva pertusa* provided the rooted outgroup. All bootstrap analyses were carried out with at least 500 replications each. All methods were applied with the default model of their respective programs, with the exception of ML, which was tested using both the HKY85 and generalized time-reversible (GTR) substitution models. The β-actin phylogeny was additionally assessed using translated amino acid sequences and nucleotide sequences excluding codon third positions. All remaining parameters were the same or equivalent to those found in Senousy et al. (2004). The *B. braunii* Berkeley only rRNA and β-actin alignments were submitted to TreeBASE (study accession no.: S2526; matrix accession no.: M4827, M4828) and rRNA alignments utilizing all five *B. braunii* strain sequences produced here were later submitted separately (study accession no.: S10552). β-actin alignments and trees utilizing Yamanaka and Songkla Nakarin strain sequences have not been submitted nor published at this time.

Genome size estimation

Sample preparation

Genome size was estimated using a procedure modified from Johnston et al. (2004, 2005, 2007). Fifty milligrams of frozen *B. braunii* cells was resuspended in 500

µL of 4 °C cold, freshly prepared Galbraith buffer. This solution was treated with 1 mg of lyticase (Sigma) at room temperature with occasional gentle mixing for at least 20 min. The mixture was then spread across a glass slide, and the aggregated cells thoroughly chopped through with a new razor blade, for at least 5 min. The liquid was collected from the glass slide and was then passed through a 50 µm filter and diluted with Galbraith buffer (Galbraith, D. W. et al. 1983) to 1 mL. This sample was then combined with the head from a female wild type strain of *Drosophila virilis*, which served as a standard (2C = 333.3 Mb; Gregory and Johnston 2008). Clean, isolated protoplasts, nuclei from the alga, and nuclei from the standard were released by grinding the chopped alga plus the *D. virilis* head in Galbraith buffer using 15 strokes of the A pestle in a Kontes 2-mL Dounce homogenizer. A *D. virilis*–only control was similarly prepared. The mixture was passed through a 50 µm filter, stained with 50 ppm propidium iodide (PI; Sigma), incubated for 30 min at 4 °C in the dark.

Flow cytometry

Flow cytometry on isolated nuclei was carried out using two instruments, a Beckman FACScan flow cytometer and a Beckman⁄Coulter Elete flow cytometer (Beckman⁄Coulter, Brea, CA, USA), using identical methods with the laser emitting 25 mW of exciting light at 488 nm. Red fluorescence from PI (intercalated into the DNA of the 2C and 4C nuclei of *D. virilis* and sample) was detected using a high bandpass filter (615 nm). To ensure that scoring included only intact nuclei free from cytoplasmic tags, counting was activated by red fluorescence, and only nuclei with low forward and low

side scatter were included in the analysis. Samples were run to produce a total of at least 1,000 nuclei under each scored peak. DNA content was determined from co-preparations of sample and standard by multiplying the ratio of the mean peak fluorescence of the diploid (2C) sample to the 2C mean fluorescent peak of *D. virilis* times the genome size of the standard (1C = 333.3 Mb for *D. virilis*) (Gregory and Johnston 2008). At least three genome size estimations for each alga were carried out over a 3-week period, and a 1C average and standard error calculated based on the produced genome sizes.

Berkeley strain GC-content estimation

A *B. braunii*, B race Berkeley strain cDNA library was previously created using a ZAP-cDNA Synthesis Kit (Stratagene; Okada et al. 2000). The library was plated, 15 random clones isolated, the contained cDNA sequenced using BigDye Terminator cycle sequencing (Applied Biosystems, Foster City, CA, USA), and gene identity determined using BLAST (Altschul et al. 1990) against the GenBank database. The 15 sequences showed high similarity with known or putative genes of green algae, most notably *Chlamydomonas reinhardtii*. These 15 genes were analyzed using the DNA sequence analysis program Seqool (http://www.biossc.de/seqool/index.html), and the bases were summed (>25 kb total) to obtain a percent GC-content and standard error for the overall GC-content.

Histochemical staining

For visualizing the nuclei of *B. braunii*, 100 µl of *B. braunii* colonies in medium were treated with 1 µl of a 1 mg/ml stock solution of 4',6-diamidino-2-phenylindole (DAPI; Sigma) dissolved in water. The cells were incubated in the dark for at least 10 minutes, but not longer than 30 minutes, prior to visualization. DAPI was also in combination with Nile red for co-staining. In that case, DAPI and Nile red were added at the same time and followed the DAPI staining procedure.

For visualization of the cell wall using Congo red (Sigma), 100 µl of *B. braunii* colonies in medium were treated with 1 µl of a 1 mg/ml stock solution of Congo red dissolved in water. For visualization of botryococcenes using Nile red (Sigma), 400 µl of *B. braunii* colonies in medium were treated with 1 µl of a stock solution of Nile red dissolved in acetone (0.15 mg/ml) so that the final concentrations of Nile red and acetone were 0.375 µg/ml and 0.25%, respectively. Both Congo red and Nile red stained samples were kept in the dark and incubated at room temperature for 15 min. Both samples were also diluted with 1 ml dH_2O, centrifuged at 10,000 x g for 30 sec, and excess solution removed by pipetting under the floating layer of algal colonies. This rinsing process was quickly repeated three times and the final stained algae samples stored in a minimal volume prior to immediate microscopy.

The fibril sheath system was visualized using a modified periodic acid-Schiff reagent (mPAS) using propidium iodide (PI; Sigma) as the Schiff reagent (Moreno et al. 2006). 270 µl of *B. braunii* colonies in medium were treated with 30 µl of a stock solution of 10% PI solution, in the dark at room temperature, for at least 30 min. The

samples were then diluted with 1 ml dH_2O, centrifuged at 10,000 x g for 30 sec, and excess solution removed by pipetting under the floating layer of algal colonies. This rinsing process was repeated three times. The samples were then resuspended in 30 µl of 10 mM, pH 8.0 PBS buffer and 1 µl of a 1 mg/ml PI stock solution added. The samples were then kept in the dark and incubated at room temperature for 20 min before an additional rinsing with dH_2O (three times) and immediate microscopy visualization. Co-staining of *B. braunii* colonies with both Nile red and an mPAS reaction followed the same procedure as an mPAS reaction alone except that 1 µl of Nile red stock solution was added to the sample during the PI incubation.

Microscopy

Microscopy imaging of *B. braunii* colonies was performed at the Texas A&M University Microscopy and Imaging Center. The Olympus FV1000 confocal microscope acquisition was supported by the Office of the Vice President for Research at Texas A&M University.

Fluorescence microscopy visualization was performed using Olympus FV1000 (Olympus America Inc., Center Valley, PA, USA), laser scanning confocal microscope equipped with UPLSAPO 100x/1.4 oil immersion objective. Excitation and emission wavelengths were set for Congo red (Ex. 543 nm, Em. 555-630 nm), mPAS-PI (Ex. 543 nm, Em. 555-620 nm), Nile red (Ex. 488 nm, Em. 540-590 nm) and Nile red + mPAS-PI double staining (Ex. 488, Em. 500-550 and 620-640 nm, sequential acquisition). Chlorophyll autofluorescence (Ex. 405 nm, Em > 650 nm) was recorded in parallel with

the dyes listed above, using line-sequential acquisition. For ratiometric imaging of Nile red staining, two images were acquired in a line-sequential mode (Ex. 488, Em. 500-530 nm), (Ex.543 nm, Em 560-585 nm) and their ratio calculated using the confocal microscope acquisition software FV10-ASW ver. 1.7.

Microscopy in support of Raman microspectroscopy studies was performed with a Zeiss Axiophot microscope equipped with a GFP filter set (excitation, 450–490 nm; emission, 500–550 nm), Plan Neofluar 100 x /1.3 oil immersion objective, and a Coolsnap CF monochrome CCD camera (Photometrics, Tucson, AZ, USA) controlled by MetaView version 5.2 software (Molecular Devices, Downingtown, PA, USA). For transmitted light imaging, differential interference contrast optics and a Nikon DXM1200C (Nikon Instruments, Melville, NY) color CCD camera were used on the same microscope.

Shell preparation

Five liters of a 4-week-old *B. braunii* culture was left undisturbed for 12 hrs allowing a majority of colonies to float and residual material to settle. This residual material was then harvested by vacuum suction with care to minimize disruption of the floating algae layer. The harvested material was then vacuum filtered though a 35 μm nylon cloth (Aquatic Eco-Systems, Inc.) to remove residual, large algal colonies. The filtrate was then centrifuged at 17,000 × g for 30 minutes to pellet the shells, bacteria, and any remaining algal colonies in solution. The supernatant was then carefully disposed of by vacuum suction while the soft, top layer of shells were gently

resuspended and transferred into fresh centrifugation tubes leaving behind a hard, bottom pellet of bacteria and algal colonies. The resuspended shells were then diluted with ddH_2O, centrifuged at 48,000 × g for 15 min, and again pelleted for isolation. This process of centrifugation, shell isolation, and dH_20 rinsing was repeated at least 4 times until there was no obvious pellet of bacteria after centrifugation. The shell fraction was then freeze-dried and analyzed by EM and gas chromatography-mass spectrometry (GC-MS).

Carbohydrate gas chromatography/mass spectrometry

All carbohydrate mass spectrometry analysis was carried out by Ian Black and Parastoo Azadi at the University of Georgia and was supported in part by the Department of Energy-funded (DE-FG02-93ER-20097) Center for Plant and Microbial Complex Carbohydrates, which is also known as the Complex Carbohydrate Research Center (CCRC).

For glycosyl composition analysis, the samples were analyzed by the alditol acetate derivatization method where the sample was depolymerized, reduced, and acetylated. The resultant alditol acetates (AAs) were analyzed by gas chromatography-mass spectrometry (GC-MS) for determination of monosaccharide identity. Specifically, 200mg of isolated shells was hydrolyzed using 2 M trifluoroacetic acid for 2 hrs in a sealed tube at 121 °C, reduced with $NaBD_4$, and acetylated using acetic anhydride/trifluoroacetic acid.

For glycosyl linkage analysis, the samples were permethylated, depolymerized, reduced, and acetylated; and the resultant partially methylated alditol acetates (PMAAs) analyzed by GC-MS as previously described by York et al. (1986). Initially, around 1 mg of the sample was suspended in 200 μL of dimethyl sulfide and the sample was left to stir for three days. The sample was then permethylated by treatment with sodium hydroxide and methyl iodide in dry DMSO (Ciucanu and Kerek 1984). The sample was subjected to the NaOH base for 15 min and then methyl iodide was added and left for 45 min. The base was then added for 15 min and finally more methyl iodide was added for 45 min. This addition of more methyl iodide and NaOH base was to insure complete methylation of the polymer. Following sample workup, the permethylated material was hydrolyzed using 2 M trifluoroacetic acid for 2 hrs in a sealed tube at 121 ˚C, reduced with $NaBD_4$, and acetylated using acetic anhydride/trifluoroacetic acid.

Both the resulting AAs and PMAAs were analyzed on an Agilent 7890A gas chromatograph (GC) interfaced to a 5975 mass selective detector (MSD) operating in the electron impact (EI) ionization mode. Separation of the AAs and PMAAS by GC was performed on a 30 m Supelco 2330 bonded phase fused silica capillary column.

Purification and identification of botryococcenes

Botryococcenes were purified from freeze-dried *B. braunii* samples as described previously (Okada et al. 1995, 1997). In brief, 10 g of freeze-dried *B. braunii* cells was extracted in *n*-hexane to remove extracellular hydrocarbons followed by a chloroform:methanol (2:1) extraction to remove intracellular hydrocarbons. Both

extracts were evaporated to dryness using a rotary evaporator, resuspended in *n*-hexane, combined, applied to an *n*-hexane gravity fed Silica Gel 60 (EMD Millipore Corporation, Billerica, MA, USA) column, and a total hydrocarbon fraction was collected as the eluate prior to the pigment front. The total hydrocarbon fraction was evaporated to dryness, resuspended in 0.5 volume of acetone, and separated by HPLC using a 20×250-mm Cosomil 5C18-AR-II column (Nacalai) with 100% MeOH mobile phase at a flow rate of 9 ml/min, detection at 210 nm. Botryococcenes eluted as follows: C_{30} botryococcene (27 min), C_{32} and C_{33} in one peak (30 min). To separate impurities from C_{30} botryococcene and to separate C_{32} and C_{33} botryococcenes, samples were applied sequentially to a 20 × 250-mm Develosil 60 silica, 3-µm HPLC column (Phenomenex, Torrance, CA, USA) with 100% *n*-hexane mobile phase at a flow rate of 8 ml/min, detection at 210 nm. Botryococcenes eluted as follows: C_{30} botryococcene (32 min), C_{32} (27 min), and C_{33} (25 min). Purity of the isolated botryococcenes was analyzed with a Shimadzu GC-2014 with a 60-m DB-1 column (J &W Science, Folsom, CA, USA), 0.25-mm inner diameter, 0.25-µm film, helium carrier gas, 250-kPa head pressure, 250 °C injection temperature, FID detector at 260 °C, and a temperature program of 50 °C for 1 min, raised to 220 °C at 10 °C/min, raised to 260 °C at 2 °C/min, hold at 260 °C for 40 min. Botryococcenes showed retention times as follows: C_{30} botryococcene (42 min), C_{32} (46 min), and C_{33} (48 min). A C_{34} botryococcene was obtained from a previous analysis (Okada et al. 1997). The molecular mass of all purified botryococcenes was confirmed by fast atom bombardment-mass spectroscopy using m-nitrobenzyl alcohol as a matrix on a JEOL SX102 mass spectrometer, and their

plane structures were confirmed by measuring ^{1}H and ^{13}C NMR spectra in $CDCl_3$ using a JEOL alpha 600 NMR spectrometer at 600 MHz and 150 MHz, respectively. The NMR data were compared with those for known botryococcenes (Okada et al. 1995; Sato et al. 2003).

Raman spectroscopy

Raman spectra of squalene (Sigma), total hydrocarbon extract, and purified botryococcenes (all in *n*-hexane in a cuvette) were obtained at Horiba Scientific (Edison, NJ, USA) using a Horiba LabRam HR 800 confocal Raman microscope. The Raman spectrometer was coupled with an Olympus BXFM microscope and a liquid nitrogen-cooled CCD detector. The excitation source was a Melles-Griot laser operating at 532 nm with a 50-mW output. A singlet lens with a focal length of 40 mm was used. Raman spectra of squalene and total hydrocarbon extract contained in vials without solvent were also recorded by Hye Jin Chun in the laboratory of Jaan Lanne, Texas A&M University, using a Jobin Yvon U-1000 double monochromator equipped with a liquid nitrogen-cooled CCD detector. A Coherent Verdi-V10 laser operating at 532 nm was utilized as the excitation source. A laser power of 2 W was typically used.

In vivo mapping by confocal Raman spectroscopy was performed at the Texas A&M Materials Characterization Facility using a Horiba Jobin Yvon LabRam IR system with an Olympus BX 41 microscope, a computer-controlled motorized XYZ microscope stage, and a liquid nitrogen-cooled CCD detector. Algae samples were applied to glass slides and trapped under glass cover slips. Excitation was achieved with a laser

wavelength of 785 nm at an output power of 20 mW. The spectral maps were recorded with a spectral resolution of 0.16 cm^{-1} and pixel size of 275 nm with an UPLSAPO 100×/1.4 oil immersion objective. Cell photobleaching was performed using a 785-nm laser at a power output of 500 mW for at least 20 minutes. Exact treatment times varied as colony cell density varied across the z-axis. Photobleaching was considered complete once the high, consistent Raman intensities across 200–3600 cm^{-1} sufficiently decreased to allow detection of individual Raman peaks and remained static for at least 2 min. All Raman spectra were collected in 60-cm^{-1} segments with accumulation times of 1000 s for each segment. Spectra were analyzed for peak wavenumbers using the LabSpec program version 5.58.25.

B. braunii, B race, Berkeley strain colonies were also trapped for Raman spectroscopy within microfluidic plates designed by Hyun Soo Kim in the laboratory of Arum Han. Briefly, the microfluidic plate was composed of polydimethylsiloxane (PDMS) and a culture sample was loaded into capture wells by syringe injection. The dimensions of the device were too large to fit the available Raman instrument properly at the time and so mapping could not be conducted, but a basic Raman spectrum could be obtained with the objective lens pressed slightly into the flexible material. These data were obtained at the Shell Oil Company Westhollow Technology Center (Houston, TX, USA) using a Horiba LabRam Aramis confocal Raman microscope. Excitation was achieved with lasers of varying wavelengths, but a 458-nm laser was primarily used at an output power of 5 mW. Operating at this wavelength the colonies were not bleached

prior to Raman spectroscopy data collection. All other specifications and methods were otherwise identical or equivalent to the previously describe LabRam IR system.

Density function theory calculations

Density function theory (DFT) calculations were conducted by Hye Jin Chun in the laboratory of Jaan Lanne, Texas A&M University, as part of a collaborative effort (Weiss et al. 2010). DFT computations used the GAUSSIAN 03 package (Frisch et al. 2004) to obtain the calculated vibrational frequencies and produce the computed Raman spectra. The B3LYP/cc-pvtz basis set was utilized. A scaling factor of 0.969 was applied for all frequencies. This value was selected to match the observed and calculated v(C=C) stretching frequencies for squalene. The computed spectra were produced using the GaussView 4.1.2 program.

Biomass/hydrocarbon analysis

Gravimetric biomass and hydrocarbon analysis requires three important considerations: one, all drying and extraction steps must be thorough and complete; two, mass measurements should be conducted on the smallest filters and flasks available to minimize instrument error; and three, all equipment must be thoroughly cleaned and nitrile gloves worn at all times to avoid human skin oils from accidently contributing to and contaminating hydrocarbon extracts.

To measure dry weight culture biomass gravimetrically, dry glass microfiber GF/C filters (Whatman, Kent, United Kingdom) were pre-weighed, the masses recorded,

and then gently rolled into a new 50 mL centrifugation tube (VWR) for storage. When algae cultures were prepared for harvesting, the growth flasks were gently, but well shaken to homogenize the culture volume, and 20 mL of culture removed by glass pipette. This 20 mL volume was then carefully pipetted onto the pre-weighed filters, under vacuum, across a minimal area of the filter. (Minimal wetted filter area speeds drying in addition to simplifying extraction steps.) The harvested sample was washed and any algae left sticking to the pipette harvested with at least 3×20 mL pipetted volumes of ddH_2O. Vacuum was additionally applied to the sample for at least 2 minutes afterwards to remove any excess water prior to the filter paper being gently rolled back into a 50 mL centrifugation tube (VWR) for storage and overnight lyophilization employing perforated tube caps. The dried filters containing the algae sample were then carefully weighed again and the masses recorded. The dry weight mass of algae alone was calculated by subtracting the previously recorded filter dry weights. Knowing the volume of the culture sample (20 mL) and total culture volume also allows for a total algae dry weight per volume media (g/L) to be calculated. The lyophilized samples should be stored air-sealed in a cool, dry, dark place.

To measure total hydrocarbons gravimetrically, the area of filter containing dried algae was carefully cut out with a clean pair of scissors, further shredded into small pieces, and deposited into a 50 mL glass centrifuge tube. Extraction was accomplished by adding 10 mL of acetone by glass pipette and sonicating the sample at 4 °C and at maximum power for 5 minutes until the filter is completed disrupted. The sonicated sample was then centrifuged for 10 min at 1000×g and the resulting yellow solution

pipetted into a clean round-bottom flask. Further solution can be released and collected by compressing the residual glass fibers with a glass stirring rod, but collection of any fibers should be minimized. This process of extraction was repeated until no additional color was derived by extraction, generally after 3-5 repeats. The total volume of acetone extract was then evaporated to dryness and the residual oils resuspended in a minimal volume of *n*-hexane.

Extracted hydrocarbons were then applied to a gravity fed, *n*-hexane equilibrate 1 cm × 5 cm Silica Gel 60 (EMD) column. An elution volume of 20 mL was initially collected and evaporated to dryness in a small, clean, pre-weighed round bottom flask. This flask was then weighed and the mass recorded. An additional 10 mL of elution volume was then added and to the round-bottom flask which was again evaporated to dryness and weighed again. This process was repeated until no additional hydrocarbon mass was accumulated. A well-packed and equilibrated column typically eluted all hydrocarbons within 20-30 mL of *n*-hexane while the initial pigmented front did not elute until at least 50 mL of volume. The final sample was further evaporated to dryness using a vacuum chamber with repeated vacuums applied and released over 20 min intervals. When completely dry, the total hydrocarbon sample should have no solvent smell and the oils will bead-up on the surface of the flask. This completely dried flask containing the total hydrocarbon sample was finally weighed one last time and the mass of the empty flask subtracted from the overall mass. This mass can again be converted into total hydrocarbons per media volume (g/L). The sample can be reserved for further

analysis by resuspending in a minimal volume of *n*-hexane and stored in a cool, dry, dark place.

TLC analysis

Thin layer chromatography (TLC) was used to visualize extracted crude botryococcene hydrocarbon compositions prior to more rigorous gas chromatography or NMR analysis. Standard TLC methods were followed using both normal and reverse phase analysis. Specifically, using an 8 in. × 8 in. C18 reverse phase TLC plate (Whatman) and a 100% acetonitrile mobile phase generated squalene and botryococcene R_f values ranging from 0.07 to 0.11. An 8 in. x 8 in. silica normal phase TLC plate (Whatman) and a 100% *n*-hexane mobile phase generated squalene and botryococcene Rf values ranging from 0.14 to 0.31. Both types of plates were visualized by iodine vapor staining for up to 20 min.

Triterpene synthase computational analysis

Triterpene sequence alignments were performed using ClustalW2. Protein structure homology modeling was performed using SWISS-MODEL software. Both programs were accessed using the ExPASy Bioinformatics Resource Portal (http://www.expasy.org). All amino acid sequences were obtained from GenBank and the structure of the human squalene synthase was obtained from the Protein Databank (accession # 1EZF).

SSL-1

Expression

The SSL-1 gene cloned into pET28a (Kan^r) using BamH1 and Xho1 restriction sites by Tom Niehaus in the laboratory of Joe Chappell, University of Kentucky. In collaboration, we obtained this vector and expressed SSL-1 as a fusion protein with a non-cleavable, N-terminal 6xHis-tag in Rosetta2(DE3)pLysS *E. coli* cells. Protein expression followed typical protocols, but additional steps were necessary to overcome poor over-expression and prevent significant C-terminal protease degradation. Specifically, the *E. coli* cells were grown at 37 °C until an OD_{600} = 0.5 and immediately placed in an ice bath for 10 minutes. The cultures were then grown at 20 °C for at least 1 hour or until cells reached an OD_{600} = 0.8 before induction using 0.1 mM IPTG. The cultures were grown for an additional 6-8 hours before being refrigerated at 4 °C while awaiting centrifugation at the same temperature at 17,000 x g. Harvested cells were immediately stored at -80 °C.

Purification

SSl-1 was purified by first resuspending harvested cells from every 1 L of culture in 80 mL of ice cold lysate buffer composed of 20 mM MOPS (pH 6.5), 500 mM NaCl, 25 mM imidazole, and 1 mM PMSF. The suspension was then kept on ice and sonicated in a glass container over 40 min(15 s pulse, 45 s rest) at 60% power. The lysate was then centrifuged at 10,000×g for 10 min in a pre-chilled centrifuge and supernatant collected. The supernatant was then loaded onto a HisTrap HP 5 ml column (GE

Healthcare), which had been stripped of Ni^{+2} and instead bound with Co^{+2}. All chromatography was carried out at 4 °C using similarly chilled buffers. Once loaded, the column was washed with at least 10 column volumes of lysis buffer (without PMSF) and 10 column volumes of wash buffer containing 20 mM MOPS (pH 6.5), 500 mM NaCl, 75 mM imidazole. Purified SSL-1 was eluted using 250 mM imidazole and immediately dialyzed at 4 °C. Dialysis used SnakeSkin pleated dialysis tubing (Thermo Scientific, Waltham, MA, USA) and two buffers. The first buffer contained 20 mM MOPS (pH 6.5) and 500 mM NaCl only while the second buffer additionally contained at least 20% glycerol. Purified SSL-1 samples were both concentrated and stored at 4 °C. All expressed protein preparations were observed using sodium dodecyl sulfate polyacrylamide gel electrophoresis (SDS-PAGE).

Stability screening

Final purification conditions were determined using the same basic process as above, but conditions that promoted greater SSL-1 stability and solubility were modified and improved over time. Key to this improvement was a method of stability screening which tested SSL-1 stability as a function of solubility. In brief, SSL-1 was collected from His-tag purification and concentrated to a blank-subtracted Abs_{280} = 1.0, equivalent to ~1.2 mg/mL. 20 µL of concentrated SSL-1 protein was then diluted with 20 µL of lysis buffer (without PMSF) to provide an unaltered control. Experimental samples were prepared by adding 20 µL of concentrated SSL-1 protein to 20 µL of test buffer for a final Abs_{280} = 0.5, equivalent to ~0.6 mg/mL. Each test sample was matched with its

only blank reaction mixture of 20 µL of lysis buffer (without PMSF) and 20 µL of test buffer. Experimental buffers varied by pH, buffering agent, salts, and stabilizing agent. All samples were stored for 24 hour periods before centrifugation at 20,000 × g. 2 µL of sample or control reaction was then removed for spectroscopy and the Abs_{280} recorded. Temperature stability was further tested using control reactions stored at different temperatures.

Because of the high amount of protein used in each sample, a visual observation of pellet formation after centrifugation was useful in confirming spectroscopy results. These observations were further substantiated for select samples of interest SDS-PAGE loaded with 5 µL volumes of centrifuged supernatant sample representing soluble protein. SDS-PAGE analysis confirmed the relative quantities of soluble protein to be similar to stability predictions based on spectroscopy, except for some buffers with high absorbency at 280 nm, like AMPSO. An observed and potential bias of this method was the tendency of SSL-1 to form a layer at the air-solution interface in a variety of samples. This interface, possibly a monolayer of protein and not truly soluble protein, could be easily observed by the formation of a notable meniscus during pipette.

Crystallization

Small, irregular crystals of SSL-1, unsuitable for crystallographic structural determination, were generated across a number of closely related conditions using the hanging drop vapor diffusion method. These conditions typically utilized purified protein at 2-8 mg/mL and half-strength well solution equilibrated over wells containing

20 mM MES (pH 6.0-6.5), 10-24% PEG 4000, and 0.2 M ammonium acetate. Additional inhibitors, such as squalestatin, or potential ligands, such as NADPH, were first mixed with the protein sample at a 1:1 molar ratio or greater.

A race NMR

Cultures of *B. braunii,* A race, Yamanaka strain were grown in the dark with gentle air-bubbled mixing by an aquarium air pump (PETCO). Heterotrophic growth and partial hydrocarbon isotopic labeling was supported by the addition of either 40 mM glucose (15% ^{13}C glucose) or 10 mM acetate (30% ^{13}C acetate). Colonies were then collected and the lipophilic crude extracted and purified using the same method previously described for the purification of total botryococcenes. The purified extract was dissolved to a final concentration of 50% in $CDCl_3$ for NMR measurements. ^{13}C NMR spectra were measured by Giridhar Sekar in the lab of Christian Hilty, Texas A&M University, using a 400 MHz NMR spectrometer fitted with a BBO probe (Bruker, Billerica, MA, USA) at 298 K using 1024 scans (51200 complex points, spectral width of 251 ppm). WALTZ-16 decoupling was applied on the ^{1}H channel at field strength of 18 kHz. Mass spectrometry analysis of the samples was carried out through submission to the Texas A&M University Laboratory for Biological Mass Spectrometry (LBMS).

Antibiotics

The following antibiotics were applied singly or in combination to *B. braunii* grown under normal conditions in liquid media and on solid media: ampicillin (75 ng/mL), carbenicillin (75 ng/mL), kanamycin (100 ng/mL), spectinomycin (50 ng/mL), and chloramphenicol (25 ng/mL). Also utilized singly or in combination were Timentin (ticarcillin [120 ng/mL] and clavulanate [7.5 ng/mL]), rifampin (20 ng/mL), and nystatin (500 ng/mL). Each growth was visually compared to a control to observe effects upon algae growth. Conversely, to observe the effects of bacteria and/or fungi contaminating algae cultures, small volumes of *B. braunii* culture (≤1 mL) were applied to LB plates containing the antibiotics. Antibiotic concentrations remained unchanged, but duplicate LB plates of each sample were grown at room temperature under benchtop illumination and at 37 °C in the dark. LB plate growth was visually assessed.

CHAPTER III

PHYLOGENETICS AND GENOME SIZE ANALYSIS OF B. BRAUNII*

Introduction

Our studies of *B. braunii* phylogenetics were carried out with two primary, short-term goals: first, to clarify the phylogenetic placement of the Berkeley strain in relation to other algae using sequencing; and second, to further interrogate representative strains from each of the *B. braunii* races in an effort to better understand the relationship of each race to the others. Pursuing each goal would also provide basic genetic information in support of several ongoing *B. braunii* genome, transcriptome, and proteome sequencing projects in which we participated. Remarkably, of the estimated 200,000 algae species worldwide (Chapman 2005), only nine species have had their genomes fully sequenced and annotated (Matsuzaki et al. 2004; Bowler et al. 2008; Misumi et al. 2008; Worden et al. 2009; Blanc et al. 2010). As a beginning step in obtaining the *B. braunii* genome sequence, we determined the genome size and GC content estimate of the Berkeley strain of *B. braunii* race B. We also confirmed the phylogenetic placement of the

---

*Portions of the following articles have been reprinted with permission from: (1) Weiss, T. L., Johnston, J. S., Fujisawa, K., Sumimoto, K., Okada, S., Chappell, J., and Devarenne, T. P. 2010b. Phylogenetic placement, genome size, and GC content of the liquid-hydrocarbon-producing green microalga *Botryococcus braunii* strain Berkeley (Showa) (Chlorophyta). *J. Phycol.* 46:534–540. Copyright 2010 © by Phycological Society of America (2) Weiss, T. L., Johnston, J. S., Fujisawa, K., Okada, S., and Devarenne, T. P. 2011. Genome size and phylogenetic analysis of the A and L races of *Botryococcus braunii. J. Appl. Phycol.* 23:833–839. Copyright 2010 © by Springer Science+Business Media B.V.

Berkeley strain in the class Trebouxiophyceae with other *B. braunii*. We additionally determined *B. braunii* race genome sizes.

With the onset of genome sequencing projects, genome sizes of organisms have become an increasingly important biological parameter to define. They are also beneficial to almost all levels of biological sciences including evolution, ecology, phylogenetics, and molecular biology (Bennett et al. 2000; Bennett and Leitch 2005; Doležel and Bartos 2005). While a large number of genome size estimates are now available for photosynthetic organisms (~6,000 reported genome sizes, http://data.kew.org/cvalues/; Bennett and Leitch 2005), of the estimated 200,000 algae species (Chapman 2005), only about 300 algae have had genome sizes determined (Kapraun 2005, 2007). Over half of these are green algae. Determination of genome sizes and phylogenetic relationships for more green algae will help to lay the foundation for understanding cellular processes of these organisms at the molecular level, which is sorely lacking.

B. braunii phylogenetics

B. braunii, B Race Berkeley phylogenetic controversy

Some disagreement exists about the phylogenetic placement of the Berkeley strain of *B. braunii*. Cell morphology was the original standard used to establish *B. braunii* taxonomy (Komárek and Marvan 1992). Subsequent studies have been based on molecular phylogenetics using nuclear small subunit (SSU; 18S) rRNA genes (Sawayama et al. 1995, Senousy et al. 2004). The first molecular phylogenetic studies

placed the Berkeley strain of *B. braunii* race B within the class Chlorophyceae (Sawayama et al. 1995). However, a follow-up study using the 18S rRNA gene sequences from one B race (Ayamé strain), two A races (CCAP 807 ⁄ 1 and Titicaca strains), and one L race (Songkla Nakarin strain) of *B. braunii* placed these races in the class Trebouxiophyceae (Senousy et al. 2004). This study by Senousy et al. (2004) included the original Berkeley strain 18S rRNA gene sequence from Sawayama et al. (1995) and left the Berkeley strain in the Chlorophyceae (Senousy et al. 2004). This placement of the Berkeley strain in the Chlorophyceae is possibly an artifact, since the original 18S rRNA gene isolated (Sawayama et al. 1995) was likely amplified from a contaminating alga belonging to the Chlorophyceae (Senousy et al. 2004).

Phylogenetic placement of *B. braunii*, B Race Berkeley

Based on the DNA sequences of rRNAs (rDNA sequence), previous studies have shown that the Berkeley strain of the B race of *B. braunii* is phylogenetically distinct from the other *B. braunii* (Sawayama et al. 1995, Senousy et al. 2004). However, it had been suggested that the 18S rDNA sequence used for this analysis was isolated from an alga other than *B. braunii* Berkeley that was a contaminant in the culture (Senousy et al. 2004). Thus, we generated a monoculture of the Berkeley strain of *B. braunii* and used RT–PCR to isolate an 18S rDNA sequence from *B. braunii* Berkeley. DNA alignments indicate that the newly isolated Berkeley 18S rDNA sequence (accession FJ807044) is distinct from the original Berkeley 18S rDNA sequence (accession X78276; Sawayama et al. 1995; Fig. 20). This result supports the suggestion that the original Berkeley 18S

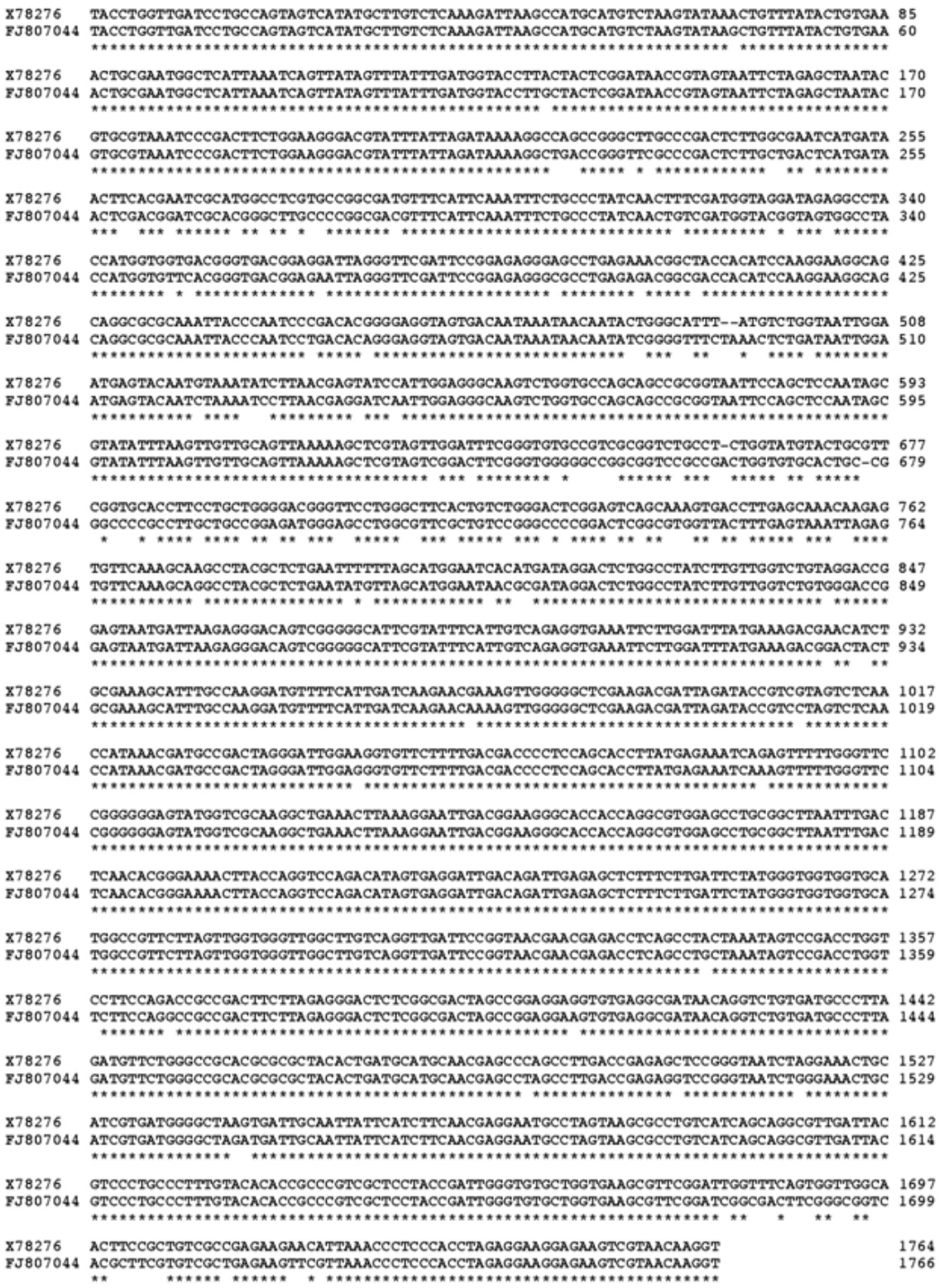

FIGURE 20. Alignment of Berkeley 18S rDNA. Sequences from the original *B. braunii*, Berkeley report (Sawayama et al. 1995) and the *B. braunii*, Berkeley sequence reported here. Sequences were aligned using ClustalW. Accession numbers: original Berkeley sequence: X78276; Berkeley sequence reported here: FJ807044. (Weiss et al. 2010b)

rDNA sequence was from a contaminating algal species, probably from the *Dunaliella* clade in the Chlamydomonadales (Sawayama et al. 1995).

To further support that our newly isolated *B. braunii* Berkeley 18S rDNA sequence does indeed originate from a *B. braunii* strain, we performed a phylogenetic analysis similar to that of Senousy et al. (2004) using neighbor-joining (NJ), minimum-evolution (ME), maximum likelihood (ML), Bayesian inference (BI), and maximum parsimony (MP) methods. All five methods gave nearly identical results overall (data not shown). The phylogenetic tree based on the ML method is shown in Figure 21 with bootstrap values from ML, BI, and MP shown. This analysis shows that the original Berkeley 18S rDNA sequence (accession X78276) clusters within the *Dunaliella* clade of the class Chlorophyceae as was reported earlier (Fig. 21; Senousy et al. 2004). Our new Berkeley 18S rDNA sequence (accession FJ807044) was placed in a cluster with the other *B. braunii* 18S rDNA sequences forming a monophyletic group within the class Trebouxiophyceae (Fig. 21). As reported previously (Senousy et al. 2004), *B. braunii* forms two lineages within this group—one containing the A race, and one containing the B and L races (Fig. 21). This coincides with the nature of the hydrocarbons produced by these races (Senousy et al. 2004). The A race produces fatty acid–derived hydrocarbons, while the B and L races produce isoprenoid-based hydrocarbons (Banerjee et al. 2002, Metzger and Largeau 2005). Importantly, our new *B. braunii* Berkeley 18S rDNA sequence forms a lineage with the B race, Ayamé strain, separate from that of the L race, Songkla Nakarin strain, which was not given in the previous analysis (Fig. 21; Senousy et al. 2004).

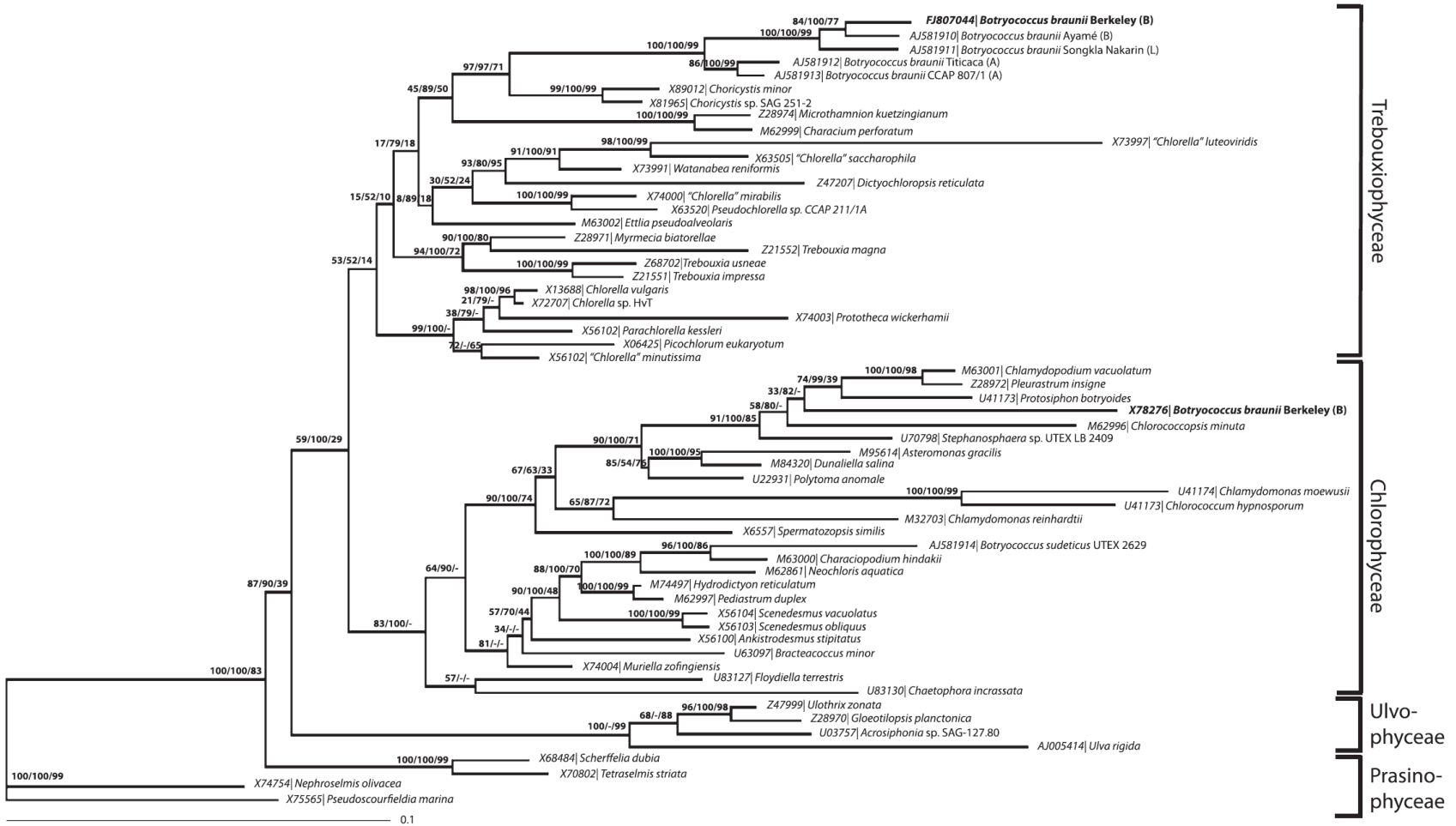

FIGURE 21. Maximum-likelihood (ML) phylogenetic tree of 18S rRNA sequences. Sequences are identified by their corresponding GenBank, DNA Data Bank of Japan (DDJB), or European Molecular Biology Laboratory (EMBL) accession numbers and organism name. Branching credibility percentages from the ML method (left), Bayesian inference (middle), and bootstrap maximum parsimony (right) are listed. Where differential branching from the ML method occurs, confidence values for the dissenting method are represented by a dash. The scale bar is for 0.1 substitutions per site. The foci of this figure, *Botryococcus braunii* Berkeley (FJ807044 and X78276), are shown in bold. (Weiss et al. 2010b)

Phylogenetic placement of the *B. braunii* races

In order to widen the view of the phylogenetic relationships between the different races and strains of *B. braunii*, we further isolated the 18S rDNA sequences from three additional strains of the B race (Yayoi, Kawaguchi-1, and Kawaguchi-2; Okada et al. 1995) and one strain of the A race (Yamanaka; Okada et al. 1995). Initially, the new *B. braunii* 18S rDNA sequences were analyzed in comparison to the 24 chlorophycean and 26 trebouxiophycean species in Weiss et al. (2010) and showed that these new *B. braunii* sequences are placed in the class Trebouxiophyceae (not shown). This is in agreement with previous studies that show all races of *B. braunii* belong to Trebouxiophyceae (Senousy et al. 2004; Weiss et al. 2010). Next, we focused the phylogenetic analysis on the distribution of *B. braunii* within Trebouxiophyceae. The phylogenetic tree based on the Bayesian inference method is shown in Fig. 22 with bootstrap values from Bayesian inference, maximum likelihood, and maximum parsimony shown. Previous phylogenetic analysis has shown that *B. braunii* forms a monophyletic group in Trebouxiophyceae with two lineages: one containing the A race and one containing the B and L races (Sawayama et al. 1995; Senousy et al. 2004; Weiss et al. 2010). Including the new *B. braunii* 18S rDNA sequences strengthens this clustering by showing that the Yamanaka strain of the A race clusters with the Titicaca strain of the A race (Fig. 22). The Kawaguchi strains of the B race cluster together, while the Yayoi strain of the B race clusters with the Ayamé strain of the B race (Fig. 22).

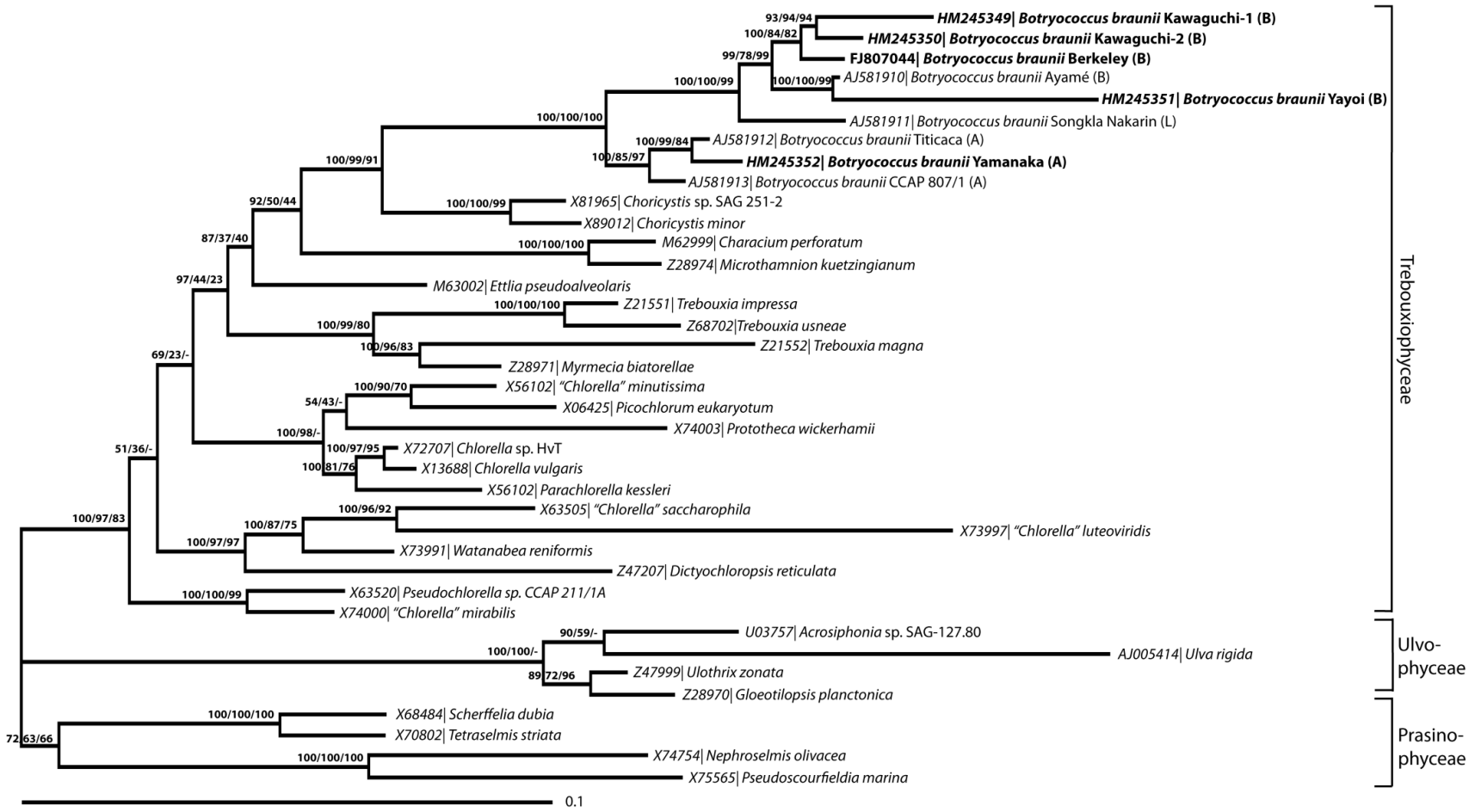

FIGURE 22. Bayesian inference (BI) phylogenetic tree of 18S rRNA sequences. Sequences are identified by their corresponding GenBank, DDJB, or EMBL accession numbers and organism name. Branching credibility percentages from the Bayesian inference (left), maximum likelihood method (middle), and bootstrap maximum parsimony (right) are listed. Where differential branching from the Bayesian inference method occurs, confidence values for the dissenting method is represented by a dash. The scale bar is for 0.1 substitutions per site. The sequences novel to this study are shown in bold. (Weiss et al. 2011)

B. braunii β-actin phylogenetics

To further support our contention that we are working with a monoculture, we isolated the β-actin cDNA from our *B. braunii* Berkeley, Yamanaka, and Songkla-Nakarin strain cultures and used these sequences for phylogenetic analysis using ML, BI, and MP. The phylogenetic tree based on ML is shown in Figure 23 and indicates that all three *B. braunii* β-actin sequences group with other algae from the Trebouxiophyceae confirming the placement of these three *B. braunii* strains based on our 18S rDNA sequence. From this we are able to conclude that β-actin phylogenetic analysis supports the conclusions of our 18S rDNA analysis. Unfortunately there are too few green algae β-actin sequences available at this time to generate such phylogenetic relationships between each *B. braunii* race free of sampling bias and with high confidence. Taken together however, our phylogenetic analyses give strong evidence that the strains we have used in our analysis are indeed pure cultures of *B. braunii* from which confident phylogenetic relationships may be drawn.

B. braunii genome size

Genome size of *B. braunii*, B race Berkeley

We used flow cytometry (Johnston et al. 2004, 2005, 2007) to estimate the genome size of *B. braunii* Berkeley as a first step in determining the whole genome sequence of the Berkeley strain. Simply put, this involves extracting nuclei, staining the nuclear DNA with saturating propidium iodide, and comparing the relative fluorescence to that of a known standard, which in our case was the 333.3 MB genome of *Drosophila*

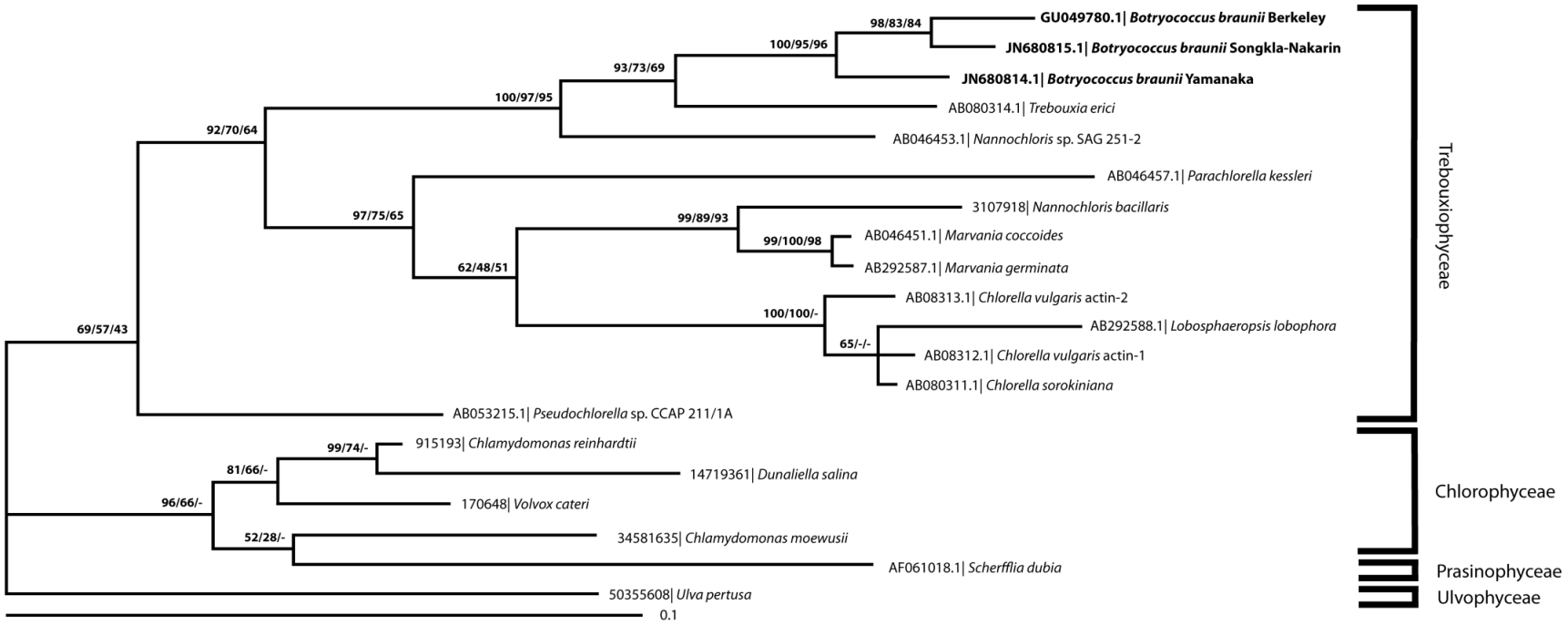

FIGURE 23. Maximum-likelihood (ML) phylogenetic tree of actin nucleotide sequences. Only the first two codon positions were used. Sequences are identified by their corresponding GenBank, DNA Data Bank of Japan (DDJB), or European Molecular Biology Laboratory (EMBL) accession numbers and organism name. Branching credibility percentages from the ML method (left), Bayesian inference (middle), and bootstrap maximum parsimony (right) are listed. Where differential branching from the ML method occurs, confidence values for the dissenting method are represented by a dash. The scale bar is for 0.1 substitutions per site. The sequences novel to this study are shown in bold. (Adopted from Weiss et al. 2010a)

virilis (Gregory and Johnston 2008). We observed that *B. braunii* Berkeley has a genome size of 166.2 ± 2.2 Mb (mean ± SE; n = 7; Fig. 24A). This translates to a 1C DNA content of 0.17 pg, based on 1 pg of DNA = 980 Mb (Bennett et al. 2000).

The estimated *B. braunii* Berkeley genome size is larger than any of the nine completed and annotated algal genomes: *Chlamydomonas reinhardtii*, 121.0 Mb; *Osterococcus tauri*, 12.6 Mb; *Osterococcus lucimarinus*, 13.2 Mb; *Cyanidioschyzan merolae*, 16.5 Mb; *Thalassiosira pseudonana*, 31.3 Mb (Misumi et al. 2008); *Phaeodactylum tricornutum*, 26.5 Mb (Bowler et al. 2008); *Micromonas* sp. RCC299, 21.1 Mb; and *Micromonas pusilla*, 21.9 Mb (Worden et al. 2009); and *Chlorella variabilis*, 46 Mb (Blanc et al. 2010). Of these, only *C. reinhardtii*, *O. tauri*, and *Micromonas sp.* are green algae (Chlorophyta), and only *C. variabilis* is from the Trebouxiophyceae. The *B. braunii* Berkeley genome size is closer to the green algae *Volvox carteri* (Chlorophyceae) genome (138 Mb), which has a standard draft sequence completed (http://genome.jgi-psf.org/Volca1/Volca1.home.html).

The genome size is not inconsistent with our phylogenetic placement of *B. braunii* Berkeley. On average, Trebouxiophyceae genome sizes (20–1,040 Mb) are larger than those of Chlorophyceae (9.8–588 Mb; Kapraun 2007). The *B. braunii* Berkeley genome size falls in the middle of each of these ranges. It has been proposed that relationships among algal genome sizes may be more related to ontogeny and reproductive modes rather than phylogenetic correlations (Kapraun 2005). Unfortunately, there is little to no information available on developmental processes or sexual cycles of *B. braunii*, which may be used to draw relationships among other

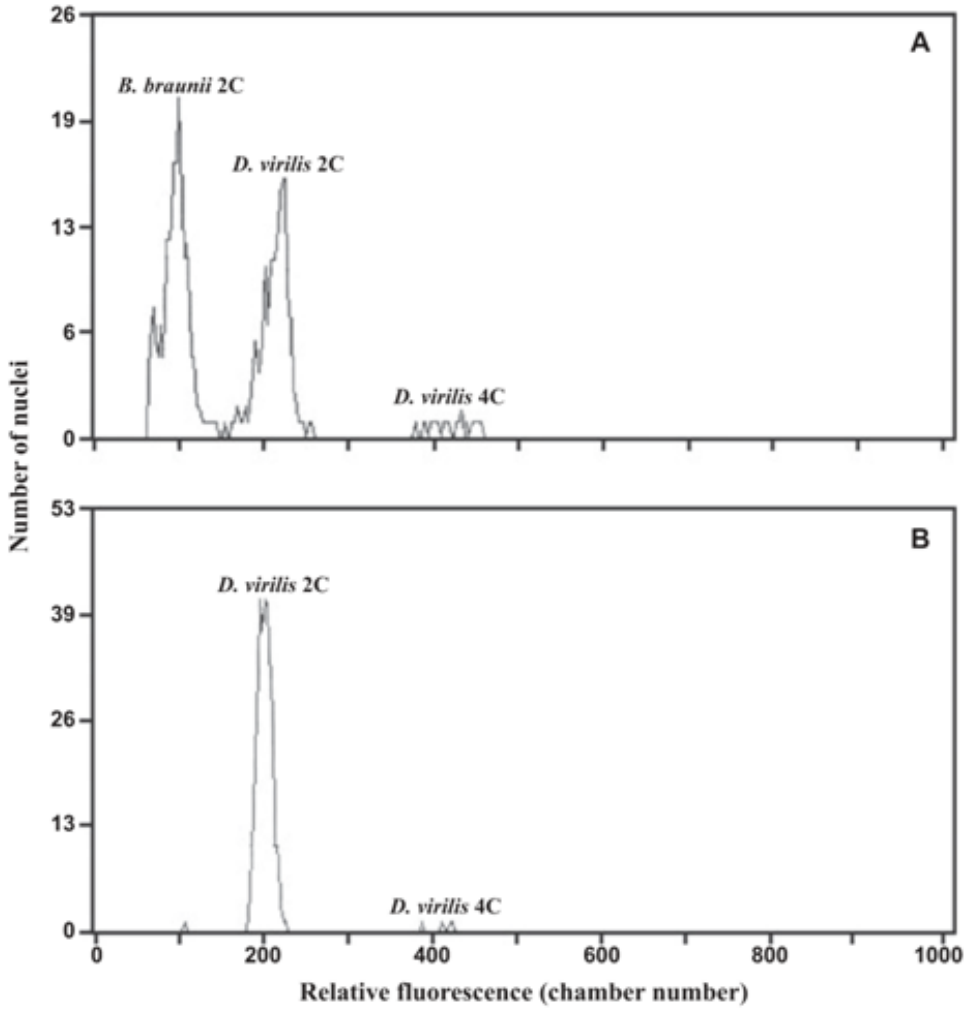

FIGURE 24. Flow cytometry analysis of *B. braunii* Berkeley for genome size determination. Diagrams show the number of nuclei with differing levels of red fluorescence from propidium iodide binding to DNA of: (A) 2C nuclei of *B. braunii* Berkeley, and 2C and 4C nuclei of *Drosophilia virilis*; (B) 2C and 4C nuclei of *D. virilis* only. (Weiss et al. 2010b)

known algal genome sizes. However, evolutionary relationships between very closely related organisms may be inferred from differences in genome sizes. For example, it is well established that there are genome size differences between species of closely related organisms such as fruit flies (Vieira et al. 2002; Bosco et al. 2007; Biemont 2008; Gregory and Johnston 2008). There is also increasing evidence that there are statistically significant differences in genome sizes between different strains of the same species (Cullis 2005; Bosco et al. 2007; Davison et al. 2007; Johnston et al. 2007; Biemont 2008; Gregory and Johnston 2008). Thus, the identification of the *B. braunii* Berkeley genome size lays the foundation for comparative genome size analysis between races and strains of *B. braunii*.

Genome size of *B. braunii*, A race Yamanaka and L race, Songkla Nakarin

Using the Berkeley strain of the *B. braunii* B race, we determined that flow cytometry was suitable for genome size determination on *B. braunii* (Weiss et al. 2010). We next used this same flow cytometry method to estimate the genome sizes for the A and L races of *B. braunii*. We found that the Yamanaka strain of the A race has a genome size of 166.0 ± 0.4 Mb (mean ± SE; n=2; Fig. 25B). This translates to a 1C DNA content of 0.17 pg, based on 1 pg of DNA = 978 Mb (Doležel et al. 2003). The Songkla Nakarin strain of the L race has a genome size of 211.3 ± 1.7 Mb (mean ± SE; n = 5; Fig. 25C), which is equal to a 0.22 pg 1C DNA content.

This A race genome size is nearly identical to that of the B race (166.2 ± 2.2 Mb; Weiss et al. 2010). However, the L race genome size is substantially larger than the B

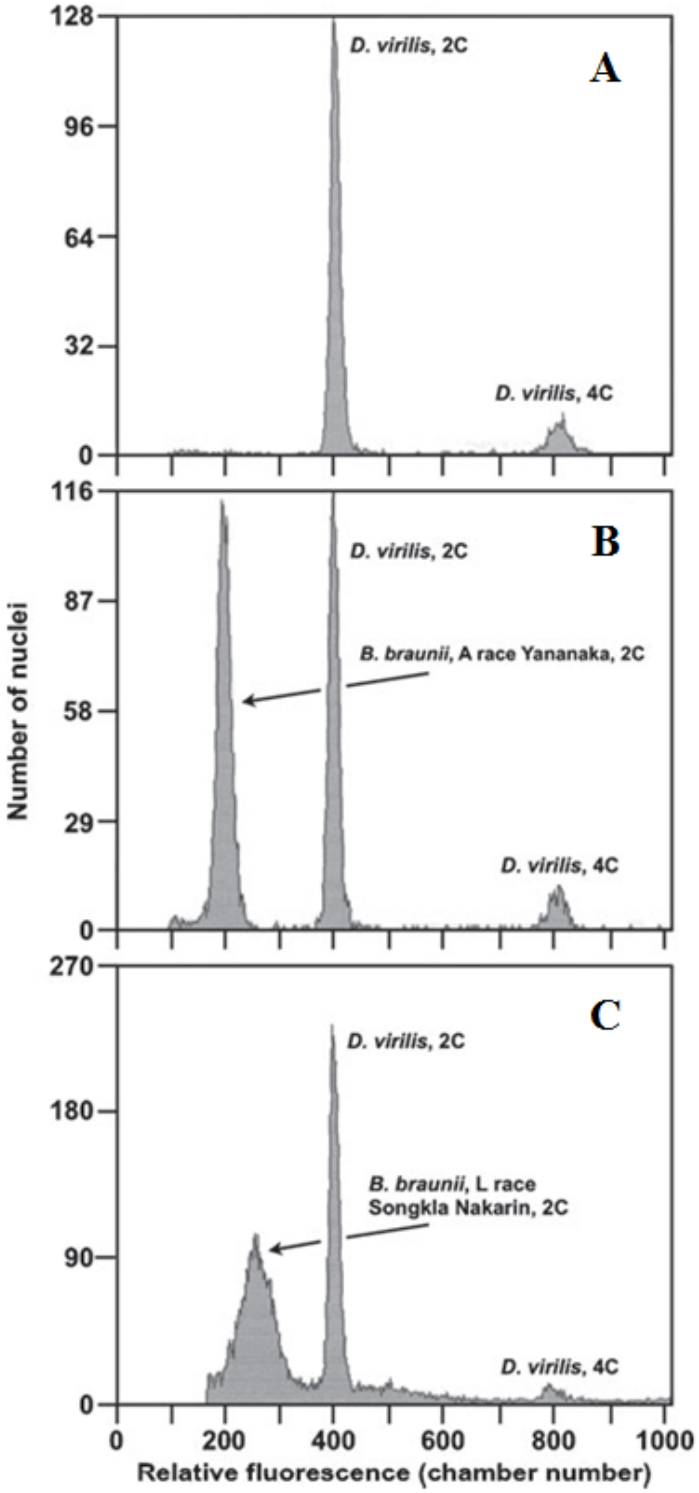

FIGURE 25. Flow cytometry analysis of *B. braunii* A and L races for genome size determination. Diagrams show the number of nuclei with differing levels of red fluorescence from propidium iodide binding to DNA of: (A) 2C and 4C nuclei of *D. virilis*; (B) 2C nuclei of *B. braunii*, A race, Yamanaka strain and 2C and 4C nuclei of *D. virilis*, and (C) 2C nuclei of *B. braunii*, L race, Songkla Nakarin strain and 2C and 4C nuclei of *D. virilis*. (Weiss et al. 2011)

and A races. The significance to this difference between the L race and the B and A races in terms of how these races diverged is not clear at this time. However, in many organisms such as flax, *Arabidopsis*, head lice, and *Drosophila*, there are significant differences in genome sizes between different strains of the same species, and these differences can be used to draw evolutionary relationships (Cullis 2005; Bosco et al. 2007; Davison et al. 2007; Johnston et al. 2007; Biemont 2008; Gregory and Johnston 2008). Unfortunately, there is not enough information on *B. braunii* genome sizes to allow such evolutionary comparisons. This will require a wider sampling of genome sizes for the different strains within each race of *B. braunii*. Since our genome size analysis included only one representative from each race of *B. braunii*, additional genome size determinations may also indicate that other strains of the A and B race have genomes of similar size to the L race. Therefore, the differences between the races shown here should be considered with caution until further analysis can be carried out.

Genome GC content of *B. braunii*, B race Berkeley

We estimated the GC content of *B. braunii* Berkeley using the coding sequences of 15 cDNAs randomly isolated from a cDNA library produced previously by us (Okada et al. 2000). The estimated GC content of these genes was determined to be 54.4 ± 1.2%. This estimate is likely to be slightly lower when introns are included in the analysis from genome sequencing since introns tend to be AT rich. For example, the whole genome of the green alga *C. reinhardtii* has a 64% GC content, while the expressed gene GC content of *C. reinhardtii* is 68% (Merchant et al. 2007).

Typical GC content for eukaryotic organisms is generally in the range of 30%–40%, with an upper limit for vertebrates and higher plants of 46% (Vinogradov 1994, 1998; Barow and Meister 2002; Meister and Barow 2007). Green algae tend to have genome GC content higher than most eukaryotes and rarely below 50%, but it can be as high as 71% (*Monoraphidium minutum*; Jarvis et al. 1992; Leon-Banares et al. 2004). All of the fully sequenced green algae genomes have a GC content of at least 58% (Misumi et al. 2008). Thus, the calculated GC content value of 54 ± 1.2% for *B. braunii* Berkeley is within the predicted range for green algae.

Conclusions

Interestingly, the B race and L race of *B. braunii* are found within the same lineage of our phylogenetic analysis, suggesting a close evolutionary relationship. It has been suggested this relationship relates to the commonality of an isoprenoid-based hydrocarbon produced by these races (Senousy et al. 2004; Weiss et al. 2010). However, their genome sizes are significantly different (Fig. 24A, 25B,C), which questions this close phylogenetic relationship. It is also questioned by the finding that the chemical composition of the A and L race cell walls are very similar, while the B race has a distinctly different cell wall chemical composition (Metzger et al. 2007, 2008). The B and L race phylogenetic relationship can be clarified in the future by obtaining 18S rDNA sequences from additional L race strains for phylogenetic analysis as well as a wider analysis of genome sizes for the different races and strains of *B. braunii*.

Meanwhile, though the genome sizes of green algae vary greatly (9.8–1,040 Mb; Kapraun 2005, 2007), the sizes of the *B. braunii* genomes shown here are larger than those of all sequenced algal genomes. The closest genome sizes to *B. braunii* are that of *Chlamydomonas reinhardtii* at 120 Mb (Merchant et al. 2007) and *Volvox carteri* at 138 Mb (Prochnik et al. 2010). This makes it interesting to speculate about the reasons for the increased *B. braunii* genome size in comparison to these sequenced algal genomes. One possibility is gene number, which ranges from ~5,300 in the 16.5-Mb genome of *Cyanidioschyzon merolae* (Matsuzaki et al. 2004) to ~14,500 in the 120- and 138-Mb genomes of *V. carteri* and *C. reinhardtii,* respectively. Thus, there appears to be a general correlation between genome size and gene number, and *B. braunii* may have a larger number of genes. Another possibility for the increased genome size of *B. braunii* as compared to other sequenced algae is a phenomenon we have noticed when cloning genes from *B. braunii*; its genes have a 3′ untranslated region (UTR) much larger than that of genes from other organisms. For example, the 3′ UTR of squalene synthase from *B. braunii* is 1,009 bp (Okada et al. 2000) while the 3′ UTR of tobacco (Devarenne et al. 1998) and *Arabidopsis* (Kribii et al. 1997) squalene synthase is 279 and 261 bp, respectively. In any case, full genome sequencing will reveal the true nature of the content of the *B. braunii* genome.

Collectively, our data presented here show that, based on genome size and GC content, the full sequence of the *B. braunii* Berkeley genome is an obtainable goal, especially since these parameters are within the range of other sequenced algal genomes. The information obtained from the Berkeley genome will aid in understanding the

molecular mechanisms employed by this organism for such processes as hydrocarbon biosynthesis, the cell cycle, and photosynthesis. Furthermore, our studies have begun to lay the foundation for increasing our knowledge about *B. braunii* molecular biology and determining the evolutionary relationships between and among the *B. braunii* races. More in-depth analysis of this kind will be invaluable in moving *B. braunii* forward as a feasible alga for biofuel production.

CHAPTER IV

B. BRAUNII CELL AND EXTRACELLULAR MATRIX*

Introduction

Though there have been numerous studies of *B. braunii* cell and colony ultrastructure, historically, most have relied upon methods of transmission light microscopy (Blackburn 1936), transmission electron microscopy (TEM) (Wolf 1981), and scanning electron microscopy (SEM) (Aaronson et al. 1983). These methods, while generally sufficient for unicellular algae studies, were less successful when applied to *B. braunii* due in part to its small cell size, amorphous colony shape, and resilient nature that makes quality microtome preparation challenging. Many of these difficulties would be overcome by the application of laser scanning confocal microscopy (LSCM) with fluorescent histology staining (Beakes and Clearly 1999). While histology stains had been applied to *B. braunii* stains for decades previously, these studies were primarily of a qualitative nature, not quantitative, and were carried out at a time prior to laboratory strains or chemical races having been identified (Blackburn 1936). Thus, even when available, uniting historical observations to current studies remains challenging. For the *B. braunii* Berkeley strain, there were no such observations at all. Therefore, we

---

*Portions of the following article has been reprinted with permission from: Weiss, T. L., Chun, H. J., Okada, S., Vitha, S., Holzenburg, A., Laane, J., and Devarenne, T. P. 2010a. Raman spectroscopy analysis of botryococcene hydrocarbons from the green microalga *Botryococcus braunii. J. Biol. Chem.* 285:32458-66.

pursued a series of LSCM observations, often utilizing fluorescent histology dyes, to observe the colony organization and composition of *B. braunii* Berkeley colonies. Key to these studies was the ability to observe colonies with the three-dimensional colony structure intact and with minimal degradation or physical alteration of the sample.

Hydrocarbons

Most of the botryococcene oils in *B. braunii*, B race, localize to the colony extracellular matrix and can be released with pressure (Fig. 26A). It is well known that *B. braunii* cells also have many intracellular oil bodies (Fig.26B; Maxwell et al. 1968; Knights et al. 1970; Banerjee et al. 2002). Both these intracellular oil bodies and extracellular oil can be visualized using the fluorescent neutral lipid-binding stain Nile red, which has been used to accurately estimate *B. braunii* oil content in high-throughput screens (Cooksey et al. 1987; Lee et al. 1998; Elsey et al. 2007). Therefore, we used fluorescence microscopy and Nile red to show the dramatic accumulation of lipids both in the extracellular matrix and in numerous intracellular oil bodies (Fig. 26B). This type of Nile red staining, though simple, reveals many important facts: one, every *B. braunii* cell possesses at least one oil body; two, the older a culture, the more numerous the oil bodies per cell and the more oil contained in the ECM; three, both the size and number of oil bodies per cell can vary greatly, even between neighboring cells of the colony; and four, the oil bodies appear randomly dispersed within the cell cytoplasm (i.e. there is no discernible organization to oil body localization). However this is not true of the *B. braunii* nucleus.

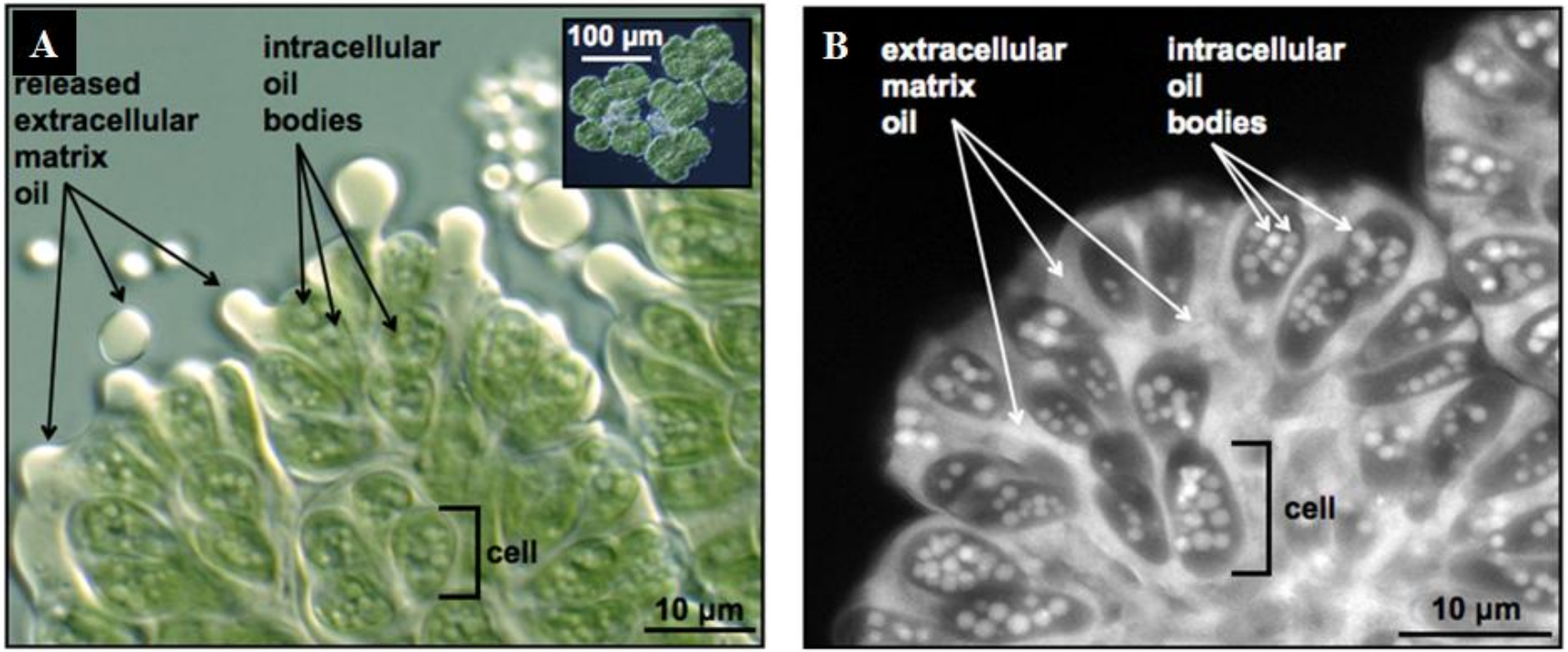

FIGURE 26. Microscopy and Nile red fluorescent imaging of *B. braunii* cells. (A) transmitted light microscope image of a partial *B. braunii* colony showing pressure-released extracellular oil and intracellular oil bodies. A *B. braunii* colony was subjected to pressure by gently pressing on the microscope slide coverslip to expel extracellular oil. Inset shows full *B. braunii* colony for perspective. (B) A colony of *B. braunii* treated with Nile red and viewed by fluorescent microscopy to visualize the Nile red-stained extracellular matrix oil and intracellular oil bodies. (Weiss et al. 2010a)

As seen using DAPI and Nile red co-stains (Fig. 27), *B. braunii* nuclei appear to be centrally located in every cell (Fig. 27A) despite the variations in the number of oil bodies in each cell (Fig. 27B). Another invariable feature of *B. braunii* is the one large chloroplast per cell, which can be visualized using autofluorescence (Fig. 27C). Its chloroplast follows the general shape of the overall cell and nearly envelopes the entire contents of the cytoplasm. Because the chloroplast is composed of one contiguous body that wraps around the cell periphery, the chloroplast has a notable cleft where the two edges of the body meet. This overall organization gives the chloroplast a distinct "U-shape" in two dimension observations when viewed by confocal microscopy: one, when viewed from a plane perpendicular to the length of the cell, the cleft between the folds of the chloroplast body appears to be the opening of the "U;" two, when viewed from a plane parallel to the length of the cell, a typical truncation away from the cell apex appears to be the opening of the "U." In three dimensional imaging however, the chloroplasts appear very similar in their "cup-like" configuration (Fig. 27C).

Though *B. braunii* colonies appear irregular or amorphous by light microscopy which often requires pressing to flatten the sample, three dimensional Nile red and autofluorescence imaging reveal a much more regimented formation of cells (Fig. 28). For instance, three dimensional imaging of native cells not pressed under a coverslip, reveals that *B. braunii* Berkeley colonies are essentially a spherical core of oily ECM in which the cells are deeply embedded up to the cell apex (Fig. 28A,B). Observation of the cell apex region alone can be achieved with two dimensional imaging alone (Fig. 29), but three dimensional imaging however also reveals that: one, the oily ECM is not

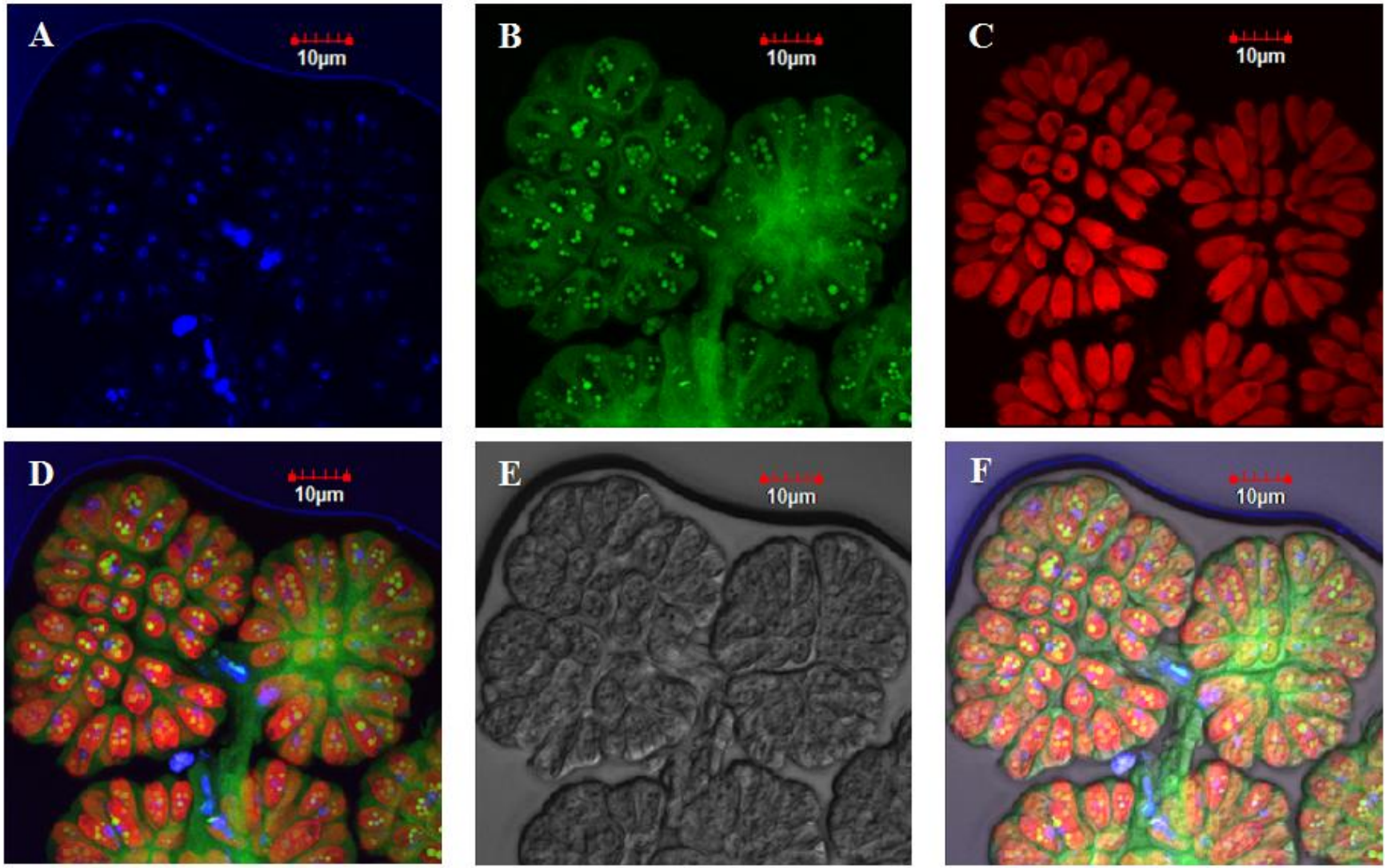

FIGURE 27. Fluorescence confocal microscopy of *B. braunii* using DAPI and Nile red co-staining. All images are an assembly of Z-stack false-color images. (A) DAPI fluorescence, (B) Nile red fluorescence, (C) Chlorophyll autofluorescence (D) Overlay of A-C, (E) DIC image (F) Overlay of D and E.

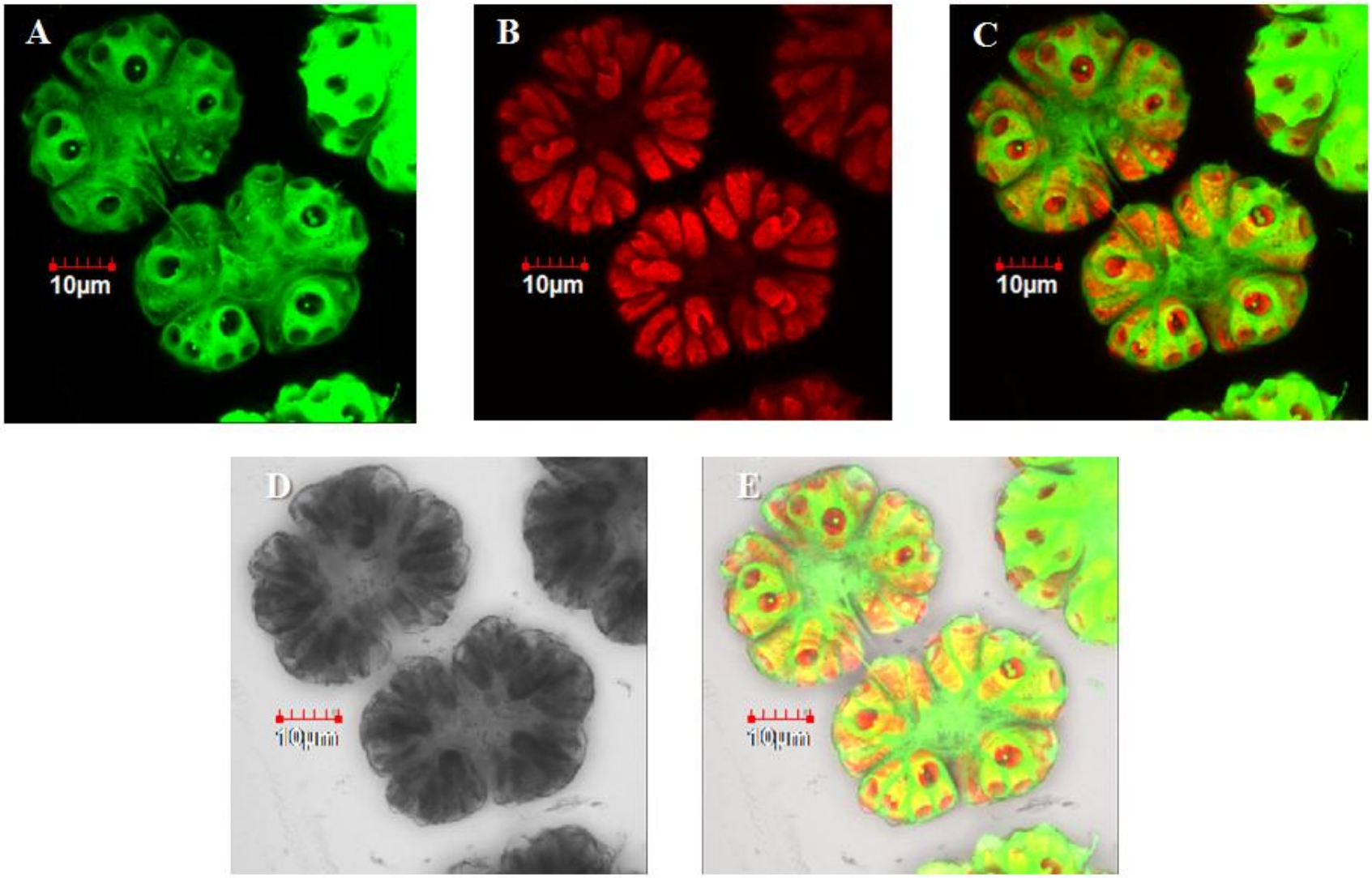

FIGURE 28. Fluorescence confocal microscopy of a *B. braunii* colony using Nile red. All images are an assembly of Z-stack false-color images. (A) Nile red fluorescence. Note the fluorescent spheres, which are oil bodies, and the non-fluorescent speckling of the oily ECM caused by inhomogeneity. (B) Chlorophyll autofluorescence (C) Overlay of A and B. (D) DIC image. (E) Overlay of C and D.

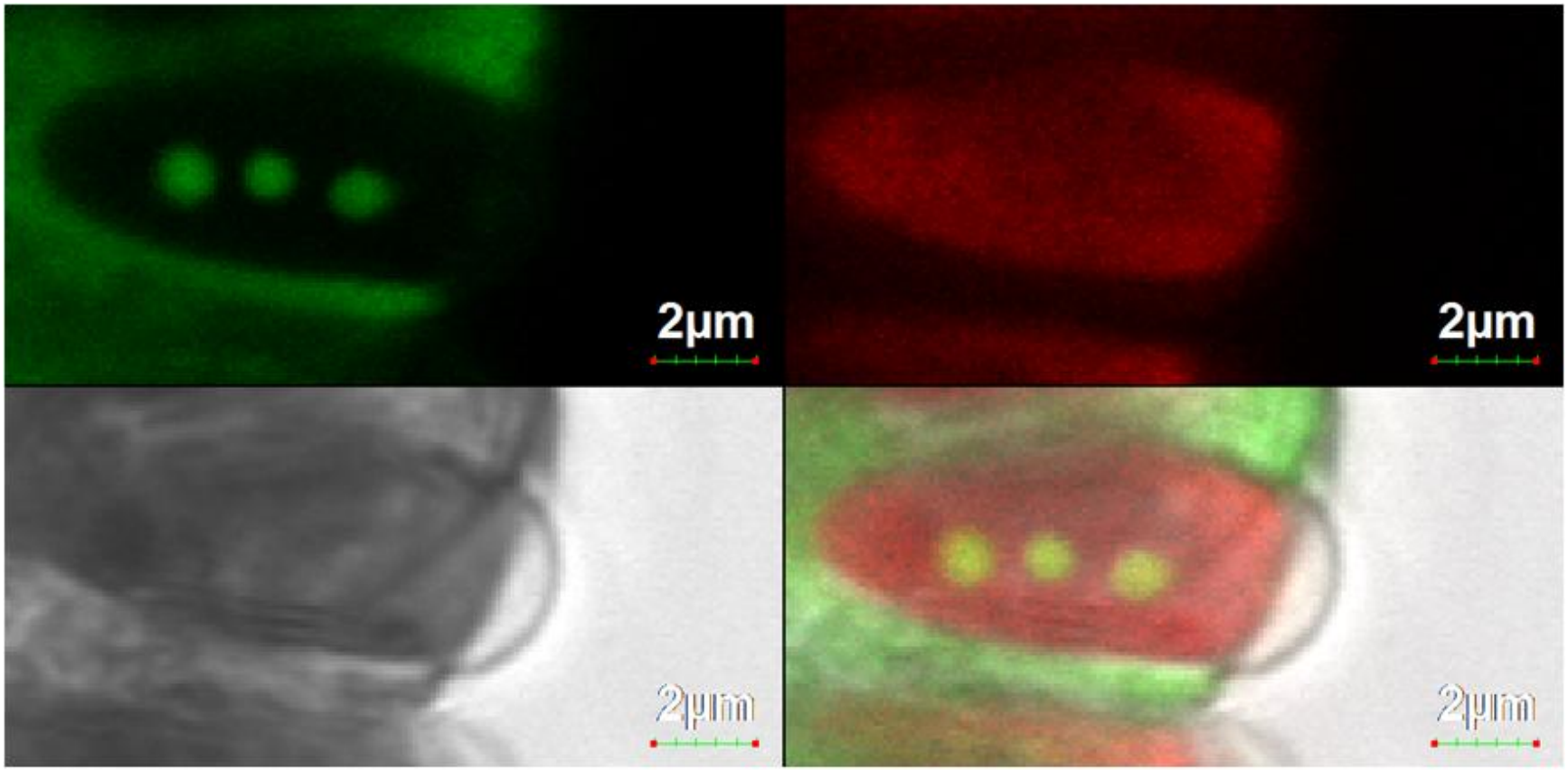

FIGURE 29. Fluorescence confocal microscopy of a *B. braunii* cell using Nile red. All fluorescence images are false-colored. (A) Nile red fluorescence (B) Chlorophyll autofluorescence (C) DIC image (D) Overlay of A, B, and C.

completely homogeneous and that there are distinct spherical bodies throughout that do not fluoresce with Nile red staining (Fig. 28A); two, that each cell does not directly contact any neighbor, but rather is completely enveloped in its own portion of oily ECM (Fig. 28A); three, that the colony appears divided and further subdivided into distinct quadrants (Fig. 28A,C); and four, that *B. braunii* Berkeley cells appear clustered in groups of three with two smaller cells in closer proximity to each other than to a third larger cell nearby (Fig. 28A,C). Three dimensional imagining with Nile red also highlights some of the inherent issues with attempting to use Nile red for quantitative experiments.

Though Nile red has been used for lipid quantitation for decades, its sensitive fluorescent properties during analysis need to be appreciated. Like many lipophilic dyes, Nile red fluorescence is quenched by water. However, unlike other dyes, Nile red maximum excitation and emission wavelengths can vary as much as 40 and 120 nm, respectively, depending upon the environment polarity (Greenspan and Fowler 1985). Furthermore, the fluorescent properties of Nile red can vary with respect to pH, temperature, and even size/volume ratios of stained bodies (Greenspan and Fowler 1985). This allows Nile red to behave as a phenomenal general lipophilic dye, but causes it to behave somewhat unpredictably under cellular conditions. This is especially noticeable using Nile red by mapping its change in emission intensity relative to excitation wavelength on stained *B. braunii* colonies (Fig. 30). In this case, Nile red is a remarkable qualitative tool which clearly shows that the polarity of the ECM is essentially homogeneous, but exhibiting some variation between the core and periphery

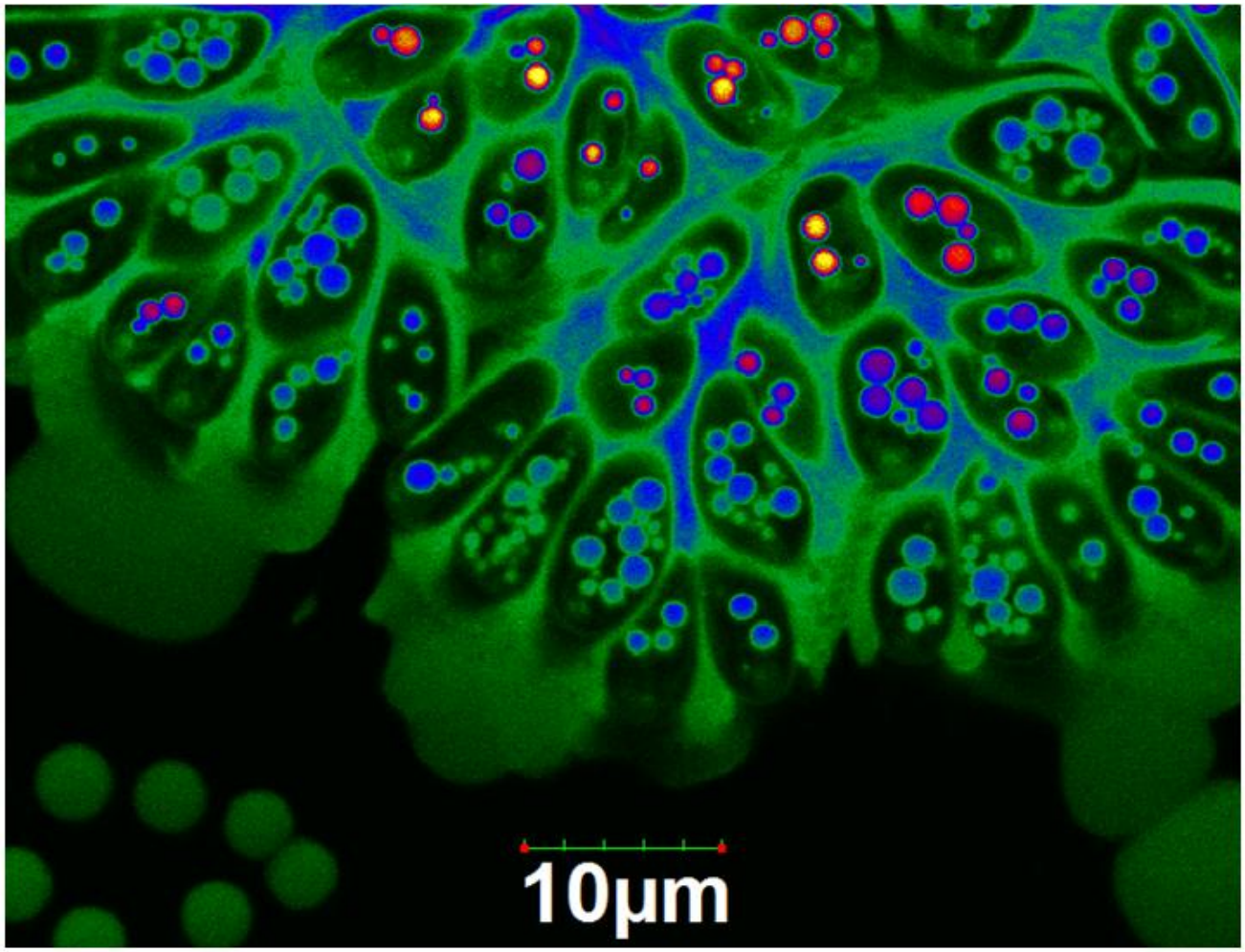

FIGURE 30. Fluorescence ratio imaging of a Nile red stained *B. braunii* colony. Both the excitation and emission wavelengths of Nile red fluorescence can vary significantly depending upon the polarity of its environment. Overlaying Nile red fluorescence excitation at 488 nm and emission at 500-530 nm, shown in blue and which indicates greater hydrophobicity, and excitation at 543 nm and emission at 560-585 nm, shown in red and which indicates greater hydrophilicity, highlights the apparent consistency of the ECM and high degree of lipid body variability.

regions—though this may in part be due to water intruding into the crushed, flat colony (Fig. 30). Moreover, this imaging also reveals that the polarity of oil bodies, and by extension likely their composition, varies cell to cell and without immediately apparent organization with respect to placement within the overall colony (Fig. 30). The oil bodies of individual cells do however exhibit the same polarity, relative to their size (Fig. 30). Most large oil bodies exhibit a hydrophobic core (shown in blue; Fig. 30) and less hydrophobic periphery (shown in green; Fig. 30); however, a few cells exhibit the opposite fluorescence pattern suggesting a more polar core (shown in red; Fig. 30). The exact meaning of this is unknown, but might suggest a changing composition of oil bodies with respect to the age of a cell or levels of oxidation that are occurring. In any case, the diversity of number, size, and composition of oil bodies in addition to an oily ECM all demonstrate the difficulty in using Nile red to quantitate hydrocarbon content in *B. braunii*.

Carbohydrates

For all that Nile red staining can tell us about the characteristics of *B. braunii* hydrophobic elements, equally engaging are the hydrophilic elements. Of primary interest was the region extending beyond the apex of the cell since, by most modes of microscopy, the cell apices appear to extend with cell walls exposed to the environment (Fig. 31A); however, this is not the case. Under high resolution, DIC imaging using a black and white camera clearly shows the faint outline of a nearly translucent retaining wall which extends beyond the apex of all cells and establishes the peripheral surface of

every colony (Fig. 31B). Several past *B. braunii* studies have identified polysaccharide fibrils around each cell (Blackburn 1936; Largeau et al. 1980; Wolf and Cox 1981; Berkaloff et al. 1984) and it seemed possible that these could compose the fibril sheath system seen here.

Congo red

The anionic dye Congo red fluoresces strongly when bound to β-(1-4)-glucanpyranoses and moderately when bound to some β-(1-3)-glucanpyranoses, with a strong favorability toward helical forms of the polysaccharides (Wood 1980). As such, though Congo red staining can detect many forms of carbohydrates, it is a favored tool for the simple detection of cellulose-like polysaccharides (Wood 1980).

When stained with Congo red, most, but not all, *B. braunii* cell walls strongly fluoresced and the fibril sheath retaining wall did not (Figs. 32, 33). This strongly suggests that in *B. braunii*: one, the fibril sheath is not composed of a cellulose-like polysaccharide; and two, that the cell wall is often, but not always, composed of cellulose-like polysaccharides (Figs. 32, 33). That a minority of cells in all colonies observed did not stain yet appear to have intact cell walls by DIC imaging (Fig. 32D) is particularly interesting. Since Congo red fluorescent positive and negative cells appear to be identical and positive cells seem well and equally saturated by fluorescent signal across the entire surface of the cell wall (Fig. 33A), this result does not appear to be a diagnostic error. One possibility is that some *B. braunii* cells lack, or transiently lack,

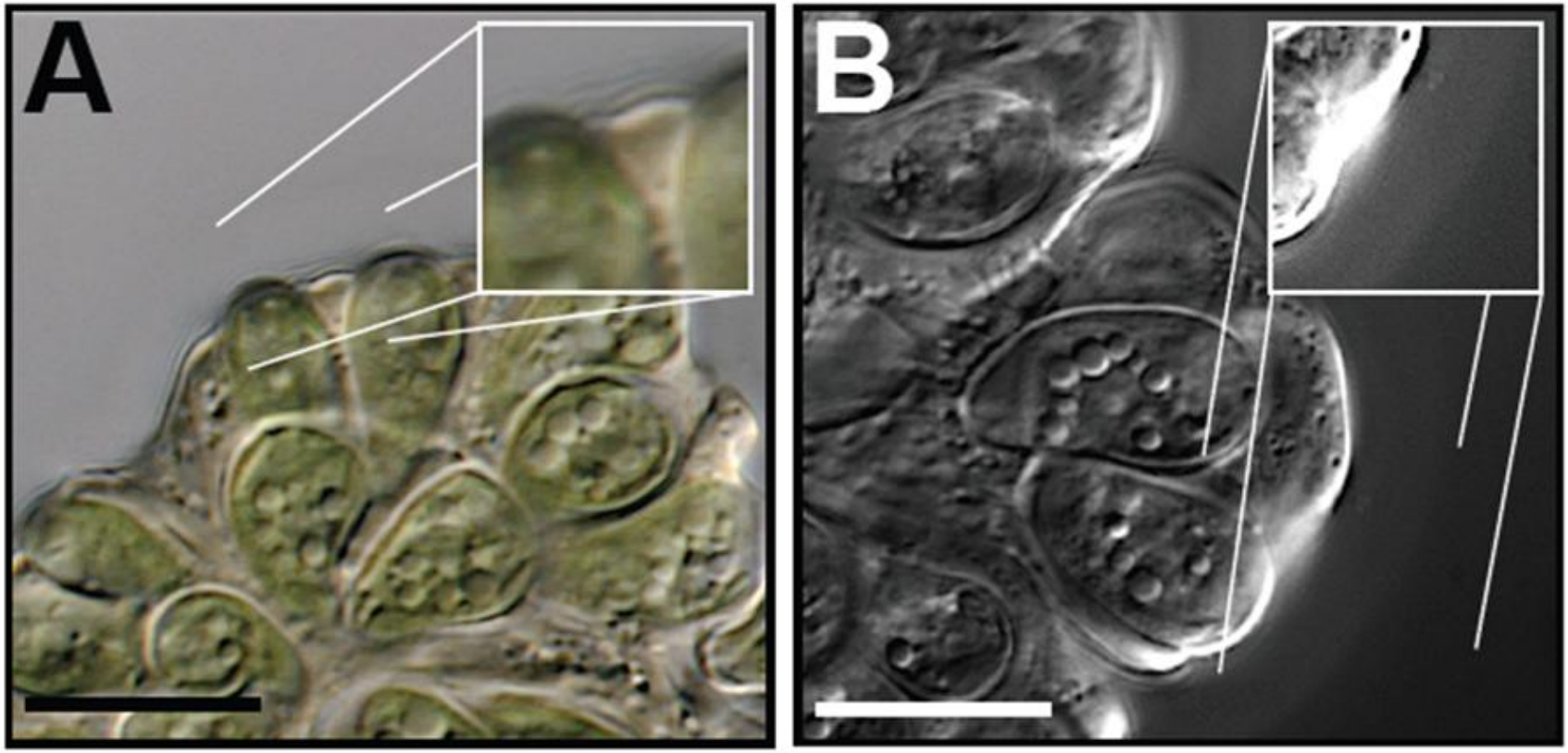

FIGURE 31. *B. braunii* colony periphery imaging. (A) DIC imaging of a *B. braunii* colony, using a color camera, in which the retaining wall is not visible. (B) DIC imaging of the same sample using, using a black and white camera, in which the retaining wall is faintly visiable extending beyond the oily ECM. The scale bars in both images is 10 μm.

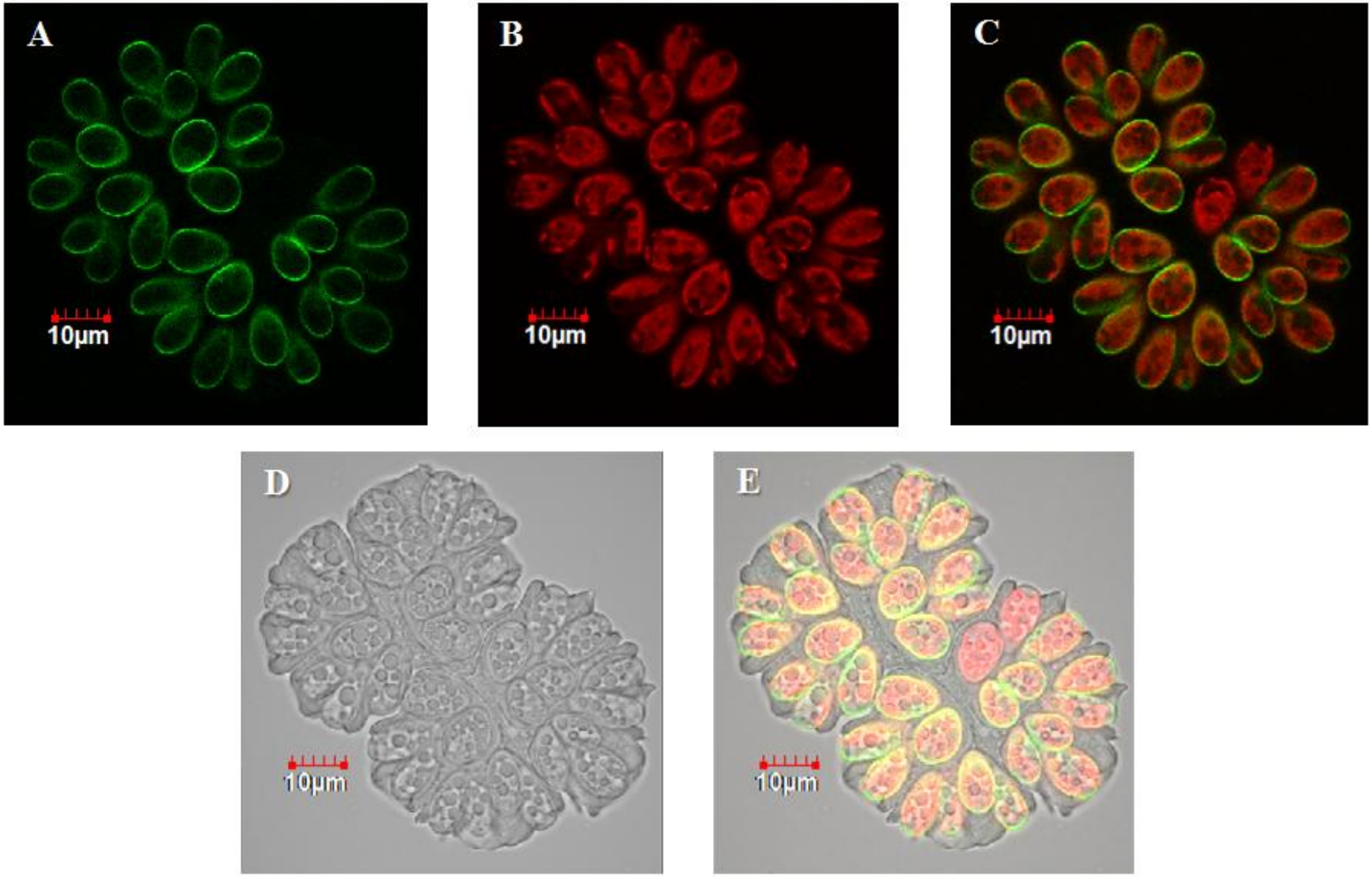

FIGURE 32. Fluorescence confocal microscopy of *B. braunii* using Congo red staining. (A) Congo red fluorescence (B) Chlorophyll autofluorescence (C) Overlay of A and B (D) DIC image (E) Overlay of C and D.

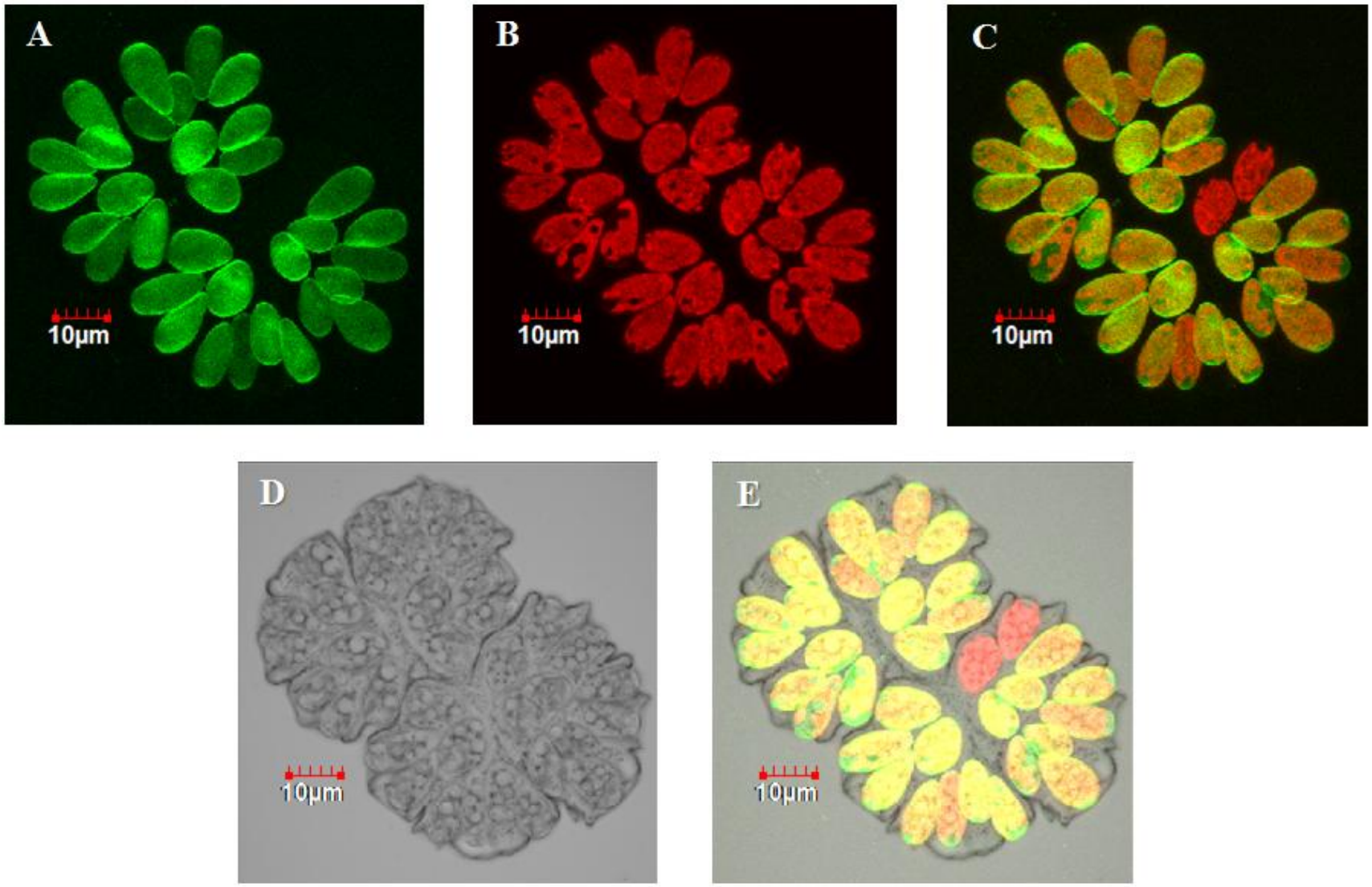

FIGURE 33. Fluorescence confocal microscopy of *B. braunii* using Congo red staining (3D imaging). All images are an assembly of Z-stack images. (A) Congo red fluorescence (B) Chlorophyll autofluorescence (C) Overlay of A and B (D) DIC image. (E) Overlay of C and D.

the cellulose-like polysaccharides with which Congo red fluorescently interacts; but, the exact meaning is not known at this time.

Modified periodic acid/Schiff reagent

Because the polysaccharidic sheath fibrils failed to stain with Congo red, the more general polysaccharide staining technique of a periodic acid/Schiff reagent (PAS) reaction was applied. Typical PAS reactions rely upon a periodic acid treatment first oxidizing vincinyl diols of carbohydrates to aldehydes which may then react, in the presence of metabisulfite, cross-linking to the fluorescent Schiff reagents fuchsine or pararosaniline (Moreno et al. 2006). After initial testing and for practical purposes during fluorescent co-staining, we used a pseudo- or modified-PAS (mPAS) reaction using propidium iodide (PI) as the Schiff reagent (Moreno et al. 2006). This mPAS-PI reaction fluorescently labeled *B. braunii* polysaccharidic sheath fibrils, cell wall, and chloroplast starch granules (Figs. 34, 35, 36).

Typical periodic acid treatments for PAS reactions utilize 1% periodic acid for 10 minutes due to ongoing tissue damage that results from prolonged treatment (Moreno et al. 2006). *B. braunii* however exhibited uncommon resilience to periodic acid treatment and so a range of periodic acid treatment times up to 90 minutes were employed. After just 10 minutes of periodic acid treatment, the polysaccharidic sheath fibrils were diffusely fluorescently labeled and chloroplast starch granules were intensely fluorescent, but little labeling of the cell wall occurred (Fig. 34A). 10 minutes of periodic acid treatment also left *B. braunii* chloroplasts overall intact (Fig. 34C) with

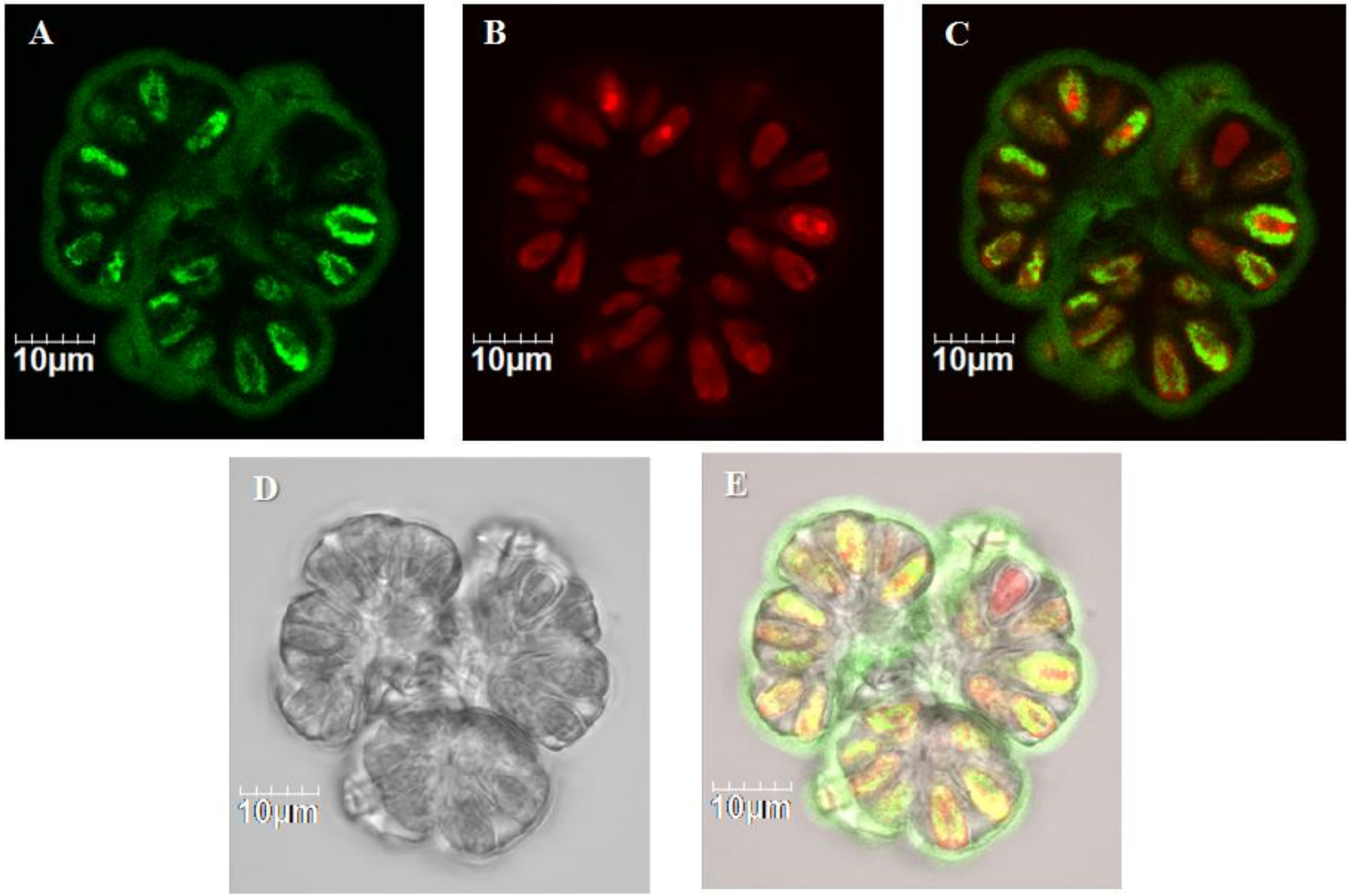

FIGURE 34. Fluorescence confocal microscopy of *B. braunii* using a brief mPAS-PI reaction. All fluorescence images are false-colored. Periodic acid treatment lasted 10 minutes. (A) mPAS-PI fluorescence (B) Chlorophyll autofluorescence (C) Overlay of A and B (D) DIC image. (E) Overlay of C and D.

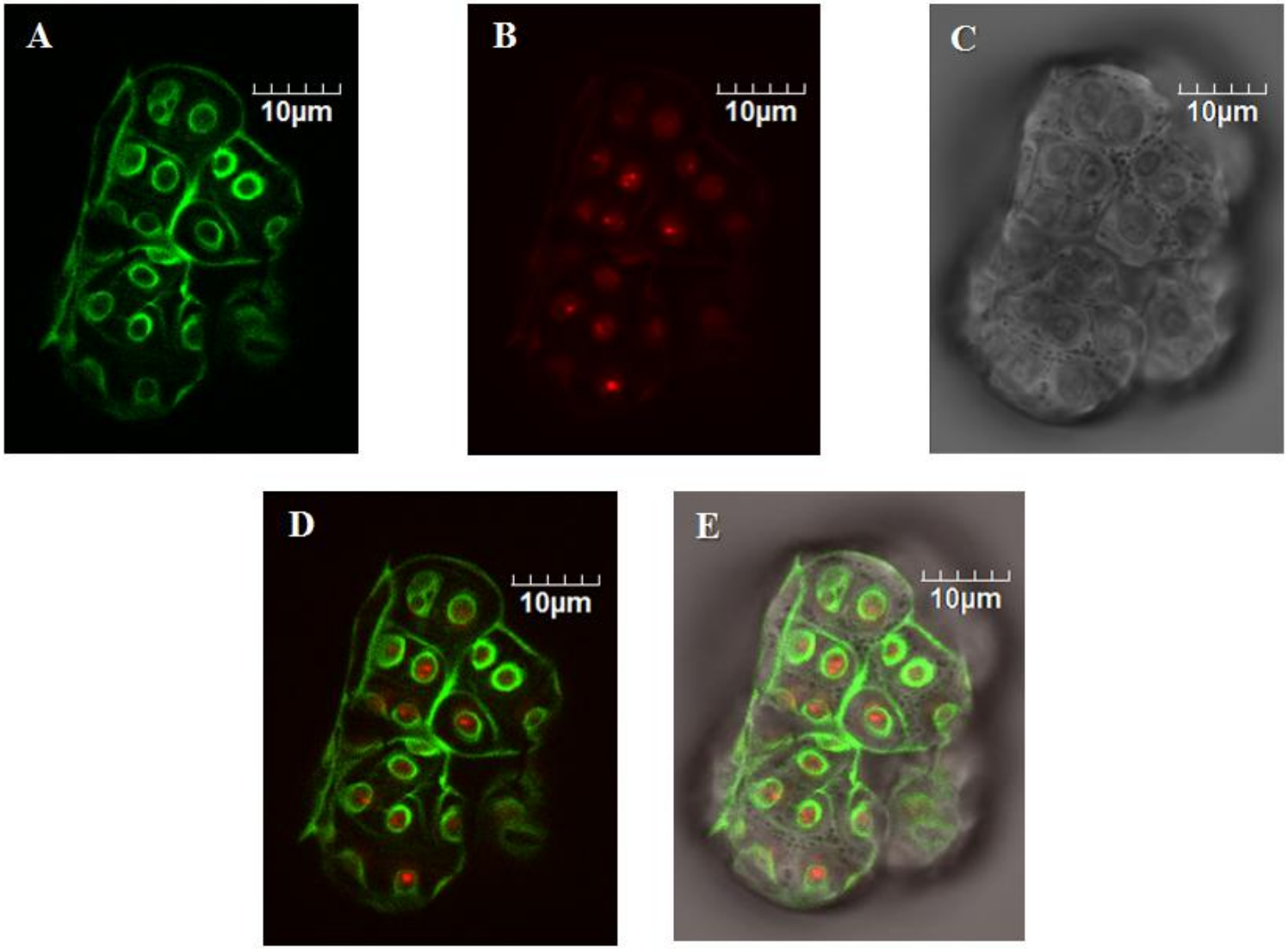

FIGURE 35. Fluorescence confocal microscopy of *B. braunii* using an extended mPAS-PI reaction. All fluorescence images are false-colored. Periodic acid treatment lasted 90 minutes. (A) mPAS-PI fluorescence (B) Chlorophyll autofluorescence (C) Overlay of A and B (D) DIC image. (E) Overlay of C and D.

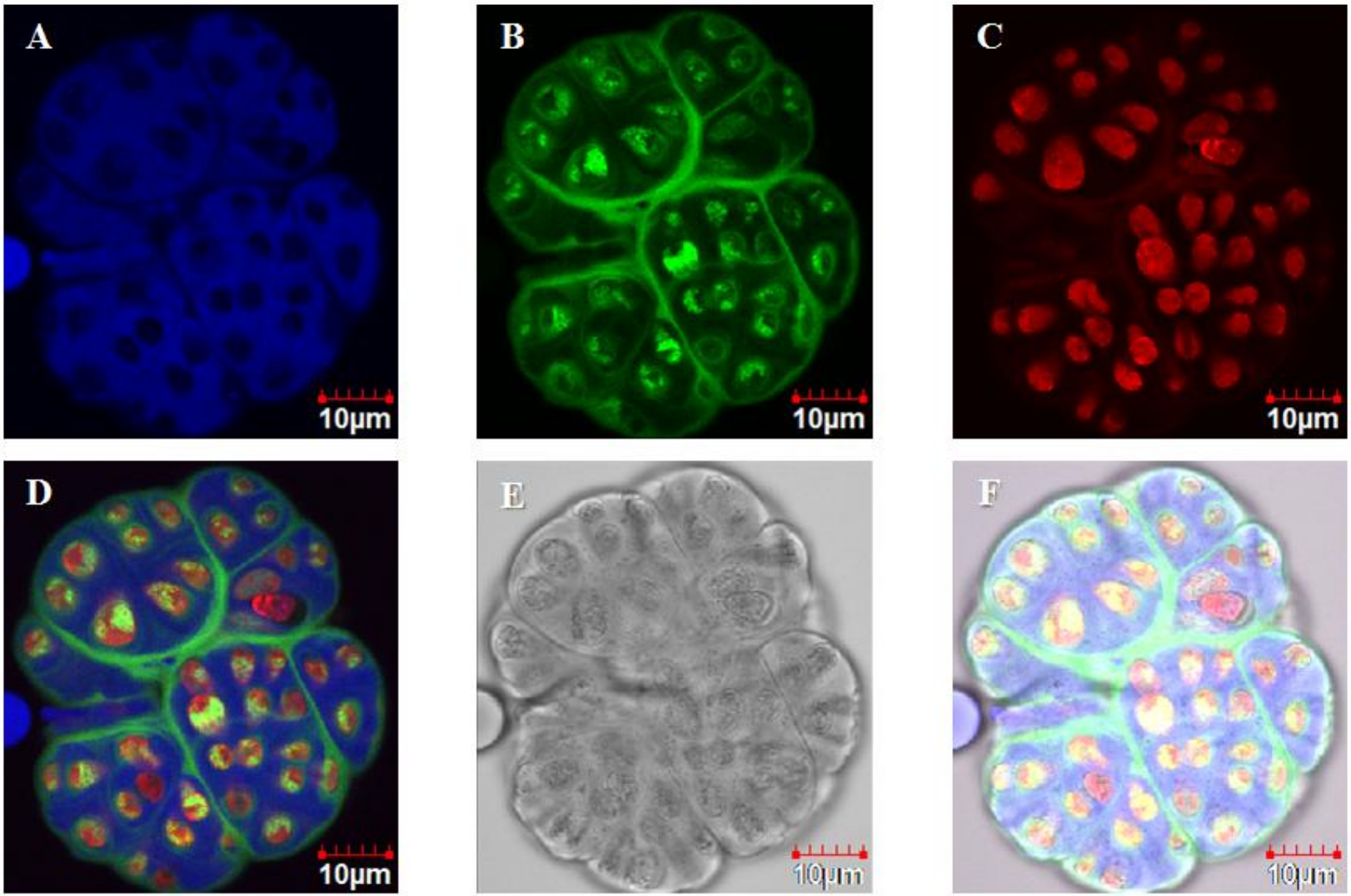

FIGURE 36. Fluorescence confocal microscopy of *B. braunii* using Nile red and mPAS-PI co-staining. All fluorescence images are false-colored. Periodic acid treatment lasted 30 minutes. (A) Nile red fluorescence (B) mPAS-PI fluorescence (C) Chlorophyll autofluorescence (D) Overlay of A-C (E) DIC image (F) Overlay of D and E.

some ultrastructure details still discernible by autofluorescence (Fig. 34B). After 90 minutes of periodic acid treatment however, chloroplasts appear to be completely obliterated (Fig. 35C) and autofluorescence is nearly absent as well (Fig. 35B). By contrast, 90 minutes of periodic acid treatment did produce an intense fluorescent labeling of polysaccharidic sheath fibrils and cell walls despite chloroplast starch granules no longer being visible (Fig. 35A). Thus while this pattern of mPAS reaction labeling presents a technical hurdle to visualizing all three major carbohydrate elements simultaneously, it could also suggest some compositional differences between them. One possible explanation is that chloroplast starch granules present a greater number of vincinyl diols than the polysaccharidic sheath fibrils and that the liquid oil surrounding each cell limits periodic acid exposure to the cell wall.

Regardless, co-staining using Nile red in addition to an mPAS-PI reaction with a moderate 30 minute periodic acid treatment clearly illustrates that the sheath fibrils form a retaining wall along the entire perimeter of the colony (Fig. 36A). This staining also reveals that the cell wall closely approaches the retaining wall at the cell apex and that these two elements together define the boundary of the oily ECM (Fig. 36D). Also interesting is the thin layer of fluorescence present between each individual cell suggesting a further polysaccharidic structure surrounds each cell and delineates the region of the oily ECM to which each individual cell contributes (Fig. 36A).

Gas chromatography/mass spectrometry

Further analysis of the polysaccharidic sheath fibrils was pursued using gas chromatography/mass spectrometry (GC/MS) carried out by Parastoo Azadi at the University of Georgia Complex Carbohydrate Research Center (CCRC). The results of this ongoing work include glycosyl composition and linkage analysis of "shells" isolated from *B. braunii* Berkeley cultures.

"Shells" are a fluffy material that accumulates in *B. braunii* cultures that can be harvested by centrifugation (Fig. 37). We have designated such material "shells" because of their apparent cup-like shape (Fig. 37). Previous studies have noted such harvested exopolysaccharides are produced by *B. braunii* and are possibly derived from the sloughing of sheath fibrils surrounding colonies (Allard and Casadevall 1990; Lupi et al. 1991, 1994).

GC/MS glycosyl composition analysis reveals that the shells and, by extension the polysaccharidic sheath fibrils of the retaining wall, are primarily composed of arabinose and galactose with only trace amounts of glucose and mannose detected (Table 1). Many other carbohydrates are conspicuously absent while the modified residues 3-methyl-arabinose and 6-methyl-galactose were detected in small amounts (Table 1). More surprising still is the presence of an as yet unidentified deoxyhexose in appreciable amounts (9.3 mol %) that did not match any standards or predicted elution times (Table 1). The results of glycosyl linkage analysis were equally uncommon.

GC/MS glycosyl linkage analysis determined that nearly all galactose residues were linked in the pyranose form with a majority doubly-linked at either the 2,3- or 2,4-

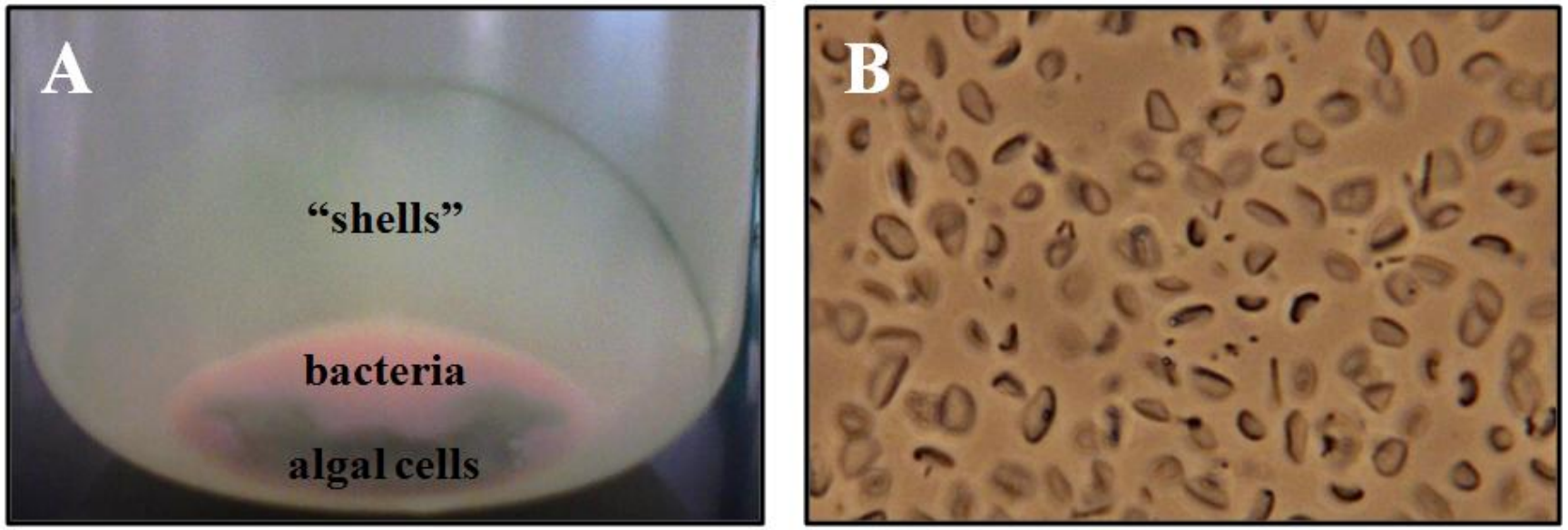

FIGURE 37. Isolation and imaging of *B. braunii* "shells." (A) Centrifugation of 35 μm filtered *B. braunii* culture pellets "shells," bacteria, and any unfiltered algal cells. (B) Microscopy of isolated "shells" reveals their namesake shape (image provided in collaboration by Ursula Goodenough and Robyn Roth of the Department of Biology at Washington University at St. Louis).

Glycosyl residue	Mass (µg)	Mol %
Arabinose (Ara)	83.5	46.7
3-Methyl-Arabinose	7.3	3.7
Rhamnose (Rha)	nd	-
Fucose (Fuc)	nd	-
Xylose (Xyl)	nd	-
Glucuronic Acid (GlcA)	nd	-
Galacturonic acid (GalA)	nd	-
Mannose (Man)	0.5	0.2
Galactose (Gal)	77.8	36.3
6-Methyl-Galactose	7.6	3.3
Glucose (Glc)	0.9	0.4
N-Acetyl Galactosamine (GalNAc)	nd	-
N-Acetyl Glucosamine (GlcNAc)	nd	-
N-Acetyl Mannosamine (ManNAc)	nd	-
Deoxyhexoses	18.3	9.3
Total carbohydrate	195.8	

TABLE 1. Glycosyl composition analysis of isolated *B. braunii* shells. Results of alditol acetate derivatized monosaccharide GC/MS. The total sample size was 200 µg. Results are expressed as a mole percent of total carbohydrate. nd = not detected.

positions (Table 2). Overall, galactose residues exhibited the most varied forms of linkages. Though some galactose residues were singly linked at multiple positions (1-,2-,3-, or 4-linked) like other residues, galactose was the only residue exhibiting any double linkages or even triple linkages, found at the 3,4,6-positions (Table 2). By contrast, arabinose was almost exclusively found in the furanose form and linked either terminally or at the 2-position (Table 2). The unidentified deoxyhexose was similarly terminally or 2-position linked (Table 2).

Collectively, GC/MS analysis establishes that the shells are almost exclusively carbohydrates and composed of arabinose and galactose, which is commonly a primary component of both land plant and algae matrices (Lamport et al. 2011). The absence of 1,4- or 1,6-linkages however is uncommon. Furthermore, while linkage analysis suggests that multi-linked galactose may be primarily forming polysaccharidic chains while singly-linked arabinose form polysaccharidic termini, too few branch points (3,4,6-galactopyranosyl) were identified to suggest an overall structure. An overall structural determination will require NMR analysis and may simultaneously permit the identification of the unknown deoxyhexose.

Conclusions

These studies have identified several physiological and morphological characteristics of the *B. braunii* B race colony. Nile red fluorescence has shown that besides the volume of the ECM not being completely filled with oil and possessing some elements of physical heterogeneity (i.e. spheres of non-fluorescence), oil bodies

Glycosyl Linkage	% present
Terminally linked Arabinofuranosyl (t-Araf)	11.9
2 linked Arabinofuranosyl (2-Araf)	19.7
4 linked Arabinopyranosyl or 5 linked Arabinofuranosyl (4-Ara or 5-Araf)	0.1
Terminally linked Deoxyhexose (t-Deoxyhexose)	6.1
2 linked Deoxyhexose (2-Deoxyhexose)	2.1
Terminally linked Mannopyranosyl (t-Man)	0.5
3 linked Mannopyranosyl (3-Man)	0.2
Terminally linked Galactofuranosyl (t-Galf)	2.1
Terminally linked Galactopyranosyl (t-Gal)	1.1
3 linked Galactopyranosyl (3-Gal)	0.7
2 linked Galactopyranosyl (2-Gal)	0.9
4 linked Galactopyranosyl (4-Gal)	4.5
2,3 linked Galactopyranosyl (2,3-Gal)	31.7
2,4 linked Galactopyranosyl (2,4-Gal)	16.6
3,4,6 linked Galactopyranosyl (3,4,6-Gal)	1.8

TABLE 2. Glycosyl linkage analysis of isolated *B. braunii* shells. Results of PMAA derivatized monosaccharide GC/MS. Values are expressed as percent of total carbohydrates detected in the sample.

themselves exhibit signs of different composition from one cell to another. Variable Congo red stain further suggests that the composition of cell walls may vary cell to cell. Together these observations hint at a dynamic clustering of cells that experience a variety of conditions or undergo a variety of individual physiological changes irrespective of their colonial organization. Separately, inspection of the polysaccharidic sheath has revealed fibrils which appear both chemically resilient and novel in composition which both delineates the boundary of the colony and provides a physical barrier to its surroundings. Goals for future studies stemming from this work would be to identify the structure of these polysaccharides and elucidate their role in mediating colony oil retention and digestive enzymatic resistance. Both of these objectives could be applied to reengineering genetic modification strategy to match *B. braunii* physiology or develop more effective means of oil extraction.

CHAPTER V

RAMAN SPECTROSCOPY ANALYSIS OF B. BRAUNII BOTRYOCOCCENES*

Introduction

Though it is well known that *B. braunii* cells have many intracellular oil bodies (Maxwell et al. 1968; Knights et al. 1970; Banerjee et al. 2002), the lipid composition of these intracellular oil bodies is not known; i.e. do they contain botryococcenes? If so, do all oil bodies consist of one molecular species of botryococcene, or are they a mixture of all botryococcenes? Because lipophilic stains like Nile red are bulk lipid-binding molecules, such stains cannot be used to address these questions because they cannot differentiate among the different botryococcenes. Thus, the ultimate goal of this objective was to use Raman microspectroscopy to detect specific botryococcenes within both the extracellular matrix and intracellular oil drops to begin to address these questions about oil body botryococcene composition. Additionally, the use of a confocal Raman microscope for the investigation of intracellular oil drops has the useful potential to eliminate the out-of-focus signal and suppress the inherently high autofluorescence background from the large chloroplast sheet enveloping the cell.

In general however, spectroscopic characterization of *B. braunii* hydrocarbons,

---

other than NMR, is extremely limited (Largeau et al. 1980; Eroglu and Melis 2010), though a characteristic absorbance spectroscopy peak for botryococcenes has been identified and used to quantitate extracted botryococcenes (Eroglu and Melis 2010). Raman spectroscopy has been used on the A race of *B. braunii* to determine that the intracellular oils were similar in nature to the extracellular oils and that these oils were composed of long chain unsaturated hydrocarbons (Largeau et al. 1980). Specific characterization by Raman spectroscopy for any hydrocarbon from any race of *B. braunii* has not been reported. There are several C=C bonds in botryococcenes that offer unique Raman spectroscopic parameters. For example, the methylation of C_{30}–C_{33} botryococcenes causes C=C bond migration from the backbone endo positions to exo positions at carbons 2, 6, 17, and 21 to create exomethylene groups (Fig. 9). Additionally, the C-26 branch C=C bond is specific to botryococcenes. In our present work we report characterization of botryococcenes from the B race of *B. braunii* by Raman spectroscopy and density function theory (DFT) calculations. Additionally, an identified Raman signature specific to methylated botryococcenes was used to map *in vivo* the presence of methylated botryococcenes in the extracellular matrix and intracellular oil bodies of live *B. braunii* cells.

Botryococcene Raman spectroscopy

Experimental analysis

To identify spectral regions that contain specificity for botryococcenes, Raman spectroscopy was applied to squalene and a total hydrocarbon extract from *B. braunii*, B

race. Squalene serves well as a known entity in comparison to botryococcenes both because of its similar structure and commercial availability. Because a total hydrocarbon extract from some strains of the B race of *B. braunii*, for example the Berkeley strain, is predominantly C_{34} botryococcene (Okada et al. 1995; Okada et al. 1997; Sato et al. 2003) and GC analysis of our total hydrocarbon extract shows C_{34} botryococcene as the primary constituent (Fig. 38), comparison of the two spectra should indicate regions unique to botryococcenes. Analysis of the two spectra indicates similarity across the spectra (Fig. 39A). However, we chose to focus on the 1600–1700 cm^{-1} region for ν(C=C) stretching vibration because the main structural differences between squalene and botryococcenes are in the C=C bond positions. Within this spectral region, squalene generated a single band at 1668 cm^{-1}, and the total hydrocarbon fraction generated two bands at 1647 and 1660 cm^{-1} (Fig. 39A). Because the subsequent analysis of purified botryococcenes was performed in *n*-hexane (see below), the Raman spectra of squalene and total hydrocarbons dissolved in *n*-hexane were analyzed to ensure that the difference in the ν(C=C) stretching region could still be detected in the presence of *n*-hexane. As shown in Fig. 39A, the 1600–1700 cm^{-1} ν(C=C) stretching region of the spectra of squalene and total hydrocarbons in *n*-hexane shows the same bands seen without *n*-hexane. However, the absolute intensity was reduced (compare Figs. 39A and B). The *n*-hexane sample alone did not show these bands (Fig. 39B).

Next, Raman spectroscopy was applied to individual botryococcenes in *n*-hexane and analyzed in the ν(C=C) stretching region to identify bands specific to the botryococcene structure. Pure C_{30}, C_{32}, C_{33}, and C_{34} botryococcenes were obtained by

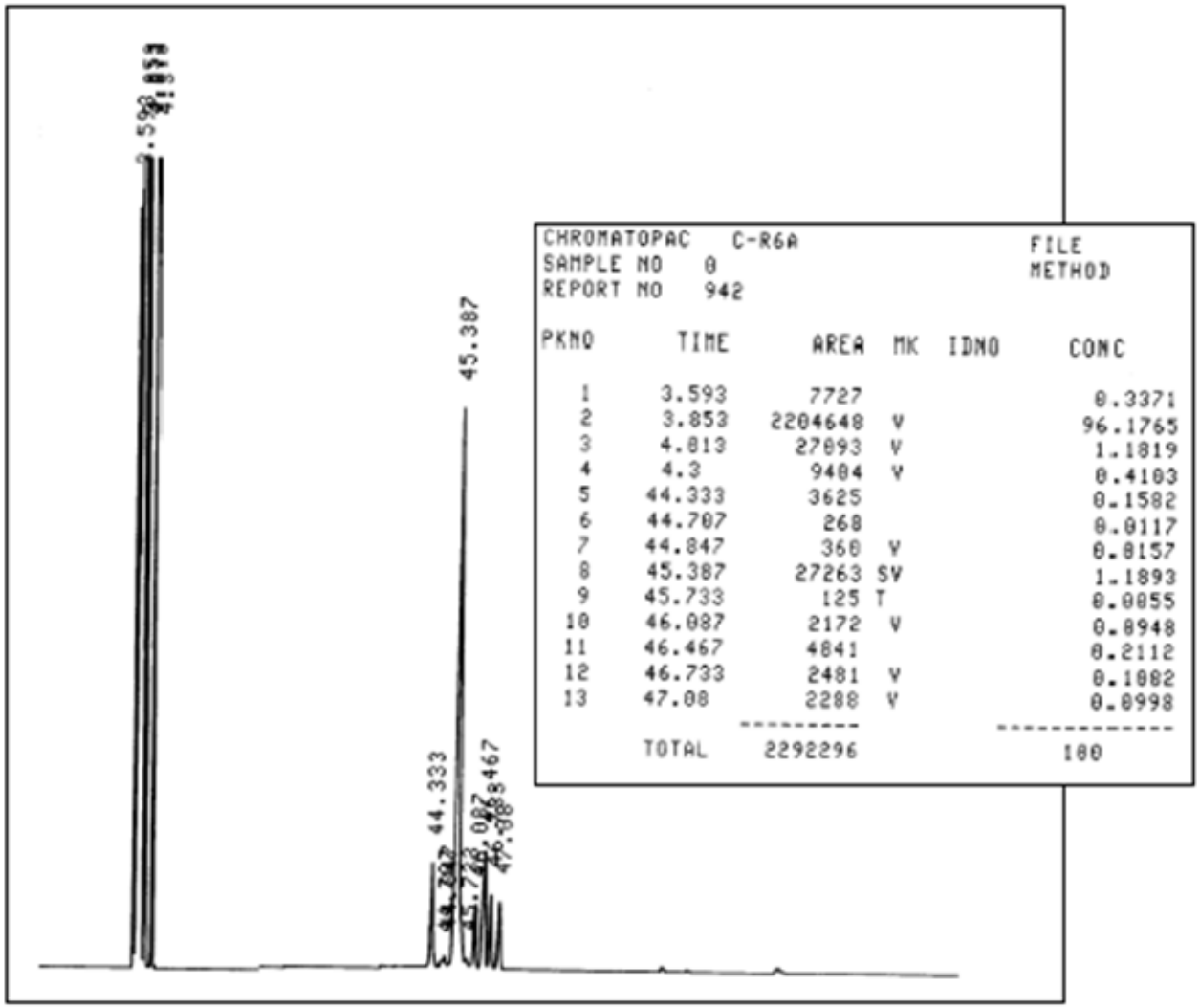

FIGURE 38. Gas chromatography of botryococcene total hydrocarbon fraction. Peaks occurring between approximately 44 and 48 minutes (peaks #5-13) correspond to the 9 compounds, at a minimum, found within the total hydrocarbon fraction. The largest peaks represent the botryococcenes isolated for this study. Peak number 8 is C_{34} botryococcene. Peaks between 3.5 and 4.3 minutes (peaks #1-4) are solvent peaks. (Weiss et al. 2010a)

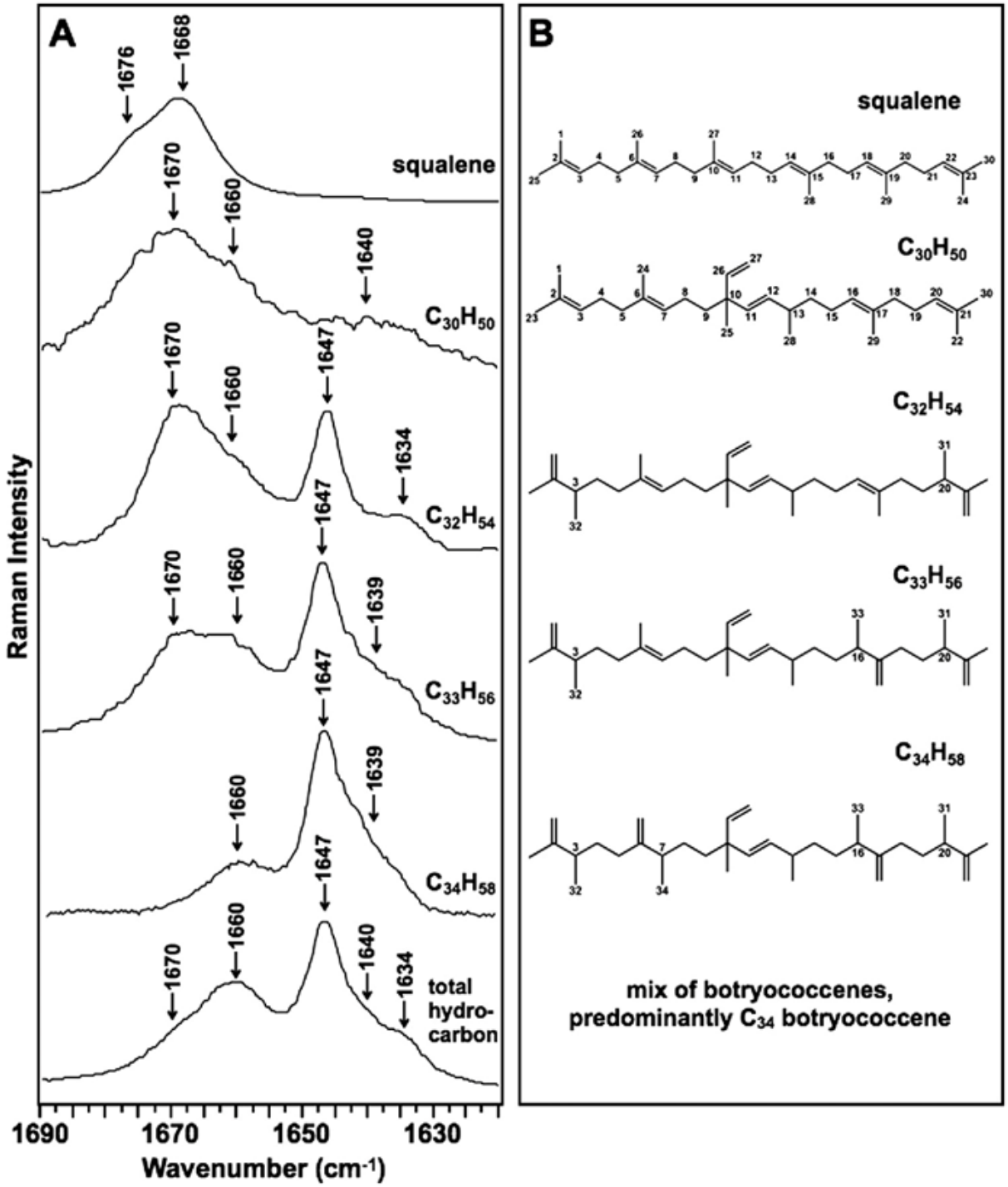

FIGURE 40. Raman spectra for the υ(C=C) stretching region of botryococcenes. (A) Indicated botryococcenes were purified from *B. braunii* by HPLC, dissolved in *n*-hexane, analyzed by Raman spectroscopy within the υ(C=C) stretching region, and compared with that for the total hydrocarbon extract and pure squalene. (B) Structures of squalene and individual botryococcenes analyzed in (A). (Weiss et al. 2010a)

HPLC, purity was confirmed by GC, molecular weights were confirmed by fast atom bombardment-mass spectroscopy, and structures were confirmed by NMR as described previously (Okada et al. 1995; Okada et al. 1997; Sato et al. 2003). We were unable to purify sufficient quantities of C_{31} botryococcene to analyze by Raman spectroscopy at this time and obtained a minimal amount of C_{30} botryococcene (3 mg) to obtain a workable spectrum. Analysis of all bands identified in the 1600–1700 cm^{-1} ν(C=C) stretching region of the spectra reveals that several of the bands can be assigned to specific bonds in botryococcenes. The band at 1647 cm^{-1} is seen in all botryococcenes except for C_{30} botryococcene (Fig. 40A). Because C_{30} botryococcene lacks methylation (Fig. 40B), this suggests that the 1647 cm^{-1} band originates from the exomethylene groups generated by the methylation events. The band at 1670 cm^{-1} is seen in all botryococcenes except C_{34} botryococcene (Fig. 40A), suggesting that it is due to the backbone C=C bonds because C_{34} botryococcene lacks these bonds with the exception of the C=C bond at C-11 (Fig. 40B). Moreover, squalene, which possesses only backbone C=C bonds, has its maximum Raman intensity at 1668 cm^{-1}. The bands at 1639 and 1660 cm^{-1} are more difficult to assign but appear to be specific to botryococcenes compared with squalene (Fig. 40A). These bands may be assigned to the branch C=C bond at C-26 and the backbone C=C bond at C-11 that are found in all botryococcenes (Fig. 40B). This is supported by the spectrum for C_{34} botryococcene (Fig. 40A), which has three major bands: 1647 cm^{-1} attributed to the exomethylene groups and 1639 and 1660 cm^{-1}, which should be attributable to the C-26 and C-11 C=C bonds because they are the only other C=C bonds in C_{34} botryococcene (Fig. 40B). However, with these data it is

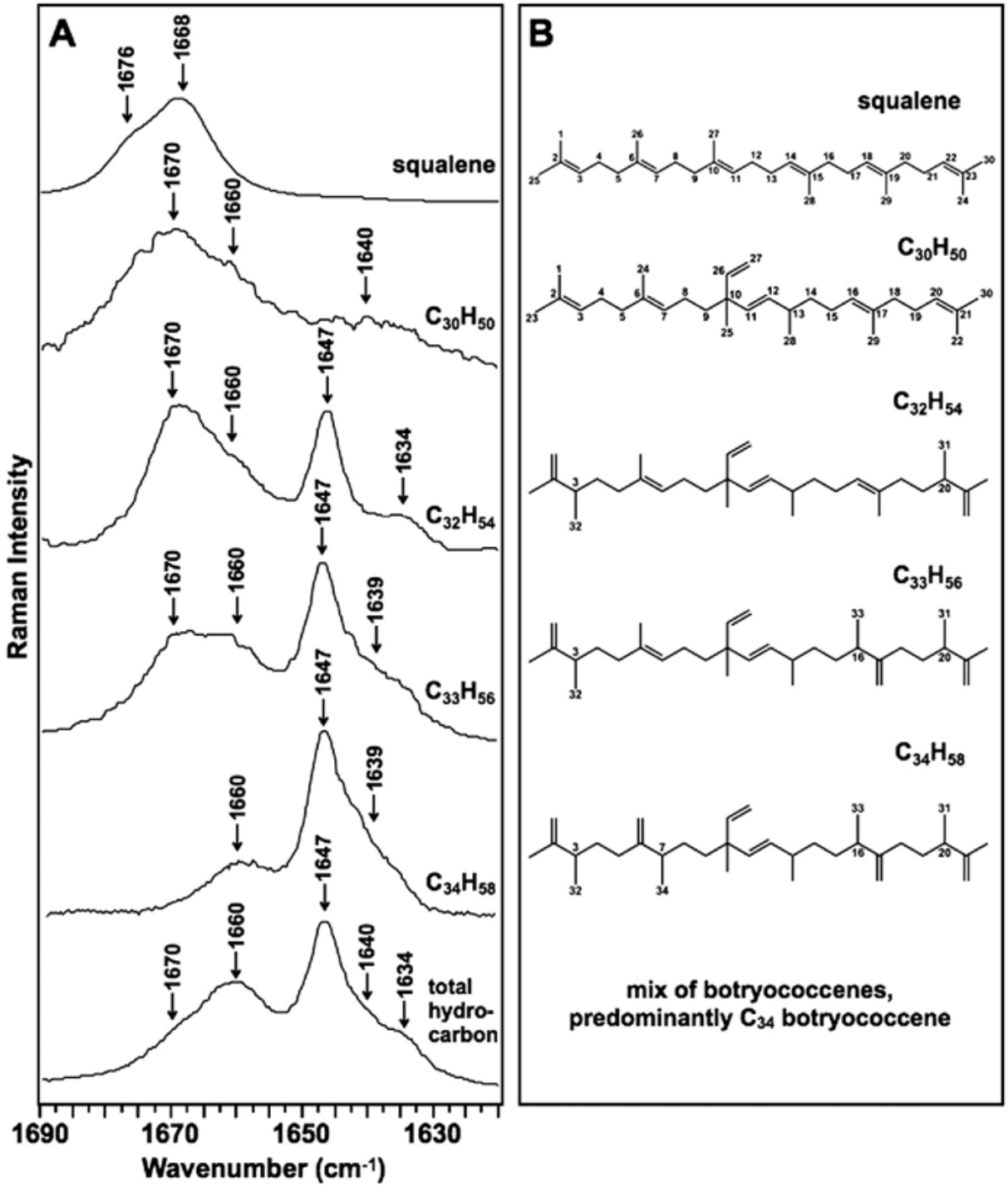

FIGURE 40. Raman spectra for the υ(C=C) stretching region of botryococcenes. (A) Indicated botryococcenes were purified from *B. braunii* by HPLC, dissolved in *n*-hexane, analyzed by Raman spectroscopy within the υ(C=C) stretching region, and compared with that for the total hydrocarbon extract and pure squalene. (B) Structures of squalene and individual botryococcenes analyzed in (A). (Weiss et al. 2010a)

difficult to assign these bands specifically to the C-26 or C-11 C=C bonds. A band at 1634 cm^{-1} is also seen in C_{32} botryococcene which cannot be assigned at this time.

These Raman spectra indicate that the Raman bands of 1639, 1647, 1660, and 1670 cm^{-1} are specific for botryococcenes. Thus, these bands could be used as diagnostic signatures for the presence of botryococcenes. The 1647 cm^{-1} band is specifically due to botryococcene methylation and may offer the best signature for Raman spectroscopy identification of botryococcenes. This is supported by the Raman spectrum of the total hydrocarbon fraction, which shows the four main botryococcene-specific bands of 1639, 1647, 1660, and 1670 cm^{-1} (Fig. 40A). Additionally, the band of 1634 cm^{-1} was detected in the total hydrocarbon fraction that was seen for C_{32} botryococcene and cannot be assigned at this time (Fig. 40A). It should be noted that the increasing methylation of botryococcenes is correlated with a shift of bands in the Raman spectra from the 1670 cm^{-1} region toward the 1647 cm^{-1} region (Fig. 40A).

Computational analysis

Because we could not obtain sufficient quantities of C_{31} botryococcene for Raman spectroscopy and could not specifically assign the 1639 cm^{-1} and 1660 cm^{-1} bands (Fig. 40), DFT calculations were used to address these problems as well as support our experimental spectra interpretation. There are two isomers of C_{31} botryococcene that have been identified in *B. braunii* by methylation of C_{30} botryococcene at C-3 or C-20 (Fig. 9; Huang et al. 1989a; Okada et al. 1995, 1997). The full Raman spectra from the calculations indicate that the major differences among all

the botryococcenes analyzed are in the *ν*(C=C) stretching region as seen in the experimental spectra (Fig. 41A). Analysis of the 1600–1700 cm^{-1} region for *ν*(C=C) stretching shows strong similarities to our experimental spectra (Fig. 41B). Fig. 41B shows the computed spectra for this region, and Figure 42B lists the calculated wavenumber values and compares them with those observed experimentally. It should be noted that each molecule has six independent *ν*(C=C) stretching frequencies, but these may overlap to produce only two or three Raman bands depending on the type (backbone, exomethylene, or branch) of C=C bond present. Fig. 42A shows the individual stretching frequency calculated for each specific C=C bond for each of the molecules. Remarkably, the stretching vibration of each individual C=C bond is shown by the calculations to be almost totally independent and uncoupled to any of the other *ν*(C=C) stretching motions or to any other vibration. What is clearly evident from Figs. 41B and 42A,B is that the three types of *ν*(C=C) stretching vibrations fall into distinct spectral regions. The backbone *ν*(C=C) stretching wavenumbers are calculated to be between 1663 cm^{-1} and 1679 cm^{-1} for all the molecules and are observed in the 1660–1670 cm^{-1} region. The exomethylene stretches are calculated to be between 1646 cm^{-1} and 1655 cm^{-1} and are all observed at 1647 cm^{-1}. The branch C=C stretches are computed to be in the 1642–1649 cm^{-1} range and are experimentally observed at 1639–1640 cm^{-1}.

Because the calculated Raman spectra were determined for fixed bonds of a linear botryococcene structure, we analyzed how different conformations of the botryococcene structure would affect the Raman spectra. The spectra for three different

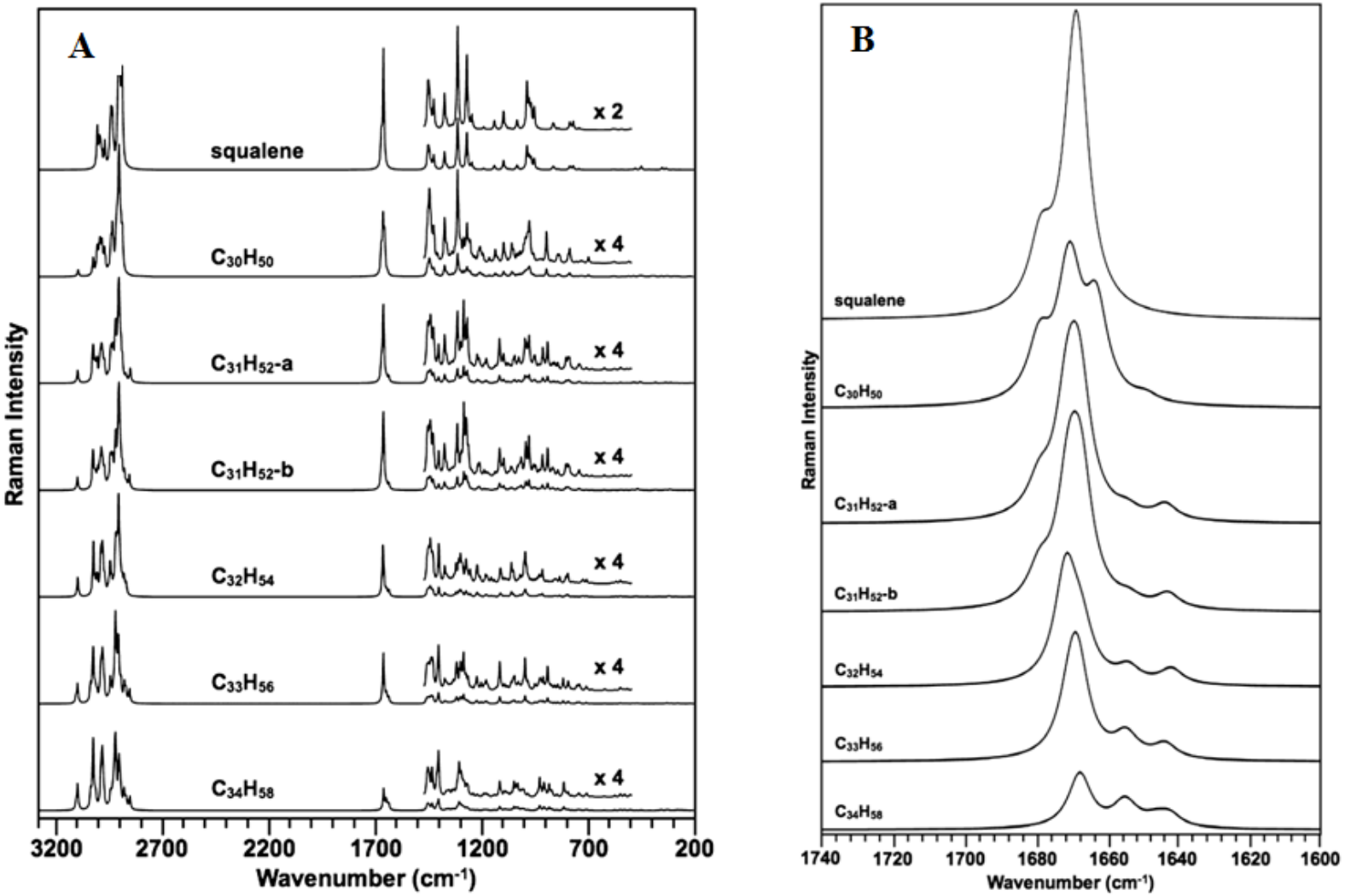

FIGURE 41. DFT-calculated Raman spectra for botryococcenes. DFT calculations were performed using the GAUSSIAN 03 package and the computed spectra were assembled using the GaussView 4.1.2 program. (A) DFT-calculated Raman spectra for squalene and the indicated botryococcenes from 200-3300 cm^{-1} and, (B) in the υ(C=C) stretching region. (Weiss et al. 2010a)

A

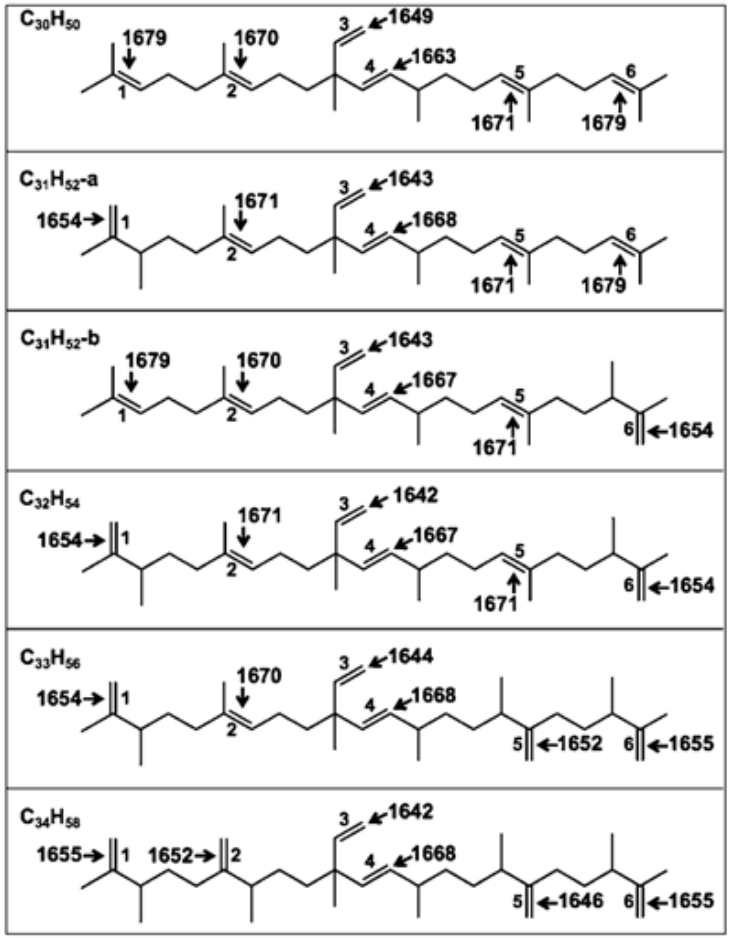

B

Molecule	C=C type	Bond number	Frequency range	
			Observed	Calculated
			cm^{-1}	cm^{-1}
$C_{30}H_{50}$	Backbone	1, 2, 4, 5, 6	1670	1663–1679
	Exomethylene	NP	NP	NP
	Branch	3	1640	1649
$C_{31}H_{52}$-a	Backbone	2, 4, 5, 6	ND	1668–1679
	Exomethylene	1	ND	1654
	Branch	3	ND	1643
$C_{31}H_{52}$-b	Backbone	1, 2, 4, 5	ND	1667–1679
	Exomethylene	6	ND	1654
	Branch	3	ND	1643
$C_{32}H_{54}$	Backbone	2, 4, 5	1670	1667–1671
	Exomethylene	1, 6	1647	1654
	Branch	3	1639	1642
$C_{33}H_{56}$	Backbone	2, 4	1670	1668–1670
	Exomethylene	1, 5, 6	1647	1652–1655
	Branch	3	1639	1644
$C_{34}H_{58}$	Backbone	4	1660	1668
	Exomethylene	1, 2, 5, 6	1647	1646–1655
	Branch	3	1639	1642

Figure 42. Calculated Raman wavenumbers for each C=C bond of individual botryococcenes. (A) Schematic of individual assignments where numbers 1–6 indicate a bond reference number in, (B) a comparison of observed and calculated Raman bands for botryococcenes. NP = not present, ND = not determined. (Weiss et al. 2010a)

conformers of C_{30} botryococcene were calculated based on rotation of the bond at C-18, C-15, or C-5 (Fig. 43A). The full Raman spectra of these conformers appear to be very similar to that of the experimental and calculated spectra for linear botryococcenes (Fig. 43A). However, analysis of the 1600–1700 cm^{-1} ν(C=C) stretching region shows that the spectra of the C_{30} botryococcene conformers have three bands similar to the linear C_{30} botryococcene, but the intensity of the bands varies depending on the conformation (Fig. 43B). This would indicate that different conformers of C_{30} and other botryococcenes may not be easily identifiable by Raman spectroscopy in a cell sample with a complex mixture of botryococcenes.

It should be noted that each of these molecules has a large number of vibrations (3N– 6 where N = number of atoms), and all of these are Raman-active. Thus, for example, $C_{34}H_{58}$ has 270 vibrations. These include 58 C–H stretching modes between 2800 and 3200 cm^{-1} and 33 skeletal stretching vibrations, including the ν(C=C) stretching modes. The remaining are various types of angle bending, twisting, wagging, rocking, etc. motions, and all are below 1500 cm^{-1}. In our present work we focus on the ν(C=C) stretching vibrations (1600–1700 cm^{-1}) because these are well separated from all other modes and provide the means for discriminating between the different botryococcenes and their three types of C=C double bonds (backbone, exomethylene, and branch).

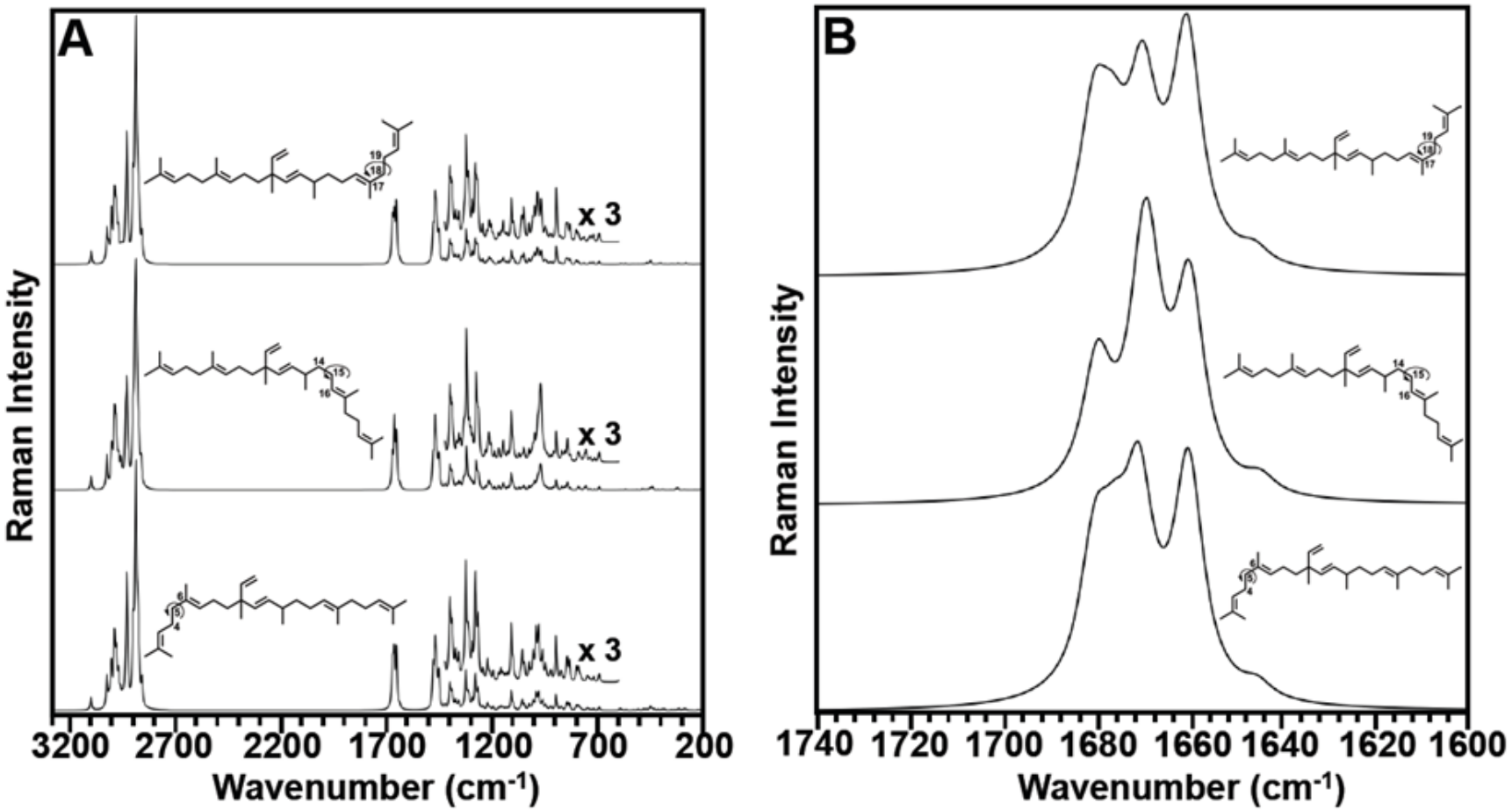

FIGURE 43. Raman spectra for three C_{30} botryococcene conformers. (A) Raman spectra of C_{30} botryococcene conformers in the 200 - 3300 cm-1 range. (B) Raman spectra of C_{30} botryococcene conformers in the 1600 - 1740 cm^{-1} ν(C=C) stretching region. Arrows indicate rotation around indicated carbon. (Weiss et al. 2010a)

In vivo Raman spectroscopy mapping

The Raman spectroscopy analysis presented here indicates that specific Raman bands can be used as markers for the presence of botryococcenes in live *B. braunii* cells and/or colonies. This is especially true for the 1647 cm^{-1} band that is specific for indicating the presence of methylated botryococcenes (Fig. 40A). Thus, Raman microspectroscopy was applied to a colony of *B. braunii* to map the presence of botryococcenes in the extracellular matrix and intracellular oil bodies. A roughly circular region within a 13 × 13-μm area of a *B. braunii* colony was scanned as shown in Fig. 44B. Raman spectroscopy required photobleaching the cells because chlorophyll autofluorescence caused high background that interfered with detection of botryococcene-specific Raman bands (Fig. 45). Spectroscopy was implemented after photobleaching, and the Raman spectrum in the 1700–1600 cm^{-1} region is shown in Fig. 44A. Detection of the botryococcene methylation-specific 1647 cm^{-1} band was evident and was the most prominent band in the spectrum (Fig. 44A). The high level of background within this spectrum prevented us from defining other botryococcene specific bands.

Next, we mapped the detection of the botryococcene methylation-specific 1647 cm^{-1} band at 54 points yielding a spectral map of the scanned region of the *B. braunii* colony. The presence of the 1647 cm^{-1} band was assigned a white color with diminishing detection levels of the 1647 cm^{-1} band scaled to gray. Because our cells were photobleached prior to Raman analysis, the cells and extracellular matrix could not be distinguished by a microscopy image. Thus, Fig. 44D shows a graphical representation

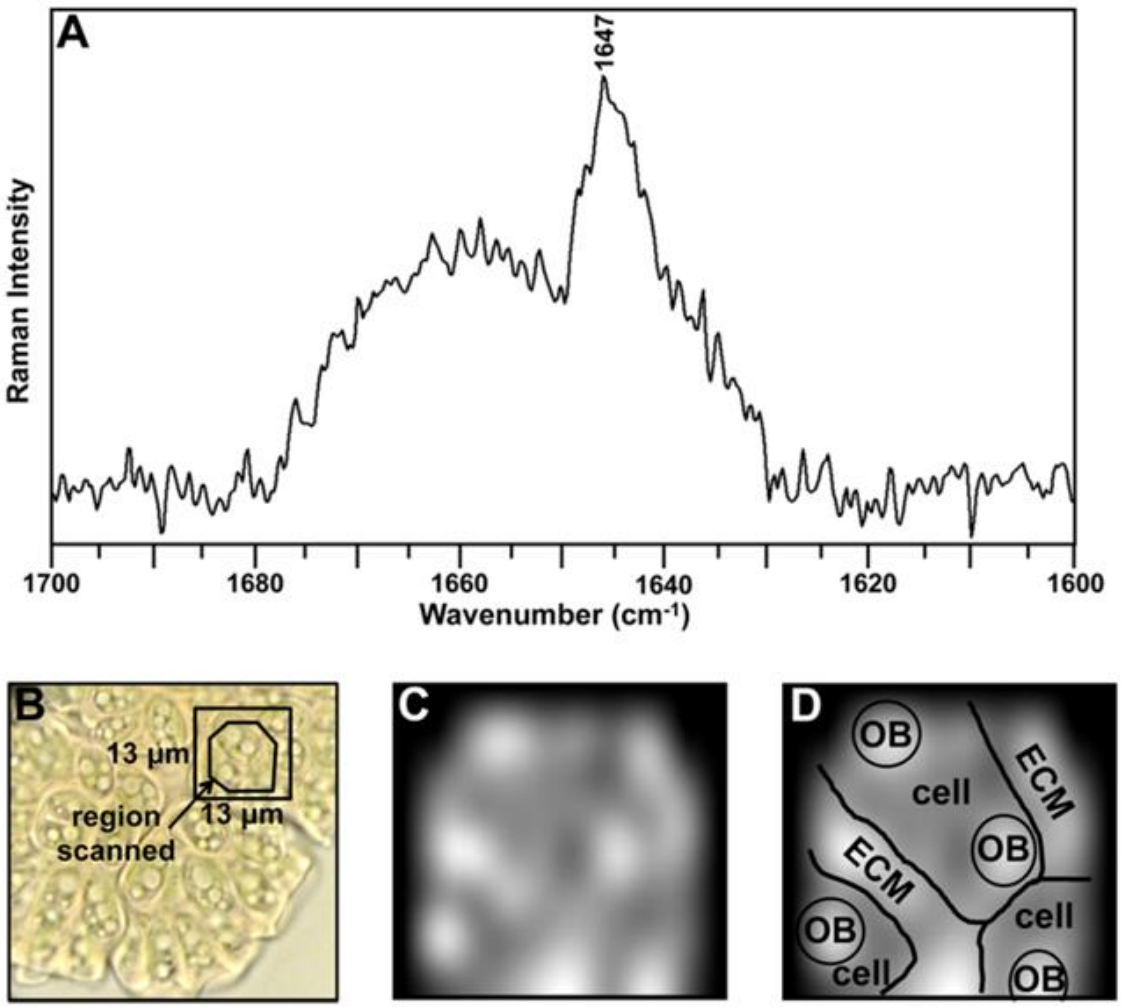

FIGURE 44. Mapping of methylated botryococcenes in a *B. braunii* colony. (A) *In vivo* Raman spectrum of a *B. braunii* colony. The laser of the confocal Raman microscope was focused on a 13×13 µm region of a colony of *B. braunii*, as shown in (B), and the Raman spectrum of the region recorded. (B) Light microscope image of the *B. braunii* colony before photobleaching for Raman spectroscopy. Boxed region indicates region used for analysis in (A). (C) Mapping of the 1647 cm^{-1}-specific botryococcene Raman band in the *B. braunii* colony. (D) Graphical representation of colony structure in (C). OB, oil body; ECM, extracellular matrix. (Weiss et al. 2010a)

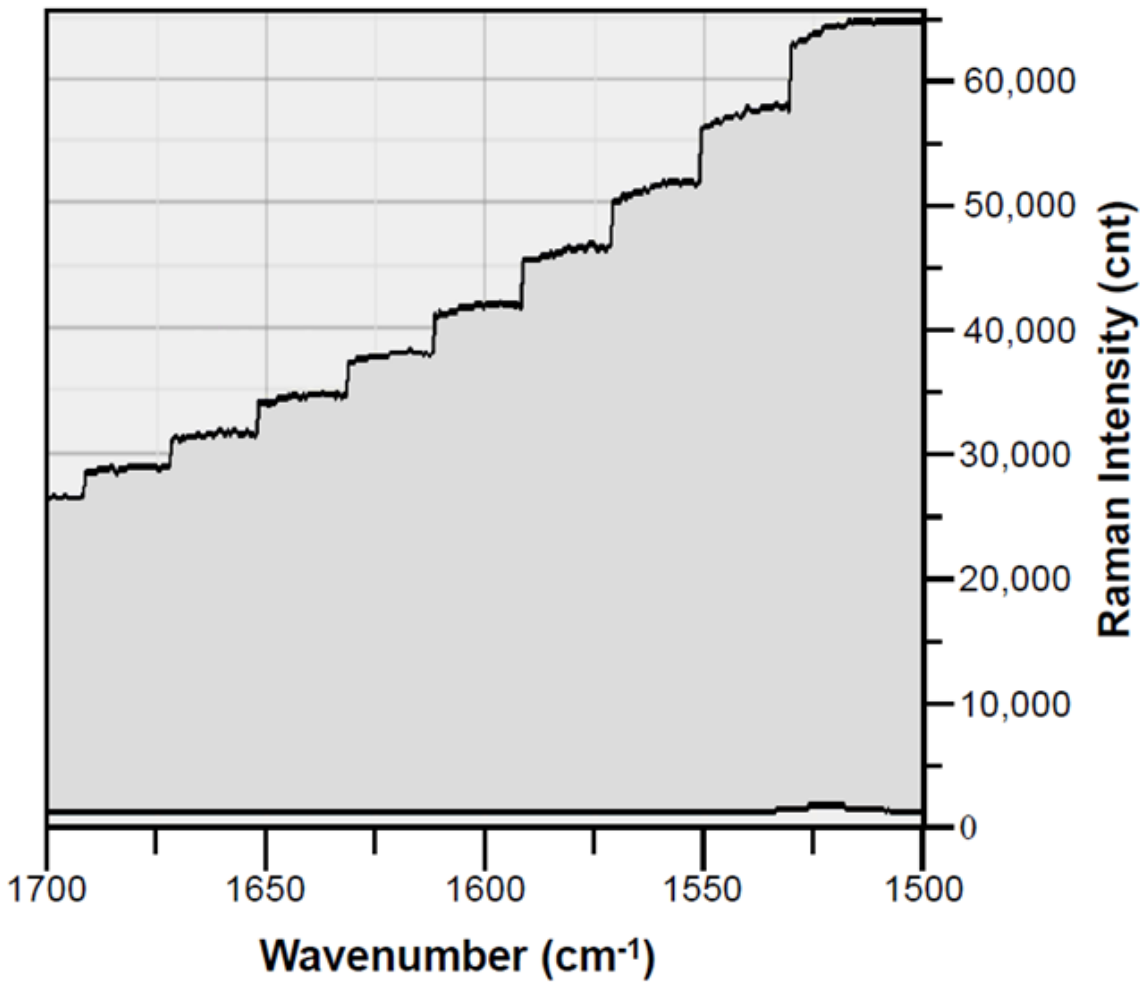

FIGURE 45. *B. braunii* autofluorescence degradation during photobleaching. *B. braunii* colonies strongly autofluoresce using a 785 nm laser, but the magnitude quickly degrades as cells are photobleached yielding a step-like spectra as each portion of wavenumbers is collected. The first spectrum (top black line) was collected from a *B. braunii* colony at the onset of a 20 minute photobleaching treatment. Each "step" equals approximately 1 minute of data collection under photobleaching conditions. Photobleaching was considered complete when a stable baseline intensity was observed. The second spectrum (bottom black line) was collected after 20 minutes of photobleaching treatment indicating the complete loss of background autofluorescence. In this second spectra, the band at ~1520 cm-1 is from carotenoids. (Weiss et al. 2010a)

of the colony and cell structure. The results show, as expected and reported (Casadevall et al. 1984; Wolf et al. 1985; Metzger et al. 1987), that the extracellular matrix has high amounts of methylated botryococcenes (Fig. 44C,D), likely C_{34} botryococcene because it is mostly found in the extracellular matrix (Maxwell et al. 1968; Knights et al. 1970; Wolf et al. 1985; Metzger et al. 1987; Banerjee et al. 2002). The intracellular oil bodies also contained methylated botryococcenes as determined by detection of the 1647 cm^{-1} band (Fig. 44C,D). Unfortunately, we were not able to determine the specific botryococcene makeup of the individual oil bodies beyond the presence of methylated botryococcenes because we were not able to assign and map additional Raman bands due to the high background in our analysis and sample degradation from prolonged interrogation (Fig. 44A).

B. braunii also produces squalene-based hydrocarbons that contain exomethylene groups similar to that found in botryococcenes. Tetramethylsqualene is produced by methylation at C-3, -7, -18, and -22 of squalene, which produces exomethylene groups at C-1, -26, -29, and -24 (Fig. 10; Huang 1989b; Okada et al. 1995; Achitouv et al. 2004). Tetramethylsqualene can also be combined with long chain polyaldehydes and carotenoids to produce polyacetals and botryoxanthins, respectively (Okada et al. 1996; Okada et al. 1998; Metzger et al. 2007). Because of the exomethylene similarities between methylated botryococcenes and tetramethylsqualene, it is possible that our detection of the 1647 cm^{-1} band in the *B. braunii* colony (Fig. 44A) is partially attributable to tetramethylsqualene and its derivatives. However, the levels of free tetramethylsqualene and botryoxanthins in *B. braunii* colonies are minute (0.009–

0.033% dry weight) (Huang et al. 1989b; Okada et al. 1995; Okada et al. 1996; Okada et al. 1998; Metzger et al. 2007) and thus, unlikely to be detected by our Raman system. However, one strain of *B. braunii*, race B, contains levels of methylated squalenes up to 4.5% dry weight (Achitouv et al. 2004). Levels of tetramethylsqualene polyacetals are much higher and can comprise up to 10% of algal dry weight (Metzger et al. 2007). This suggests that *in vivo* Raman microspectroscopy detection may be possible and that these compounds may contribute to the detection and mapping of the 1647 cm^{-1} band in Fig. 44. But it should be noted that tetramethylsqualene polyacetals are found predominantly within the *B. braunii* cell walls and not in oil bodies (Metzger et al. 2007). Exact wavenumber assignment to the C=C bonds in tetramethylsqualene and its derivatives will require isolation of pure compounds and Raman spectroscopy analysis. Given the difficulty in isolating milligram quantities of these compounds, DFT calculations may offer the best approach for estimating wavenumber assignments.

Conclusions

These studies have identified specific Raman spectroscopic characteristics for botryococcenes of *B. braunii*, B race. Additionally, as a botryococcene methylation-specific Raman signature can be detected in living *B. braunii* cells, this indicates that intracellular oil bodies are indeed composed of botryococcenes. It also suggests that Raman spectroscopy is a powerful tool that can be applied to advancing studies on botryococcene biosynthesis. A goal for future studies is to refine the Raman microspectroscopy using instrumentation appropriate to very small photosynthetic cells

to fine-map the presence of the different botryococcene homologs in a colony of *B. braunii*. Of particular interest will be the location of the different botryococcenes within the cells to determine whether there is a biosynthetic, or composition difference among the many intracellular oil bodies. Additionally, Raman spectroscopy could be applied to analyze botryococcene levels and quality during the development of a *B. braunii* culture to determine when oil levels are of both maximal quantity and quality for cell harvesting.

CHAPTER VI

COMPUTATIONAL ANALYSIS OF B. BRAUNII TRITERPENE SYNTHASES AND SSL-1 PURIFICATION FOR X-RAY CRYSTALLOGRAPHY

Introduction

As a ubiquitous enzyme providing a critical cellular function, squalene synthase (SS) has been studied in a variety of organisms, though none more so than in humans where it plays a critical role in cholesterol synthesis (Bergstrom et al. 1993). As a reflection of this importance, the *Homo sapiens* squalene synthase (HsSS) has been crystallized and its structure solved (Thompson et al. 1998; Pandit et al. 2000). Since then however, no other SS structures from other organisms have been solved. This may be in part due to the significant challenges and limitations to the HsSS crystallization process (Thompson et al. 1998; Pandit et al. 2000). In any event, the HsSS remains the primary source of SS structural information. This narrow foundation poses one of the most significant impediments to understanding the enzymatic mechanism of botryococcene synthesis in the *B. braunii* B race.

Because the function of SS is so well conserved, sequential differences between SS from different organisms appear generally cosmetic. The publication of Niehaus et al. (2010) however has shown that cosmetically similar BSS, SSL-1, SSL-2, and SSL-3 possess differentiation enzymatic function. So in a situation where it is not intuitively obvious how an enzyme like BSS, but not SSL-1, can catalyze the formation of

squalene, understanding how botryococcenes are synthesized also requires a reexamination of the mechanism of squalene formation in detail.

In pursuit of such a reexamination and to understand what specific residues contribute to the differentiated enzymatic activities of BSS, SSL-1, SSL-2, and SSL-3, we have conducted computational sequential and homology modeling analysis. Additionally, we have successfully expressed, purified, and sufficiently stabilized SSL-1 for promising results in early crystallography experiments.

Triterpene synthase computational analysis

Sequence alignment

Using sequence alignment, in general, the four triterpene synthases of *B. braunii* appear highly conserved, but in fact possess several key differences (Fig. 46). These differences can be most easily dissected into the following categories: N- and C-terminal domain length, “flap”, numbered domains, FPP binding residues, and the NADPH binding domain.

The most obvious terminal disparities are small variations in the number of N-terminal residues and significantly longer C-terminal hydrophobic tails of BSS and SSL-2 (Fig. 46; Niehaus et al. 2010). This is important since the hydrophobic tail of SS has been shown to be ER associated (Stamellos et al. 1993) and the length and content of the C-termini suggest both BSS and SSL-2 may be similarly associated (Niehaus et al. 2010). Without such a hydrophobic tail, the possible differences in localization or mobility of the botryococcene biosynthetic enzymes SSL-1 and SSL-3 are not clear.

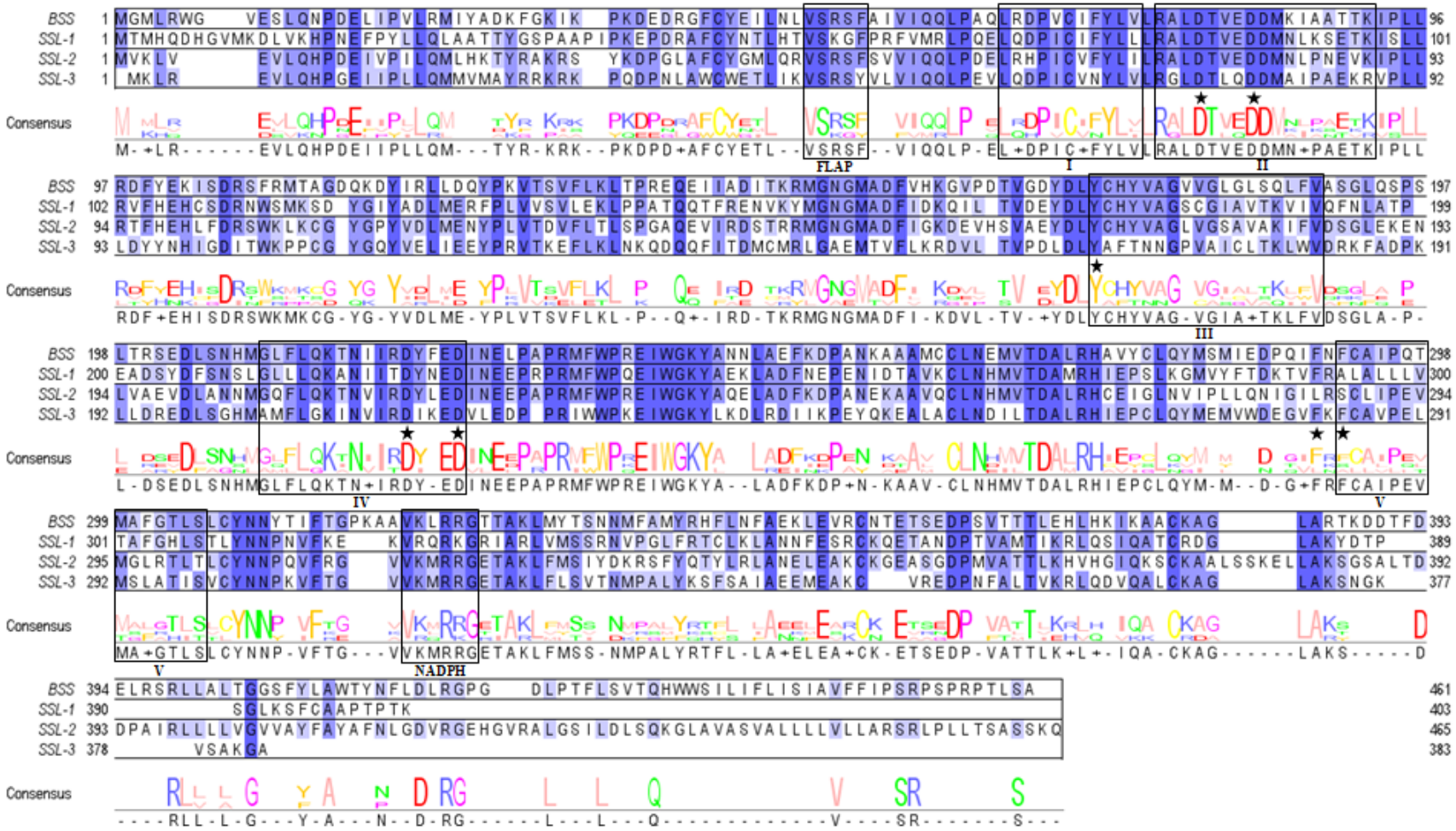

FIGURE 46. Amino acid sequence alignment of *B. braunii* triterpene synthases. Residues highlighted in dark blue are identical and light blue are similar. The "FLAP," NADPH binding, and five conserved domains (I-V) of squalene synthases are boxed (Robinson et al. 1993). Residues critical for squalene synthase activity are starred (Gu et al. 1998; Pandit et al. 2000). Note that BSS and SSL-2 have C-terminal, hydrophobic tails while SSL-1 and SSL-3 do not.

With respect to the highly conserved "flap," which seals off one open end of the catalytic channel between helices A and B, BSS and SSL-2 are again highly similar in that they share the identical sequence "VSRSF" (Fig. 46; Pandit et al. 2000). By contrast the flap of SSL-1 and SSL-3 are both different containing two and one dissimilar residues, respectively (Fig. 46). This difference is noteworthy for several reasons. First, the sequence of the SS flap is among the most highly conserved sequence among all species (Pandit et al. 2000). Second, the flap plays a critical enzymatic role in capping and excluding water from the hydrophobic channel that makes up the active site (Pandit et. al 2000). Third, several SS inhibitors have been shown to function by binding to and disrupting flap motion (Pandit et al. 2000). Altogether, the nonconserved sequence of SSL-1 and SSL-3, which together uniquely catalyze the formation of botryococcene, is extremely interesting.

While the descriptions of the *B. braunii* triterpene synthase termini and flap may break down clearly into BSS and SSL-2 vs. SSL-1 and SSL-3, discussions of the SS numbered domains are not so clear. In general, domains I and IV are highly identical, domain V is moderately similar, and, except for SSL-3, domains II and III are roughly half identical and half similar (Fig. 46). The difference of SSL-3 sequence in comparison to the other enzymes is perhaps most striking. The first ten residues of domain II in BSS, SSL-1, and SSL-2 are identical (RALDTVEDDM) while SSL-3 is different by three non-similar residues (RGLDTLCRRM; Fig. 46). This difference, though noticeable, seems small in comparison to the differences within domain III. In this case, the first seven residues of domain III in BSS, SSL-1, and SSL-2 are again identical

(YCHYVAG) while SSL-3 is this time different by five residues non-similar (YAFTNNG; Fig. 46). While parsing out how each nonconserved residue might contribute to different product outcomes would be very difficult, the conserved portions of each numbered domain do contain residues known to be critical for catalytic function (Gu et al. 1998).

The conserved residues critical for SS function can be roughly broken down into three categories: substrate binding, intermediate interaction, or product formation. For substrate binding, SS has two recognized motifs: one, DxxxDD, is found in domain I, and a second, DxxED, is found in domain IV (Fig. 46; Pandit et al. 2000). These sequences appear to be closely similar to the sequence DDxxD, which is a recognizable motif for the binding of diphosphate moieties using Mg^{+2} ions in Class I isoprenoid biosynthetic enzymes (Pandit et al. 2000). In this light, it is not surprising that all four *B. braunii* triterpene synthases retain these critical aspartate residues. More informative perhaps is the single identified critical residue of domain III.

Domain III begins with a highly conserved tyrosine residue, which in SS has been specifically implicated in several interactions which facilitate PSPP formation (Fig. 46; Gu et al. 1998; Pandit. et al. 2000). It is believed this tyrosine accomplishes this through π orbital stabilization of the carbocation intermediate and proton donation (Gu et al. 1998). What is notable about this residue however is that though this important tyrosine residue appears conserved in all *B. braunii* triterpene synthases, the surrounding residues of SSL-3 do not (Fig. 46). Given the critical and multi-purpose role of this tyrosine in squalene synthesis, it may be reasonable to hypothesize that altering the

spatial orientation of this residue may be important in directing botryococcene synthesis instead. However, similar consideration should be given to a pair of phenylalanine residues at the start of domain V (Fig. 46).

Overall, domain V is the least conserved domain of the *B. braunii* triterpene synthases (Fig. 46). This is especially noteworthy because domain V and its two phenylalanine residues have been directly implicated in catalyzing the second step of squalene formation from the PSPP intermediate (Gu et al. 1998). If true, conservation of these phenylalanine residues might be expected to direct squalene synthesis while different variations allow for the alternative formation of botryococcenes. This speculation does not correlate to enzymatic activities however. Though BSS possess these two phenylalanine residues (F290 and F292), SSL-2, which also catalyzes the synthesis of squalene, does not possess either phenylalanine while SSL-3, which catalyzes the synthesis of botryococcene, possesses both (F283 and F285; Fig. 46). This is completely counterintuitive to expectations. Such expectations are further complicated by the fact that SSL-1, which only participates in the first catalysis of squalene synthesis, PSPP formation, possesses one conserved phenylalanine residue (F292). Since a close inspection of critical residues is not immediately informative, one last region of interest is the pattern of conservation in the NADPH binding domain.

BSS, SSL-2, and SSL-3 all catalyze a reaction requiring NADPH, so it is not so surprising that they each posses nearly identical, six-residue NADPH binding domains (Fig. 46). SSL-1 however, which only catalyzes PSPP formation, does not utilize NADPH and appears to have low sequence consensus with the triterpene synthases that

do (Fig. 46). While a narrow view of the NADPH domain sequence seems to indicate a straightforward correlation to NADPH binding, the importance of protein structure between this domain and domain V casts some uncertainty on this relationship (Fig. 46). This intermediary region, known as the J-K loop by Pandit et al (2000), was therefore examined in greater detail using structure homology modeling.

Structure homology modeling

Homology modeling is essentially an attempt to predict the structure of a target protein computationally using a similar homologous protein structure as a template. We used SWISS-MODEL (http://swissmodel.expasy.org/) and the sequences of all four *B. braunii* triterpene synthases, *Nicotiana tabacum* SS, and *Homo sapiens* SS built upon the *H. sapiens* SS crystal structure. Modeling the *H. sapiens* protein onto itself was an important control to identify regions of poor prediction and cover gaps where residues had not been solved in the crystal structure. Our modeling suggests little divergence except for helix J, helix K, and especially the region between them, the J-K loop (Fig. 47; Pandit et al. 2000). The J-K loop region plays a critical role in the model of *H. sapiens* SS function as it provides a flexible linker between the catalytically important helix J and NADPH binding helix K (Pandit et al. 2000). In fact, the J-K loop was so named because it was so flexible that the region was unsolved by X-ray crystallography (Pandit et al. 2000). This lies in stark contrast to all other sequences modeled, even the *N. tabacum* SS, which are predicted to be helical (Fig. 47). The reasoning for this

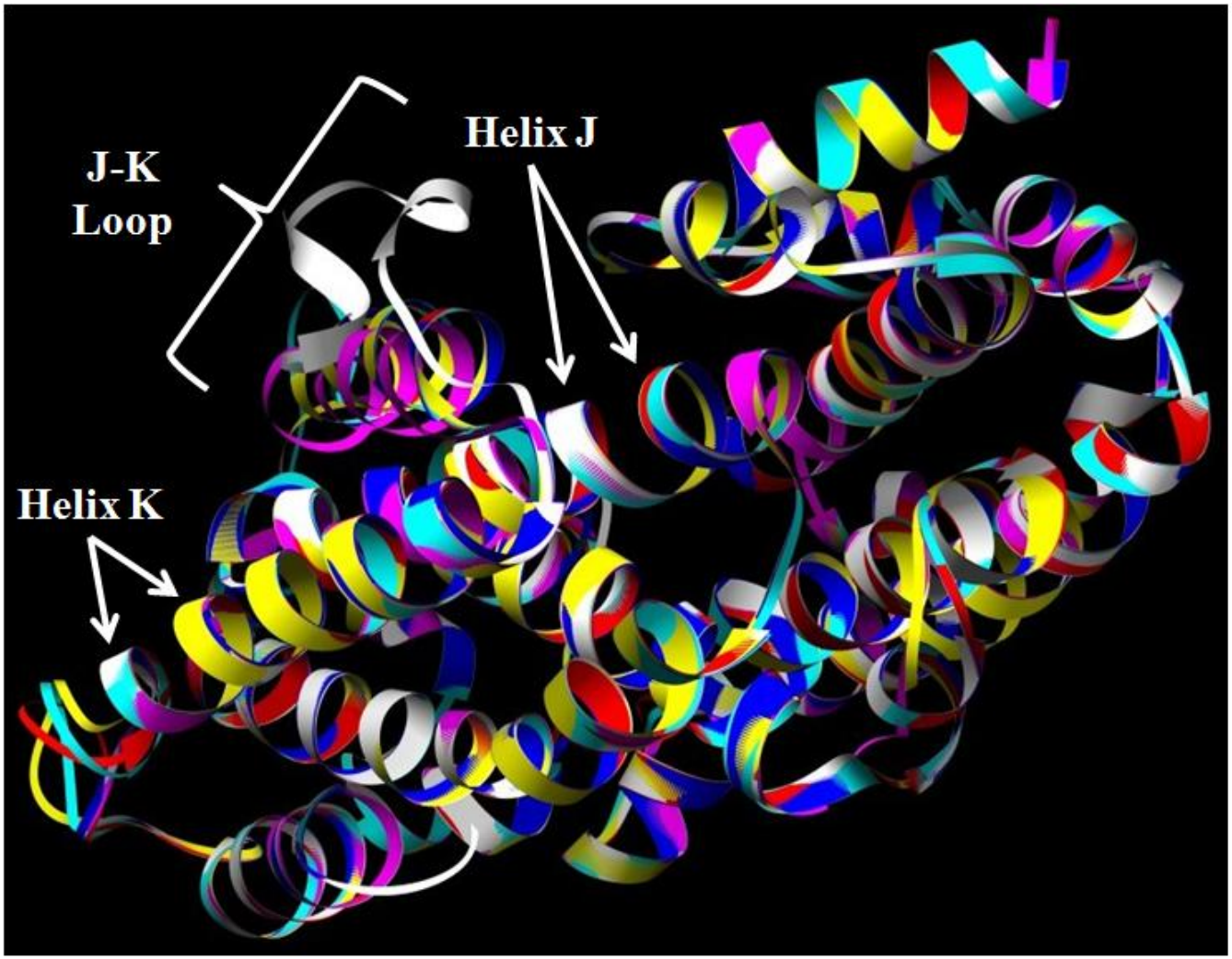

FIGURE 47. ***B. braunii*** **triterpene synthase homology modeling.** Homology models of BSS (cyan), SSL-1 (red), SSL-2 (yellow), SSL-3 (blue), *Nicotiana tabacum* squalene synthase (SS; purple), and *Homo sapiens* SS (white)based on the crystal structure of the *H. sapiens* SS from Pandit et al. (2000). Helix J roughly corresponds to Domain V, while the J-K loop and Helix K to the NADPH binding domain of Robinson et al. (1993). Each synthase appear highly similar except for a predicted helix in the region of the *H. sapiens* J-K loop.

prediction becomes more obvious when looking at a sequence alignment of this specific region for all six modeled sequencing (Fig. 48).

Alignment of the J-K loop region reveals several surprises: one, the J helix appears somewhat conserved while the K helix is not; two, the NADPH binding domain appears nearly identical in the SSL-2, SSL-3, and *N. tabacum* SS, but divergent in the remaining sequences; and three, BSS possesses a unique three amino acid insertion in the J-K loop (Fig. 48). This last observation is perhaps most surprising of all since BSS is the only *B. braunii* triterpene synthase which functions as a true squalene synthase. Thus, though the J-K loop region appears helical in all but the *H. sapiens* SS, what significance, if any, this region contributes in determining *B. braunii* triterpene synthase function remains unclear.

SSL-1 purification and crystal screening

Computational analysis generated several regions of interest to study in determining the critical residues in triterpene synthase function, but alone failed to hint at any clear relationships. Thus we decided to pursue an X-ray crystallography study of each triterpene synthase. Due to significant technical impediments in dealing with the proteins however, we have not yet achieved this goal. With respect to SSL-1 specifically however, we have taken many of the necessary steps of successfully designing a purification strategy, stabilizing the purified protein, and generating some promising initial crystallography results.

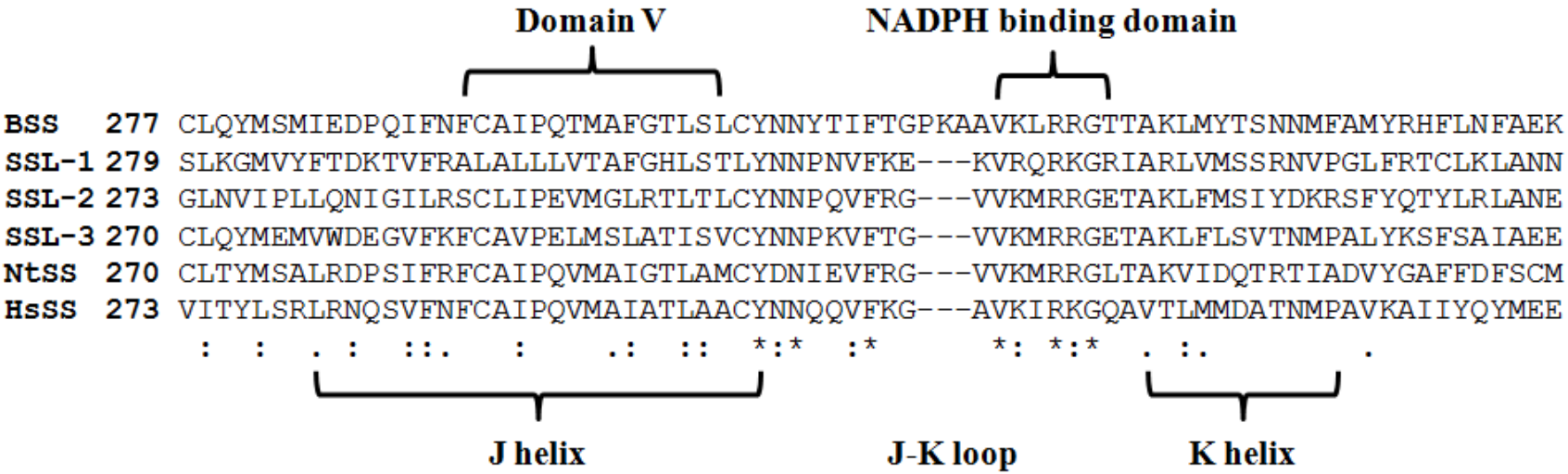

FIGURE 48. Sequence alignment of select *B. braunii* triterpene synthase J-K helices. Alignment of the four *B. braunii* triterpene synthases plus squalene synthases from *Nicotiana tabacum* (NtSS) and *Homo sapiens* (HsSS). The Domain V and NADPH binding domains indicated were assigned to the HsSS by Robinson et al. (1993). The J helix, J-K loop, and K helix indicated were assigned to the HsSS by Pandit et al. (2000).

SSL-1 purification relies upon an N-terminal 6× histidine tag (N-6xHis) using a Co^{+2} affinity column like that described by our collaborators in Niehaus et al. (2010). While this basic purification process was successful, it proved inadequate for crystallography studies due to protein degradation and instability at room temperatures. Compensating for protein degradation was resolved by a thorough cold-shock treatment prior to induction, expression at low temperatures, and purification using pre-chilled equipment maintained at 4 °C at all times. More problematic however was the need to maintain N-6xHis-SSL-1 solubility at or near the temperatures at which crystallography would be conducted. Such stability screening assays based on the absorption of soluble protein would eventually generate conditions which either improved upon or completely replaced those used by Niehaus et al. (2010).

The first stage of N-6xHis-SSL-1 stability screening focused on pH, salt, basic stabilizing agents, and temperature (Table 3). This screening revealed that after 24 hours, N-6xHis-SSL-1 was more stable: at pHs slightly above or below neutral; in the presence of NaCl more than other salts; in the presence of glycerol; and at low temperatures (Table 3). None of these results were surprising except for pH, which suggested that the calculated pI = 7.2 of N-6xHis-SSL-1 may not be an accurate reflection of its true pI since it appeared more stable at pH 7 than at pH 8. This result suggested that previous purifications at pH = 8.0 were unfavorable. So to next test a new range of pHs, new buffers also needed to be screened.

The second stage of N-6xHis-SSL-1 stability screening focused on buffers near the pH of their maximum buffering capacity and stabilizing agents while temperature

Condition	Abs_{280}			% Abs_{280} Remaining
	Blank	Sample	Difference	24 hours
pH (500 mM Tris)				
5.7	0.696	0.637	-0.059	-11.8
7	0.625	0.741	0.116	23.2
8	0.676	0.667	-0.009	-1.8
9	0.681	0.689	0.008	1.6
9.9	0.652	0.710	0.058	11.6
11.6	0.675	0.898	0.223	44.6
Salt (500 mM)				
NaCl	1.122	1.185	0.063	12.6
KCl	0.648	0.651	0.003	0.6
LiCl	1.104	1.104	0.000	0.0
$MgCl_2$	0.648	0.658	0.010	2.0
Stabilizing agent				
10% glycerol	0.968	0.995	0.027	5.4
20% glycerol	0.679	0.786	0.107	21.4
500 mM imidazole	0.814	0.789	-0.025	-5.0
Temperature (°C)				
4	1.255	1.530	0.275	55.0
23	1.255	1.261	0.006	1.2
37	1.255	nd	nd	nd

TABLE 3. N-6xHis-SSL-1 stability assay #1 results. All test samples contained 10 mM Tris, pH 8.0 from the initial purification in addition to the specific reagent listed and was stored at 23 °C unless otherwise specified. Each sample also contained a standard starting condition with sufficient protein for $Abs_{280} = 0.5$. nd = not determined due to sample evaporation.

remained a comparative control (Tables 4, 5). Building upon the results of the last screening, the conditions all included NaCl and glycerol which greatly enhanced the stability of N-6xHis-SSL-1 requiring a second day of screening. While a few conditions were obviously better after 24 hours (Table 4), when the best were reassessed after 48 hours, N-6xHis-SSL-1 was most stable with buffers MOPS (pH 6.5), TEA (pH 8.5), and AMPSO (pH 8.5) and also was further stabilized by the addition of even higher amounts of glycerol (Table 5). To confirm these results and to make sure buffer absorption was not biasing the results a third stage of stability screening was conducted.

The third and final stage of N-6xHis-SSL-1 stability screening focused comparing the most promising results of the previous absorption-based assays using SDS-PAGE (Fig. 49). This screening revealed that after 72 hours, N-6xHis-SSL-1 was most stable using MOPS (pH 6.5) or TEA (pH 8.5) and that the addition of glycerol and use of low temperatures were extremely conducive to N-6xHis-SSL-1 stability (Fig. 49). This further revealed that: one, AMPSO (pH 8.5) was not as beneficial as predicted by absorption measurements; and two, that conditions have been found under which pure N-6xHis-SSL-1 could be purified and used for crystallography screening without rapid precipitation under the necessary conditions.

Initial crystallography screening trials using purified protein (Fig. 50) failed to generate any crystal useful for structural analysis, but would routinely produce irregular microcrystals under a variety of conditions similar to those used by Pandit et al. (2000) to crystallize a truncated version of the *H. sapiens* SS (Fig. 51). Because these

Condition	Abs_{280}			% Abs_{280} Remaining 24 hours
	Blank	Sample	Difference	
Buffer (500 mM*)				
Na Acetate, pH 5.6	0.739	1.031	0.292	58.4
Na Cacodylate, pH 6.5	0.750	0.773	0.023	4.6
MES, pH 6.5	0.710	0.996	0.286	57.2
MOPS, pH 6.5	0.691	1.014	0.323	64.6
PIPES, pH 6.6	0.695	0.975	0.280	56.0
HEPES, pH 7.6	0.711	0.924	0.213	42.6
BisTris Propane, pH 8.4	-0.301	0.037	0.338	67.6
Tris, pH 8.5	0.777	1.153	0.376	75.2
Tricine, pH 8.5	0.701	1.045	0.344	68.8
TAPS, pH 8.5	0.924	1.186	0.262	52.4
TEA, pH 8.5	0.675	1.026	0.351	70.2
Na Malonate, pH 8.5	0.706	1.017	0.311	62.2
AMPSO, pH 8.5	1.673	2.252	0.579	115.8
Bicine, pH 8.5	0.744	0.959	0.215	43.0
CHES, pH 8.5	0.682	1.024	0.342	68.4
CAPS, pH 8.5	0.816	1.059	0.243	48.6
Stabilizing agent				
30% glycerol	0.978	1.334	0.356	71.2
40% glycerol	0.951	1.370	0.419	83.8
6% 1,4-butanediol	0.759	1.120	0.361	72.2
6% 2-methyl-2,4-pentanediol	0.719	1.068	0.349	69.8
5% ethylene glycol	0.973	1.220	0.247	49.4
10% ethylene glycol	0.900	1.201	0.301	60.2
Temperature (°C)				
4	1.070	1.450	0.380	76.0
23	1.093	1.405	0.312	62.4

TABLE 4. N-6xHis-SSL-1 stability assay #2 results (24 hours). All test samples contained 10 mM Tris, pH 8.5 and 500 mM NaCl from the initial purification plus 20% glycerol in addition to the specific reagent listed and was stored at 23 °C unless otherwise specified. Each sample also contained a standard starting condition with sufficient protein for Abs_{280} = 0.5. *All additive buffers were tested at 500 mM except for AMPSO and CHES, which were tested at 250 mM due to solubility limitations.

Condition	Abs_{280}			% Abs_{280} Remaining 48 hours
	Blank	Sample	Difference	
Buffer (500 mM*)				
MOPS, pH 6.5	0.692	1.020	0.328	65.6
BisTris Propane, pH 8.4	0.156	0.358	0.202	40.4
Tris, pH 8.5	0.768	0.875	0.107	21.4
Tricine, pH 8.5	0.707	0.871	0.164	32.8
TEA, pH 8.5	0.703	1.068	0.365	73.0
AMPSO, pH 8.5	1.692	2.156	0.464	92.8
CHES, pH 8.5	0.819	0.941	0.122	24.4
Stabilizing agent				
30% glycerol	0.981	1.301	0.320	64.0
40% glycerol	0.952	1.343	0.391	78.2
6% 1,4-butanediol	0.745	0.886	0.141	28.2
6% 2-methyl-2,4-pentanediol	0.702	0.856	0.154	30.8
Temperature (°C)				
4	1.046	1.357	0.311	62.2
23	1.081	1.316	0.235	47.0

TABLE 5. N-6xHis-SSL-1 stability assay #2 results (48 hours). All test samples contained 10 mM Tris, pH 8.5 and 500 mM NaCl from the initial purification plus 20% glycerol in addition to the specific reagent listed and was stored at 23 °C unless otherwise specified. Each sample also contained a standard starting condition with sufficient protein for Abs_{280} = 0.5. *All additive buffers were tested at 500 mM except for AMPSO and CHES, which were tested at 250 mM due to solubility limitations.

A

Condition	Abs_{280}			% Abs_{280} Remaining
	Blank	Sample	Difference	72 hours
Temperature (°C)				
23	1.095	1.330	0.235	47.0
4	1.068	1.379	0.311	62.2
Buffer (500 mM*)				
Tris, pH 8.5	0.778	0.885	0.107	21.4
Na Cacodylate, pH 6.5	0.750	nd	nd	nd
MOPS, pH 6.5	0.692	1.020	0.328	65.6
TEA, pH 8.5	0.676	1.041	0.365	73.0
AMPSO, pH 8.5	1.671	2.135	0.464	92.8
CHES, pH 8.5	0.682	0.804	0.122	24.4
Stabilizing agent				
30% glycerol	0.977	1.297	0.320	64.0
40% glycerol	0.952	1.343	0.391	78.2

B

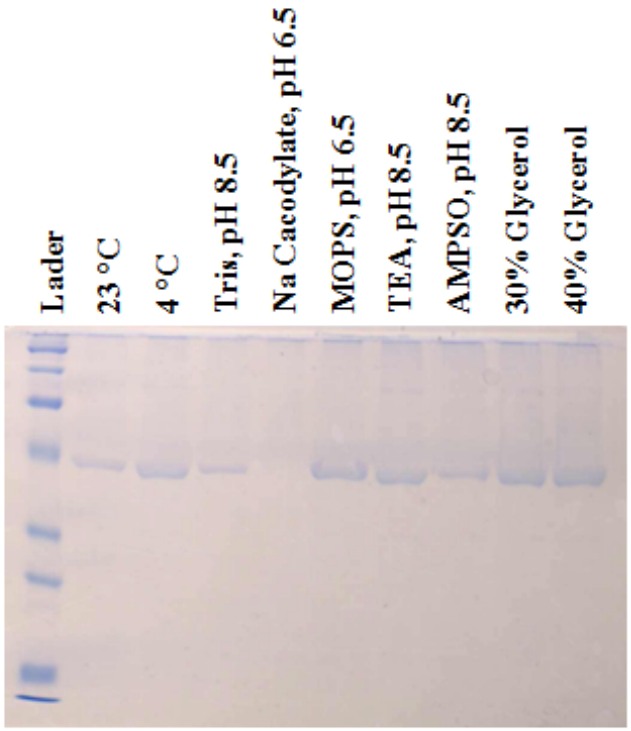

FIGURE 49. N-6xHis-SSL-1 stability assay #3 results. (A) Solubility as measured by Abs_{280}. (B) Solubility as visualized by SDS-PAGE. The two methods appear in agreement except for AMPSO, which strongly absorbs at 280 nm. All test samples contained 10 mM Tris, pH 8.5 and 500 mM NaCl from the initial purification plus 20% glycerol in addition to the specific reagent listed and was stored at 23 °C unless otherwise specified. Each sample also contained a standard starting condition with sufficient protein for Abs_{280} = 0.5. *All additive buffers were tested at 500 mM except for AMPSO and CHES, which were tested at 250 mM due to solubility limitations.

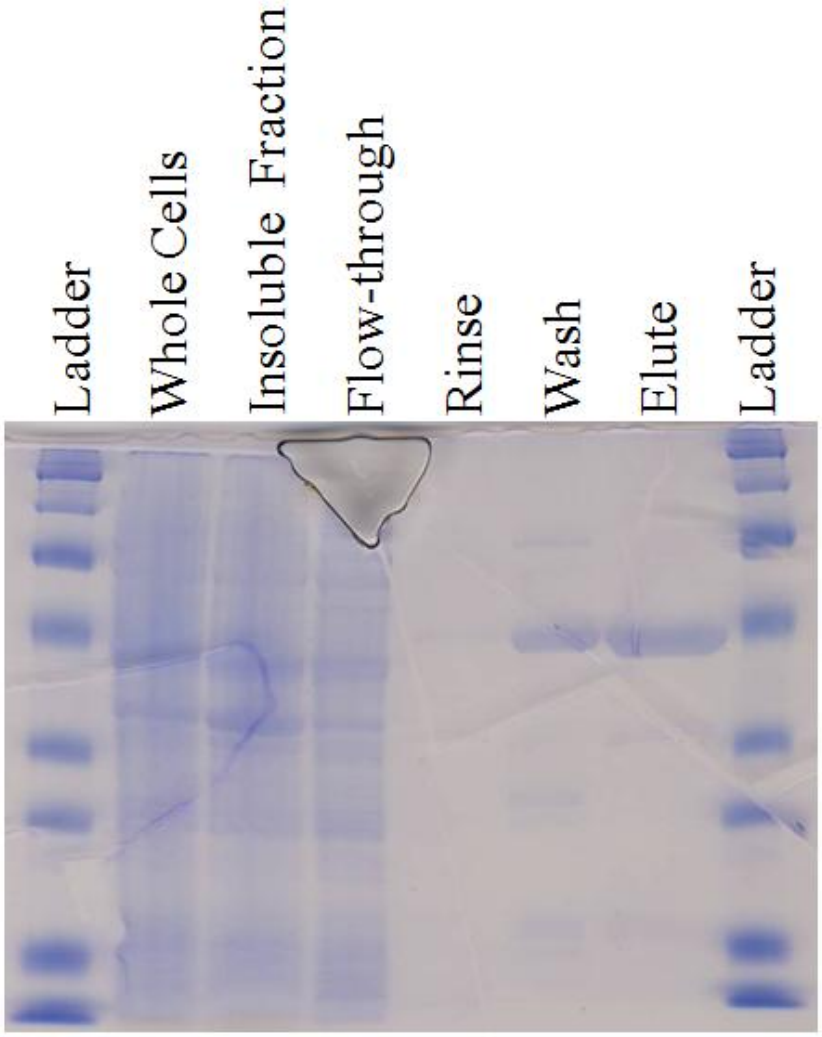

FIGURE 50. N-6xHis-SSL-1 purification. SDS-PAGE illustrating the results of 3 L of E. coli culture purified on a 5 mL Co^{+2} affinity column. Buffers contained 20 mM MOPS, pH 6.5 and 500 mM NaCl. Imidazole concentrations: rinse = 25 mM, wash = 75 mM, and elute = 250 mM. N-6xHis-SSL-1 consistently eluted at two distinct imidazole concentrations with greater impurities observed at the lower concentration.

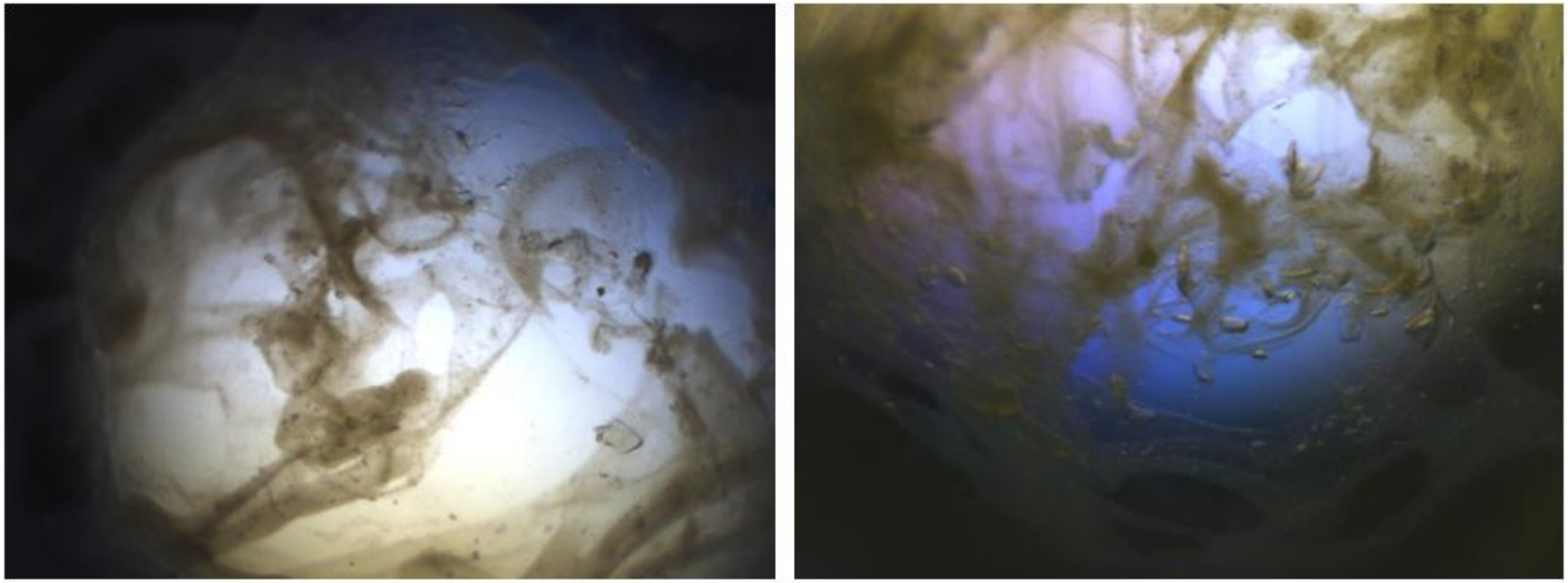

FIGURE 51. N-6xHis-SSL-1 microcrystals. N-6xHis-SSL-1 illustrated a propensity for rapid precipitation across a variety of conditions, but also frequently formed irregular microcrystals. Similar microcrystals were previously described during the crystallization of a twice truncated human squalene synthase (Pandit et al. 2000).

microcrystals formed easily and under a variety of similar conditions (MOPS pH 6-8 and PEG 4000 18-24%), this gives hope that SSL-1 might someday be crystallized.

Conclusions

Computational studies of the *B. braunii* triterpene synthases reveal that the question of how each enzyme derives its specificity will not be answered without further experimental structural studies. Towards this goal, though N-6xHis-SSL-1 was never successfully crystallized, the critical improvements in discovering stable conditions for the purified protein may benefit any *in vitro* assay requiring purified SSL-1. Fortunately, the detailed study and stabilization of SSL-1 should also contribute the technical feasibility of additional studies regarding the other *B. braunii* triterpene synthases. As even the *H. sapiens* SS could never be crystallized without a bound inhibitor however, the success of future crystallography trials for each enzyme may require significant screenings of appropriate inhibitors and/or additional detergents.

CHAPTER VII

NMR ANALYSIS OF B. BRAUNII, A RACE YAMANAKA ALKADIENE SYNTHESIS AND ISOMERIZATION

Introduction

One of the more interesting aspects of the *B. braunii* A race hydrocarbon synthesis has always been the prevalence of *trans* isomers at each unsaturated position. As A race hydrocarbons are thought to be derived from fatty acids, which contain *cis* double bonds, this seems very strange since only some bacteria, like *Vibrio* and *Pseudomonas* are known to transiently isomerize *cis* double bonds for the formation of *trans* fatty acids in response to high temperature or chemical attack (Morita et al. 1993; von Waalbrunn et al. 2003; Ferreri et al. 2007). *Vibrio* and *Pseudomonas* do so only after fatty acid synthesis is complete and use a special fatty acid isomerase which does not necessitate a positional shift of the double bond (Morita et al. 1993; von Waalbrunn et al. 2003). So how the *B. braunii* A race can utilize *trans* fatty acids as substrates during hydrocarbon synthesis and then accumulate *trans* bond containing products in large quantities is both exceptionally rare and not well understood (Templier et al. 1991; Metzger and Largeau 2005).

In order to study these *trans* alkenes and observe if environmental stimuli had any effect on their synthesis we began an investigation using ^{13}C NMR and the *B. braunii* A race strain Yamanaka. Because the Yamanaka strain only synthesizes a roughly equal mixture of C_{27} and C_{29} ω9 alkadienes it offers a simpler system for this

purpose than other strains (Okada et al. 1995). While the study was unfortunately hampered by severe culturing problems soon after the experiments began, the preliminary data we successfully collected strongly indicate that the ω9 alkadiene *cis*:*trans* population is notably affected by environmental stimuli and implicate a post-synthesis isomerization event.

Results

Because of the high abundance of alkadienes that can be extracted from *B. braunii*, A race Yamanaka biomass and roughly 1% natural occurrence of ^{13}C, 1D ^{13}C NMR was easy to use with and without the introduction of additional isotope and generated distinct peaks corresponding to terminal and double-bond adjacent carbons under different growth conditions (Fig. 52). All spectra corresponded with previously documented spectra and assignments (Metzger et al. 1986). Some carbons could not be individually assigned (k), because they belong to long stretches of saturated carbon-carbon bonds (Fig. 52). Samples were also further analyzed by mass spectrometry to monitor any change in the populations of different length alkadienes; however, regardless of the growth condition, every sample remained similar with primarily 45% C_{27} and 50% C_{29} alkadienes—a makeup previously described by Okada et al (1995). Because mass spectrometry cannot be used to specifically observe ω9 alkadiene bond orientation and formation alone, the study was therefore conducted in two parts with and without heterotrophic ^{13}C isotopic labeling.

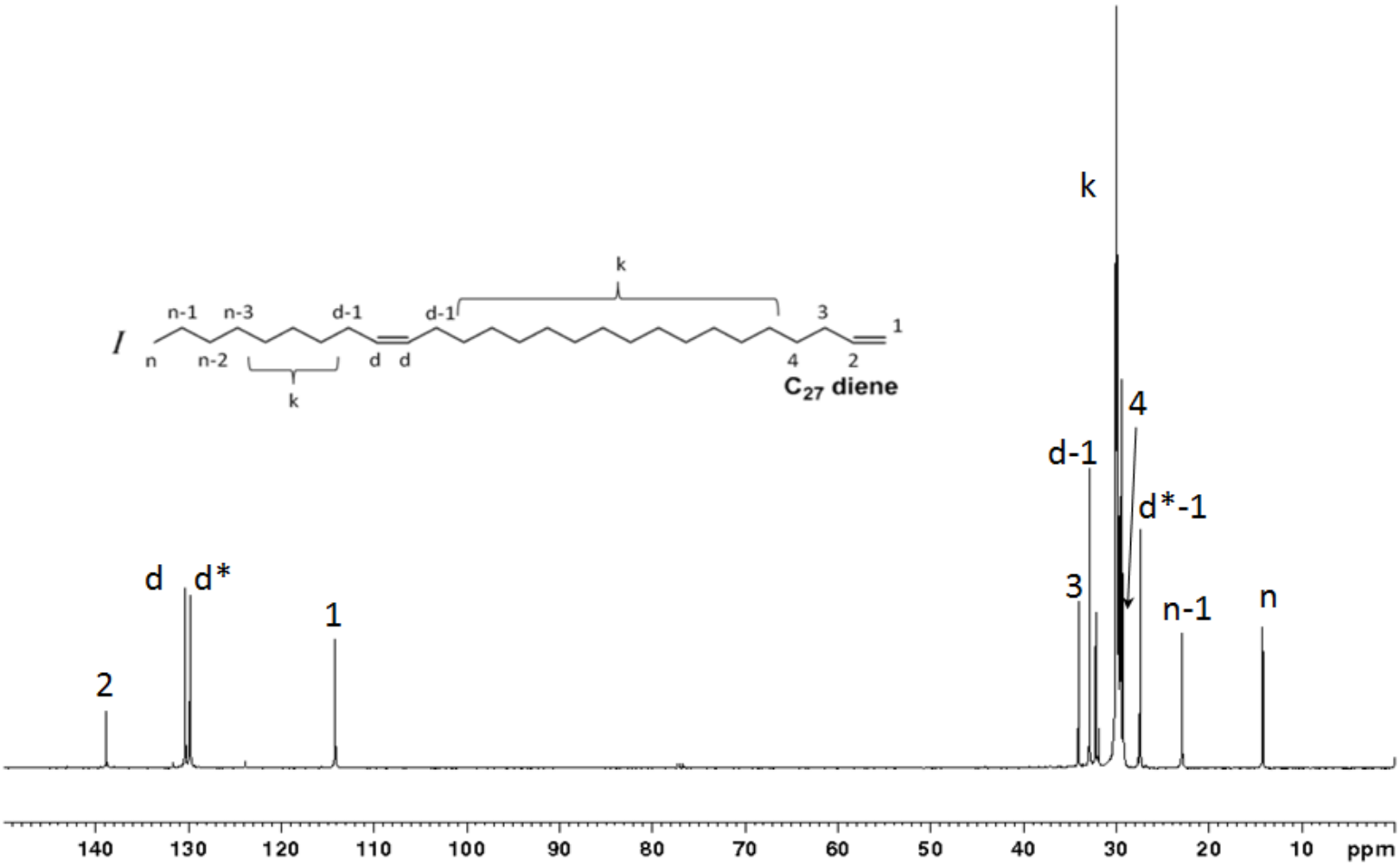

FIGURE 52. ***B. braunii*** **A race alkadiene NMR spectra.** Example NMR spectra of natural abundance, 1D ^{13}C NMR of *B. braunii*, A race Yamanka extracted alkadienes. Assigned peaks are demonstrated on a C_{27} diene. Bonds in the k regions cannot be distinguished. Peaks d and d-1 correspond to the *cis* conformation of the ω9 bond, as shown, but that peaks d* and d*-1 correspond to the *trans* conformation of the same bond. The sample analyzed here contained a roughly equal mixture of each isomer.

Our observations of the ω9 alkadiene bond orientation using unlabeled, phototrophic growth vs. dark, heterotrophic growth using glucose or acetate generated several findings (Fig. 53). Among the findings: first, phototrophic growth yields a nearly equal ratio of ω9 alkadiene *cis*:*trans* isomers (49:51); second, the ^{13}C isotope from glucose was successfully integrated into alkadienes synthesis but not from acetate; third, heterotrophic growth conditions generated an identical, new *cis*:*trans* ratio (29:71); and fourth, that the *cis*:*trans* ratios of naturally ^{13}C labeled and artificially ^{13}C labeled ω9 alkadienes were identical using a glucose carbon source (Fig. 53). This last finding was especially surprising and takes advantage of the fact that ^{13}C labeled carbons experience an isotopic shift. Since the heterotrophic growth used a mixture of 15% ^{13}C labeled and 85% unlabeled glucose, isotopically shifted ω9 carbon peaks could only have been introduced into alkadienes by ^{13}C labeled glucose metabolism at the time of heterotrophic growth while non-isotopically shifted ω9 carbon peaks would be the additive result of alkadienes synthesized and accumulated before and after heterotrophic growth. So in essence, since the *cis*/*trans* ratios of new alkadienes vs. new plus old alkadienes are equal and not 49:51, it can be concluded that heterotrophic growth somehow leads to the promotion of the *trans* isomer post-synthesis. Dissecting the causative factor found in heterotrophic growth was further examined in a second series of observations.

To dissect the factors of light and carbon availability a screen of *B. braunii*, A race Yamanaka cultures were made using ± light and ± 2.5% CO_2 (Fig. 54). Because this culturing screen took advantage of naturally occurring ^{13}C, no additional carbon

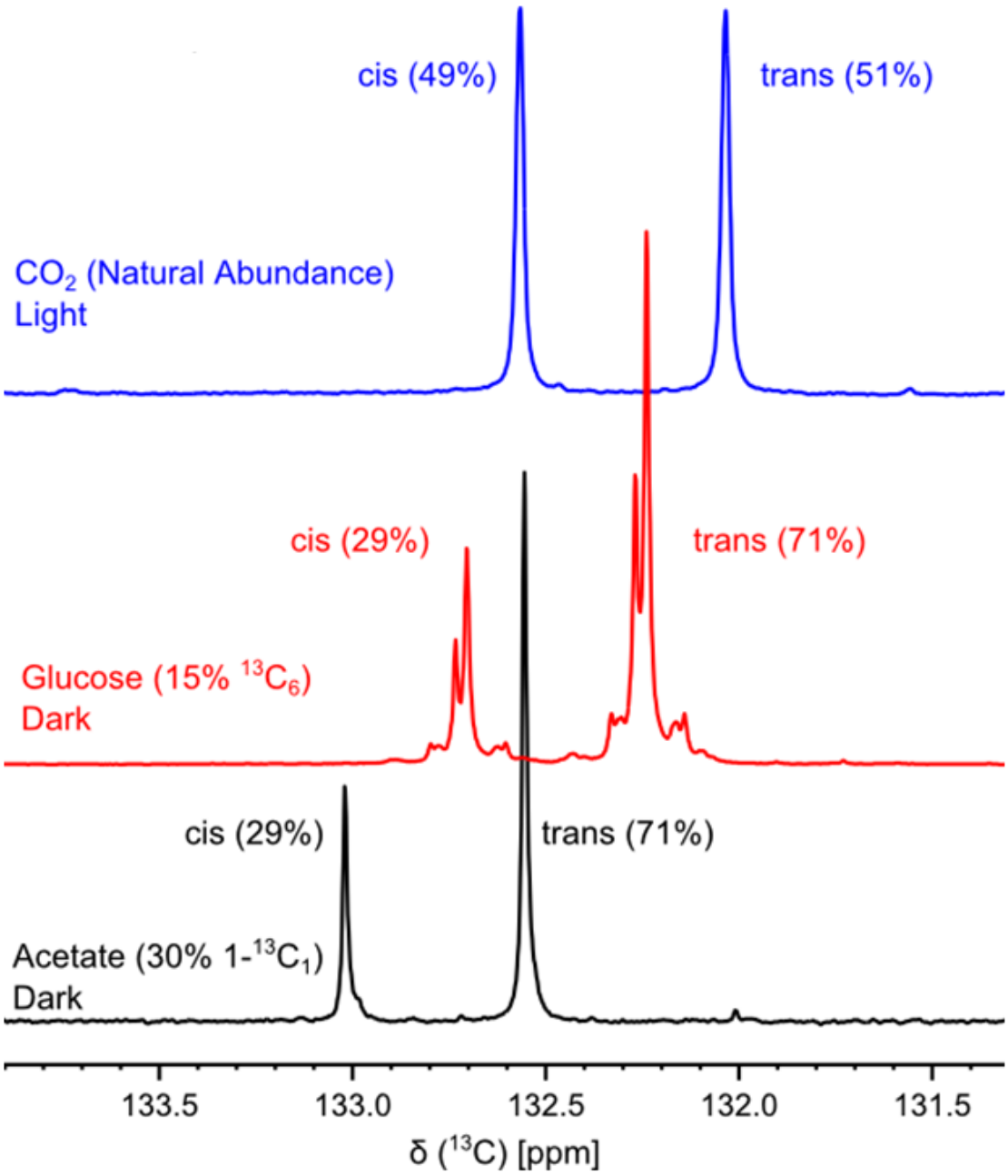

FIGURE 53. ***B. braunii*** **A race alkadiene ω9 conformation under heterotrophic conditions.** Three alkadiene samples corresponding to growth with CO_2 in the light (blue), with 15% $^{13}C_6$ glucose in the dark (red), or 30% $^{13}C_1$ acetate in the dark (black). The select NMR peaks correspond to the alkadiene ω9 bond and each sample is offset for easy viewing. Under typical growth conditions, the Yamanka strain accumulates *cis* and *trans* ω9 isomer alkadienes equally (blue). While in the dark, *B. braunii* easily incorporate $^{13}C_6$ glucose into alkadienes so that they contain both new labeled alkadienes and old, naturally labeled alkadienes which can be distinguished by isotope shift (red). This indicates that both old and newly synthesized alkadienes are equally isomerized to favor the *trans* ω9 bond orientation under such conditions. This same isomerization can be seen in the acetate experiment even though the label was not incorporated into alkadiene synthesis (black).

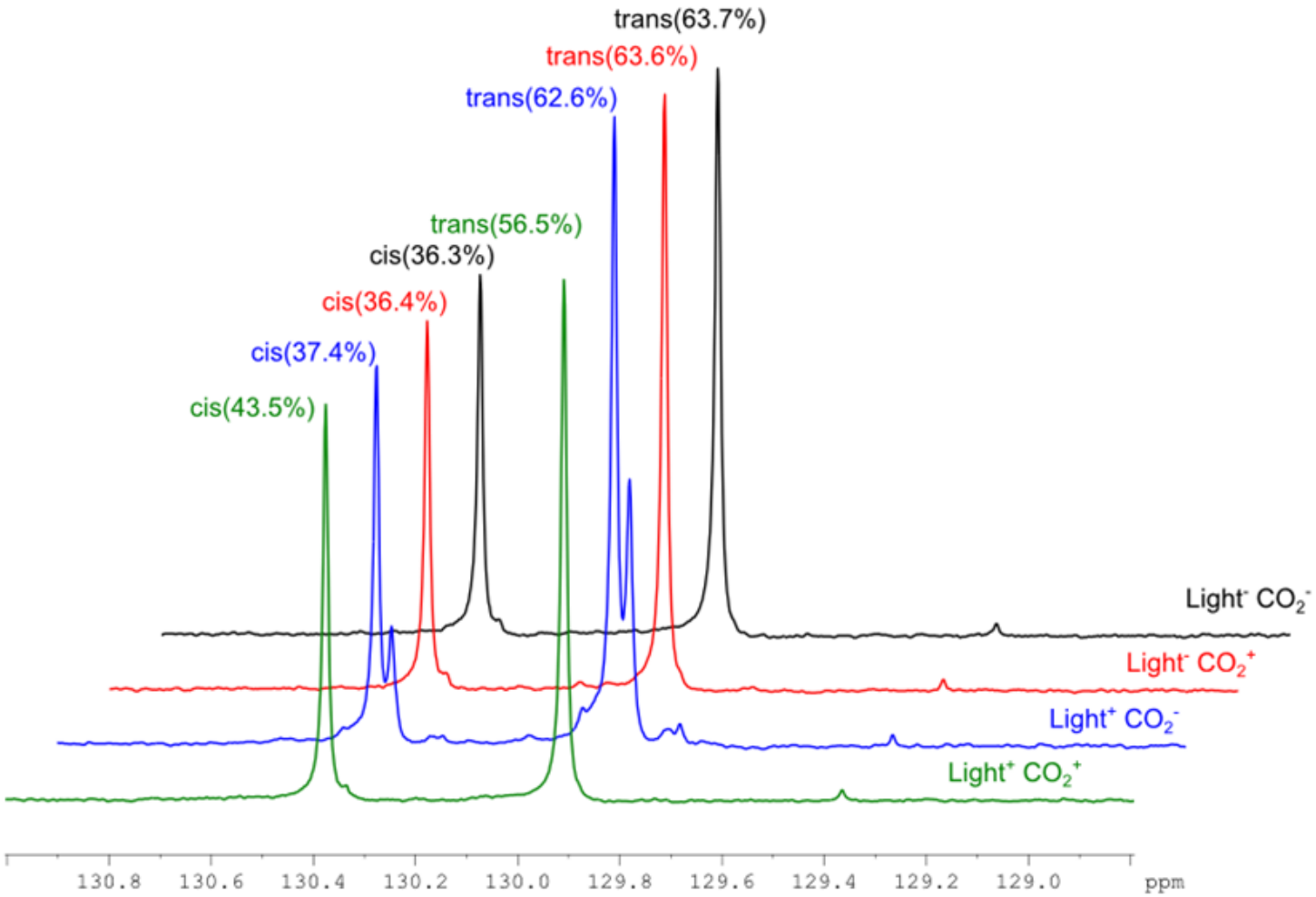

FIGURE 54. ***B. braunii*** **A race alkadiene ω9 conformation under phototrophic conditions.** The select NMR peaks correspond to the alkadiene ω9 bond and each sample is offset for easy viewing. Under a screen of four conditions (+/- light and +/- CO_2) *B. braunii* shifted to favor a *trans* ω9 conformation under any non-ideal phototrophic condition and at near identical ratios (black, red, blue). The double-peaks of the +light, -CO_2 condition was the result of labeled alkadiene contamination from an incompletely washed flask and should be ignored. Additionally, over the course of this ten day experiment, the supply of CO_2 was interrupted for two days which was sufficient to cause a small shift of the cis trans ratio compared to constant phototrophic conditions (green line).

source besides CO_2 was added and all growth was strictly phototrophic. However, during the course of the ten day experiment, the supply of 2.5% CO_2 was exhausted on day 3 and was not replaced until day 5. As a result, the experiment actually benefitted from the additional information garnered by comparing the interrupted 10 day phototrophic growth to the uninterrupted 10 day phototrophic growth of the first set of observations. It is important to note that because every culture was bubbled with air even the "– 2.5% CO_2" conditions received an input of 0.039% atmospheric CO_2. With each of these important caveats in mind, the findings of the phototrophic conditions screening include: first, even a brief interruption in 2.5% CO_2 supply was sufficient to alter the ω9 alkadiene *cis*:*trans* ratio from the previously measured 49:51 to 43.5:56.5; second, the *cis*:*trans* ratio of – light/+ 2.5% CO_2 and – light/– 2.5% CO_2 were nearly identical at 36.4:63.6 vs. 36.3:63.7, respectively; and third, the ω9 alkadiene *cis*:*trans* ratio was 37.4:62.6, which is smaller than the ideal phototrophic condition, but larger than the non-ideal phototrophic conditions. Despite the + light/– 2.5% CO_2 sample being partially compromised by contamination, these results overall suggest that the shift in ratios favoring the ω9 alkadiene *trans* conformation is not a function of light nor available CO_2 alone, but rather somehow a reflection of both. More specifically, remembering that heterotrophic growth on glucose or acetate generated identical ω9 alkadiene *cis*:*trans* ratios, the favorability *trans* alkadienes accumulation seems directly linked to the favorability of photosynthesis and not levels of carbon input.

Conclusions

Collectively, these new NMR studies of the *B. braunii* A race open several new avenues of alkadiene synthesis studies. Though now only suggestive, the possibility that the *B. braunii* A race may respond to environmental stimuli and isomerize alkadienes is exciting and novel. Questions also remain as to how or why the *B. braunii* A race benefits from the synthesis of *trans* alkadienes at all. Whether such mechanisms are similar or novel in comparison to bacteria like *Vibrio* and *Pseudomonas* also remains to be seen. As alkadienes are predominately stored outside the cell however and the magnitude of observed *cis*/*trans* ratio shift suggests these extracellular hydrocarbons may be isomerized, the possibility of a novel extracellular isomerase which does not require the positional shift of the double bond is tantalizing. Such studies would not only be a benefit to the understanding of the mechanisms of the A race, but to *B. braunii* studies as a whole and possibly the usefulness of alkadienes in biofuel production.

CHAPTER VIII

SUMMARY AND FUTURE DIRECTIONS

The results of the experiments, data, and analysis of this study have collectively produced information which adds to and even changes our knowledge about *B. braunii*. Beyond just *B. braunii* however, these studies have also contributed to the development of tools and methods useful for studying algae, non-model organisms, and lipid synthesis in general.

Our phylogenetic analyses not only corrected a generally accepted error in the literature, but also established the relation of the three races of *B. braunii*. Though sequencing clearly suggests that the isoprenoid synthesizing B and L races are more closely related to each other than to the A race, these same data will contribute to much broader sequencing projects as well. Sharing 18S rDNA sequences on world-wide servers will help others to identify *B. braunii* in the future especially when sampling from the environment. While these are future applications, just contributing the sequences of genes to databases is important because so few algae sequences are available to represent such a vast number of species. Adding our sequences slowly adds to this ever growing body of knowledge which will support further phylogenetic studies in the future. Adding our estimated genome sizes helps similarly.

While our genome sizing specifically reveals that the L race genome is significantly larger than the A or B, this discovery may also suggest how the three *B. braunii* races diverged to evolve along their own separate path. Our estimations are also

critical foundational information for genome sequencing projects which, at the time of our work, are underway for both the A and B race (www.jgi.doe.gov). Transcriptomic and proteomic studies by and with collaborators are similarly underway. All of these sequencing projects will collectively establish a strong foundation for *B. braunii* and green algae molecular studies in general. It will also speed the isolation of novel genes and projects which require genetic modification. Both aims may lead to improvements in algae biofuel feedstock. Such pursuits will also require better tools however and one such tool could be Raman microspectroscopy.

We were the first to collect the individual Raman spectra of several botryococcenes and apply this knowledge to map their locations within living *B. braunii* cells. This research not only lays out a methodical approach to the cellular mapping of individual molecules of interest, but also opens other paths of inquiry into analytical Raman spectroscopy. Our computational analysis of theoretical botryococcene Raman spectra proved that the υ(C=C) stretching of large molecules could be accurately predicted by DFT. The comparison and contrast of these predictions to our experimental data, in addition to what is already known about squalene, provide the basis for refining and improving Raman prediction of large molecules. Improvements in such predictions would be immeasurably helpful in the study of molecules which cannot be individually purified for experimental use. In some ways however this application is dwarfed by the potential applications of Raman microspectroscopy to algae.

While Raman spectroscopy has been applied to algae for many years, our research shows that it is possible to derive qualitative and semi-quantitative lipid data

from a single, live cell. This lies in stark contrast to current methods which generally require the destruction of many cells, lipid extraction and isolation, and/or rely on variable lipophilic fluorescent indicators. Raman spectroscopy is also particularly suited to working with algae, because it is not sensitive to water so that algae may be monitored with minimal sample preparation or even in their native environment. We have taken advantage of this already in our collaboration with Dr. Arum Han and Hyun Soo Kim of the Department of Electrical and Computer Engineering at Texas A&M University. Detailed in a manuscript in preparation, they have designed microfluidic plates which may capture, culture under a screen of conditions, and allow for the analysis of individual *B. braunii* colonies using various forms of microscopy. We have already found that Raman spectroscopy may be successfully applied to the analysis of colonies trapped within the devices. This opens a world of possibilities where in screening both qualitatively and quantitatively for a biofuel product in algae might be possible under a host of growth conditions. So too might the technology be applied to high-throughput screening of isolated mutants for a desired genetic trait. While these microfluidic plates would be a new tool for the study of photosynthetic cells, we have also helped pursue the improvement of Raman spectroscopy for the purpose of biological imaging. In collaboration with Dr. Wei-Chuan Shih and Ji Qi of the Department of Electrical and Computer Engineering at the University of Houston, we have begun to document many improvements in the preparation of algae for Raman spectroscopy and they seek to create an instrument capable of interrogating several points simultaneously. Such an improvement would allow for rapid 2D or even 3D imaging of samples and reduce

sample degradation—a key concern in biological Raman spectroscopy. Such applications are more far-flung than just studies of *B. braunii*, but we have expanded areas into this focus as well.

Where Raman spectroscopy may not be a suitable tool for studying the *B. braunii* A race hydrocarbons, we have shown that isotopic labeling and NMR may be applied to simultaneously interrogate molecular characteristics of alkadiene synthesis and modification in response to the phototrophic environment. While it is known that *trans* bonds in fatty acids are rare, we still do not know what biological purpose the accumulation of *trans* alkadienes might serve in *B. braunii*. Why *B. braunii* would promote the population of *trans* over *cis* alkadienes through isomerization is another question. While these questions only hint at the possibility of a novel isomerase activity it supports the premise that the synthesis of *B. braunii* hydrocarbons is not simply a matter of floatation and that the cells act to modify their hydrocarbons in direct response to their environment. Clearly the synthesis of these oils is more complicated than initial appearances would suggest, much like *B. braunii* botryococcene synthesis.

In our collaboration with Dr. Joe Chappell and Tom Niehaus of the Department of Plant and Soil Sciences at the University of Kentucky we learned that botryococcenes are synthesized not by one enzyme, but by two and that an alternative mechanism exists in *B. braunii* to synthesize squalene. Our own efforts have clearly shown that understanding what enzymatically differentiates makes each of the four *B. braunii* triterpene synthases will require more than just computational analysis. And while our X-ray crystallography approach has yet to generate data, our method of SSL-1

purification and stabilization will undoubtedly prove helpful in further *in vitro* studies of SSL-1. Given the high degree of similarity between the four *B. braunii* triterpene synthases the preparation of SSL-1 should also serve as a guide for the purification and stabilization of the BSS, SSL-2, and SSL-3 as well. Beyond *B. braunii* and beyond algae even, our studies have demonstrated the weaknesses of a human-centric squalene synthase model. Features and motifs which have been assigned special significance in the *H. sapiens* SS and are presumed to be highly conserved in all species do not appear in BSS by sequence or homology modeling. Thus, studies of the *B. braunii* triterpene synthases may well alter and improve the general model of squalene synthase function. Further studies will also undoubtedly be required for the genetic modification of *B. braunii* or genetic engineering of other organisms to produce botryococcenes for use in biofuel production. However modification of *B. braunii* will also require a better basic knowledge of *B. braunii* molecular biology and that is perhaps where we have made the most contributions.

Our studies of *B. braunii* structural elements from a histochemical perspective have revealed that *B. braunii* structural polysaccharides may be as novel as its hydrocarbons. We have found that the exterior of colonies is wrapped in a layer composed solely of neutral residues of arabinose and galactose, both with occasional methyl modifications, and also an unknown deoxyhexose. This polysaccharide composition is novel and NMR studies are now underway in collaboration with Dr. Parastoo Azadi at the University of Georgia Complex Carbohydrate Research Center to assess its molecular structure and identify the unknown deoxyhexose. Equally novel is

the isolation of shells which suggests *B. braunii* actively disperses pieces of the colony outer layer into solution in a manner perhaps similar to the shedding of bark on trees. Also interesting is that fluorescence microscopy suggests each individual *B. braunii* cell is encompassed by its own polysaccharide retaining wall. This would mean that each individual cell makes its own individual contribution to the oily extracellular matrix surrounding it in a compartmentalized fashion designed to retain the oil in close proximity to the cell. Nile red staining also showed that there are spots of inhomogeneity in the oily extracellular matrix in and around the cells which have not been previously described. The significance of this inhomogeneity is not known at this time nor is the reasoning for some, but not all, cell walls to stain with Congo red suggesting cellulose-like composition. All of these questions and many more are currently being explored using electron microscopy in collaboration with Dr. Ursula Goodenough and Robyn Roth of the Department of Biology at the University of Washington in St. Louis. These experiments have already begun to yield many more interesting findings on the unique nature and composition of *B. braunii* cells that contributes to their unique ability to produce large quantities of hydrocarbons.

While *B. braunii* studies will likely remain driven by a focus on algae biofuel research for the foreseeable future, we have found so many novel and unique qualities about *B. braunii* that there is strong justification to continue basic biological research as well. For as much as we believe *B. braunii* is unique, the truth is that we cannot be certain with so few other algae being studied in equal detail. It may well be that the many unique traits we associate with *B. braunii* are quite common, if simply less

pronounced, in many algae. So while further study of *B. braunii* would certainly benefit biofuels it may well also reshape our entire thinking about algae as a whole.

REFERENCES

Aaronson, S., Berner, T., Gold, K., Kushner, L., Patni, N. J., Repak, A., and Rubin, D. 1983. Some observations on the green planktonic alga, *Botryococcus braunii* and its bloom form. *J. Plankton Res* 5:693-700.

Achitouv, E., Metzger, P., Rager, M-N., and Largeau, C. 2004. C_{31}-C_{34} methylated squalenes from a Bolivian strain of *Botryococcus braunii*. *Phytochem.* 65:3159–3165.

Adam, P., Schaeffer, P., and Albrecht, P. 2006. C_{40} monoaromatic lycopane derivatives as indicators of the contribution of the alga *Botryococcus braunii* race L to the organic matter of Messel oil shale (Eocene, Germany). *Org. Geochem.* 37:584–596.

Adl, S. M., Simpson, A. G. B., Farmer, M. A., Andersen, R. A., Anderson, O. R., Barta, J. R. et al. 2005. The New Higher Level Classification of Eukaryotes with Emphasis on the Taxonomy of Protists. *J. Eukaryot. Microbiol.*, 52:399–451.

Allard, B. and Casadevall, E. 1990. Carbohydrate Composition and Characterization of Sugars from the Green Microalga *Botryococcus braunii*. *Phytochem.* 29:1875-1878.

Altschul, S. F., Gish, W., Miller, W., Myers, E. W., and Lipman, D. J. 1990. Basic local alignment search tool. *J. Mol. Biol.* 215:403–10.

Audino M., Grice K., Alexander R., and Kagi R. I. 2002. Macrocyclic alkanes in crude oils from the algaenan of *Botryococcus braunii*. *Org. Geochem.* 33:979–984.

Banerjee, A., Sharma, R., Chisti, Y. and Banerjee, U. C. 2002. *Botryococcus braunii*: a renewable source of hydrocarbons and other chemicals. *Crit. Rev. Biotechnol*. 22:245–79.

Barow, M. and Meister, A. 2002. Lack of correlation between AT frequency and genome size in higher plants and the effect of nonrandomness of base sequences on dye binding. *Cytometry* 47:1–7.

Beakes, C. W. and Cleary, A. L. 1999. Visualization of plastids and lipophilic components in living colonies of a wild strain of the hydrocarbon-forming green alga *Botryococcus* by laser scanning confocal microscopy. *Appl. Phycol*. 10:435-446.

Behar F., Derenne S., Largeau C. 1995. Closed pyrolyses of the isoprenoid algaenan of *Botryococcus braunii*, L race: geochemical implications for derived kerogens. *Geochim. Cosmochim. Acta.* 59:2983–2997.

Bennett, M. D., Bhandol, P. and Leitch, I. J. 2000. Nuclear DNA amounts in angiosperms and their modern uses-807 new estimates. *Ann. Bot.* 86:859–909.

Bennett, M. D. and Leitch, I. J. 2005. Nuclear DNA amounts in angiosperms: progress, problems and prospects. *Ann. Bot.* 95:45–90.

Bergstrom, J. D., Kurtz, M. M., Rew, D. J., Amend, A. M., Karkas, J. D., Bosterdor, R. G., et al. 1993. Zaragozic acids: A family of fungal metabolites that are picomolar competitive inhibitors of squalene synthase. *Proc. Natl. Acad. Sci. USA* 90:80-84.

Biemont, C. 2008. Genome size evolution: within-species variation in genome size. *Heredity* 101:297–8.

Blackburn, K. B. 1936. *Botryococcus* and the algal coals. I. A reinvestigation of the alga *Botryococcus braunii* Kützing. *Trans. Roy. Soc. Edinb.* 58:841-854.

Blanc, G., Duncan, G., Agarkova, I., Borodovsky, M., Gurnon, J., Kuo, A. et al. 2010. The *Chlorella variabilis* NC64A Genome Reveals Adaptation to Photosymbiosis, Coevolution with Viruses, and Cryptic Sex. *Plant Cell* 22:2943-2955.

Bosco, G., Campbell, P., Leiva-Neto, J. T. and Markow, T. A. 2007. Analysis of Drosophila species genome size and satellite DNA content reveals significant differences among strains as well as between species. *Genetics* 177:1277–90.

Bowler, C., Allen, A. E., Badger, J. H., Grimwood, J., Jabbari, K., Kuo, A., Maheswari, U., et al. 2008. The *Phaeodactylum* genome reveals the evolutionary history of diatom genomes. *Nature* 456:239–44.

Brahma, S. K., Hargraves, P. E., Howard, W. F., and Nelson, W. H. 1983. A Resonance Raman Method for the Rapid Detection and Identification of Algae in Water. *Appl. Spectrosc.* 37:55–58.

Brassel, S.C., Eglinton, G., Mo, F.J. 1986. Biological marker compounds as indicator of the depositional history of the Maoming oil shale. *Org. Geochem.* 10:927–941.

Brown, A. C., Knights, B. A. and Conway, E. 1969. Hydrocarbon content and its relationship to physiological state in the green alga *Botryococcus braunii*. *Phytochem.* 8:543–7.

Cane, R. F. 1977. Coorongite, balkashite and related substances—an annotated bibliography. *Trans. R. Soc. S. Aust.* 101:153–154.

Casadevall, E., Metzger, P., and Puech, M. P. 1984. Biosynthesis of triterpenoid hydrocarbons in the alga *Botryococcus braunii*. *Tetrahedron Lett.* 25:4123–4126.

Cavalier-Smith, T. 2004. Only six kingdoms of life. *Proc. R. Soc. Lond. B* 271:1251–1262.

Chapman, A. D. 2005. *Numbers of Living Species in Australia* and *the World*. Report for the Department of the Environment and Heritage, Canberra, Australia, pp. 1–64.

Chapman, A. D. 2009. *Numbers of Living Species in Australia* and *the World*. Report for the Australian Biological Resources Study, Canberra, Australia, pp. 1–84.

Chen, A. and Poulter, C. D. 1993. Purification and characterization of farnesyl diphosphate/geranylgeranyl diphosphate synthase. *J. Biol. Chem.* 268:11002-11007.

Chen, M., Zeng, H., Larkum, A. W., and Cai, Z. L. (2004) Raman properties of chlorophyll d, the major pigment of *Acaryochloris marina*: studies using both Raman spectroscopy and density functional theory. *Spectrochim. Acta A. Mol. Biomol. Spectrosc.* 60:527–534.

Chisti, Y. 2007. Biodiesel from microalgae. *Biotechnol. Adv.* 25:294–306.

Chisti, Y. 2008a. Biodiesel from microalgae beats bioethanol. *Trends Biotechnol.* 26:126–31.

Chisti, Y. 2008b. Response to Reijnders: do biofuels from microalgae beat biofuels from terrestrial plants? *Trends Biotechnol.* 26:351–2.

Chisti, Y. 20010. Fuels from microalgae. *Biofuels* 1:233–235.

Ciucanu, I., and Kerek, F. 1984. A Simple and Rapid Method for the Permethylation of Carbohydrates. *Carbohyd. Res.* 131:209-217.

Cooksey, K. E., Guckert, J. B., Williams, S. A., and Callis, P. R. 1987. Fluorometric-determination of the neutral lipid-content of microalgal cells using Nile red. *J. Microbial. Methods* 6:333–345.

Cordoba, E., Salmi, M., and León, P. 2009. Unravelling the regulatory mechanisms that modulate the MEP pathway in higher plants. *J. Exp. Bot.* 60: 2933–2943.

Cullis, C. A. 2005. Mechanisms and control of rapid genomic changes in flax. *Ann. Bot. (Lond.)* 95:201–6.

Davison, J., Tyagi, A. and Comai, L. 2007. Large-scale polymorphism of heterochromatic repeats in the DNA of *Arabidopsis thaliana*. *BMC Plant Biol.* 7:44.

Derenne, S., Largeau, C., Casadevall, E., Berkaloff, C. 1989. Occurrence of a resistant biopolymer in the L race of *Botryococcus braunii*. *Phytochem.* 28:1137–1142

Devarenne T. P., Shin, D.H., Back, K., Yin, S., and Chappell, J. 1998. Molecular characterization of tobacco squalene synthase and regulation in response to fungal elicitor. *Arch Biochem Biophys* 349:205–215.

Doležel, J., Bartos, J., Voglmayr, H., Greilhuber, J. 2003. Nuclear DNA content and genome size of trout and human. *Cytom. A* 51:127–128, author reply 129.

Doležel, J., Bartos, J. 2005. Plant DNA flow cytometry and estimation of nuclear genome size. *Ann. Bot. (Lond)* 95:99–110.

Edwards, H. G. M., de Oliveira, L. F. C., Cockell, C. S., Ellis-Evans, J. C., and Wynn-Williams, D. D. 2004. Raman spectroscopy of senescing snow algae: pigmentation changes in an Antarctic cold desert extremophile. *Int. J. Astrobiol.* 3:125–129.

Eisenreich, W., Bacher, A., Arigoni, D. and Rohdich, F. 2004. Biosynthesis of isoprenoids via the non-mevalonate pathway. *Cell. Mol. Life Sci.* 61:1401-1426.

Elsey, D., Jameson, D., Raleigh, B., and Cooney, M. J. 2007. Fluorescent measurement of microalgal neutral lipids. *J. Microbiol. Methods* 68:639–642.

Engebrecht, J., Brent, R., and Kaderbhai, M. A. 1991. Minipreps of plasmid DNA. *Curr. Protoc. Mol. Biol.* 15:1.6.1-1.6.10.

Eroglu, E., and Melis, A. 2010. Extracellular terpenoid hydrocarbon extraction and quantitation from the green microalgae *Botryococcus braunii* var. Showa. *Bioresource Technol.* 101:2359–2366.

Ferreri, C., Panagiotaki, M., and Chatgilialoglu, C. 2007. Trans Fatty Acids in Membranes: The Free Radical Path. *Mol. Biotechnol.* 37:19–25

Frisch, M. J., Trucks, G. W., Schlegel, H. B., Scuseria, G. E., Robb, M. A., Millam, J. M., et al. 2004. GAUSSIAN, Version 0.3, Gaussian, Inc., Wallingford CT.

Galbraith, D. W., Harkins, K. R., Maddox, J. M., Ayres, N. M., Sharma, D. P. and Firoozabady, E. 1983. Rapid flow cytometric analysis of the cell cycle in intact plant tissues. *Science* 220:1049–51.

Galbraith, M. N., Hillen, L. W., and Wake, L. V. (1983) Darwinene: a branched hydrocarbon from a green form of *Botryococcus braunii*. *Phytochem.* 22:1441–1443.

Gelpi, E., Oro, J., Schneider, H. J. and Bennett, E. O. 1968. Olefins of high molecular weight in two microscopic algae. *Science* 161:700–2.

Glikson, M., Lindsay, K., Saxby, J. 1989. *Botryococcus*—A planktonic green alga, the source of petroleum through the ages: transmission electron microscopical studies of oil shales and petroleum source rocks. *Org. Geochem.* 14:595–608.

Greenspan, P. and Fowler, S. D. 1985. Spectrofluorometric studies of the lipid probe nile red. *J. Lipid Res*. 26:781-789.

Gregory, T. R. and Johnston, J. S. 2008. Genome size diversity in the family Drosophilidae. *Heredity* 101:228–38.

Grung, M., Metzger, P., and Liaaen-Jensen, S. 1989. Primary and secondary carotenoids in two races of the green alga *Botryococcus braunii*. *Biochem. Syst. Ecol.* 17:263–9.

Gu P. D., Ishii, Y., Spencer, T. A., and Shechter, I. 1998. Function-structure studies and identification of three enzyme domains involved in the catalytic activity in rat hepatic squalene synthase. *J. Biol. Chem.* 273:12515–12525.

Guindon, S. and Gascuel, O. 2003. A simple, fast, and accurate algorithm to estimate large phylogenies by maximum likelihood. *Syst. Biol.* 52:696–704.

Guiry, M. D. and Guiry, G. M. 2012. AlgaeBase. World-wide electronic publication, National University of Ireland, Galway. http://www.algaebase.org; searched on 23 April 2012.

Hall, B. G. 2001. *Phylogenetic Trees Made Easy: A How-to Manual for Molecular Biologists.* Sinauer Associates, Sunderland, Massachusetts, 179 pp.

Heraud, P., Wood, B. R., Beardall, J., and McNaughton, D. 2006. Effect of pre-processing of Raman spectra on *in vivo* classification of nutrient status of microalgal cells. *J. Chemometrics* 20:193–197.

Heraud, P., Beardall, J., McNaughton, D., and Wood, B. R. 2007. *In vivo* prediction of the nutrient status of individual microalgal cells using Raman microspectroscopy. *FEMS Microbiol. Lett.* 275:24–30

Hillen, L. W., Pollard, G., Wake, L. V. and White, N. 1982. Hydrocracking of the oils of *Botryococcus braunii* to transport fuels. *Biotechnol. Bioeng.* 24:193–205.

Hu, Q., Sommerfeld, M., Jarvis, E., Ghirardi, M., Posewitz, M., Seibert, M., and Darzins, A. 2008. Microalgal triacylglycerols as feedstocks for biofuel production: perspectives and advances. *Plant J.* 54:621–639.

Huang, Y. Y., Beal, C. M., Cai, W. W., Ruoff, R. S., and Terentjev, E. M. 2010. Microalgal triacylglycerols as feedstocks for biofuel production: perspectives and advances. *Biotechnol. Bioeng.* 105:889–898.

Huang, Z., and Poulter, C. D. (1989a) Stereochemical Studies of Botryococcene Biosynthesis: Analogies between 1'-1 and 1'-3 Condensations in the Isoprenoid Pathway. *J. Am. Chem. Soc.* 111:2713–2715.

Huang, Z., and Poulter, C. D. (1989b) Isoshowacene, A C_{31} hydrocarbon from *Botryococcus braunii* var. showa. *Phytochem.* 28:3043–3046.

Huang, Z., and Poulter, C. D. (1989c) Tetramethylsqualene, a triterpene from *Botryococcus braunii* var. showa. *Phytochem.* 28:1467–1470.

Huelsenbeck, J. P. and Ronquist, F. 2001. MRBAYES: Bayesian inference of phylogenetic trees. *Bioinformatics* 17:754–5.

Jarvis, E. E., Dunahay, T. G. and Brown, L. M. 1992. DNA nucleoside composition and methylation in several species of microalgae. *J. Phycol.* 28:356–62.

Jazwinski, S.M. 1990. Preparation of extracts from yeast. *Methods Enzymol.* 182:154–174.

Johnston, J. S., Ross, L. D., Beani, L., Hughes, D. P. and Kathirithamby, J. 2004. Tiny genomes and endoreduplication in Strepsiptera. *Insect Mol. Biol.* 13:581–5.

Johnston, J. S., Pepper, A. E., Hall, A. E., Chen, Z. J., Hodnett, G., Drabek, J., Lopez, R. and Price, H. J. 2005. Evolution of genome size in Brassicaceae. *Ann. Bot. (Lond.)* 95:229–35.

Johnston, J. S., Yoon, K. S., Strycharz, J. P., Pittendrigh, B. R. and Clark, J. M. 2007. Body lice and head lice (Anoplura: Pediculidae) have the smallest genomes of any hemimetabolous insect reported to date. *J. Med. Entomol.* 44:1009–12.

Kapraun, D. F. 2005. Nuclear DNA content estimates in multicellular green, red and brown algae: phylogenetic considerations. *Ann. Bot. (Lond.)* 95:7–44.

Kapraun, D. F. 2007. Nuclear DNA content estimates in green algal lineages: Chlorophyta and Streptophyta. *Ann. Bot. (Lond.)* 99:677–701.

Kitazato, H., Asaoka, S. and Iwamoto, H. 1989. Catalytic cracking of hydrocarbons from microalgae. *Sekiyu Gakkaishi* 32:28–34.

Knights, B. A., Brown, A. C., Conway, E. and Middleditch, B. S. 1970. Hydrocarbons from the green form of the freshwater alga *Botryococcus braunii*. *Phytochem.* 9:1317–24.

Komárek, J. and Marvan, P. 1992. Morphological differences in natural populations of the genus *Botryococcus* (Chlorophyceae). *Arch. Protistenkd.* 141:65–100.

Kribii, R., Arro, M., Del Arco, A., Gonzalez, V., Balcells, L., Delourme, D., et al. 1997. Cloning and characterization of the *Arabidopsis thaliana* SQS1 gene encoding squalene synthase—involvement of the C-terminal region of the enzyme in the channeling of squalene through the sterol pathway. *Eur. J. Biochem.* 249:61–69.

Kubo, Y., Ikeda, T., Yang, S.-Y., and Tsuboi, M. 2000. Orientation of carotenoid molecules in the eyespot of alga: *in situ* polarized resonance Raman spectroscopy. *Appl. Spectrosc.* 54:1114–1119.

Kützing, F. T. 1849. Species Algarum. *Lipsiae* [Leipzig]. F.A. Brockhaus. pp. [i]-vi, [1]-922.

Lamport, D.T., Kieliszewski, M. J. Chen, Y., and Cannon, M. C. 2011. Role of the extension superfamily in primary cell wall architecture. *Plant Physiol.* 156:11-19.

Largeau, C., Casadevall, E., Berkaloff, C., and Dhamelincourt, P. 1980. Sites of accumulation and composition of hydrocarbons in *Botryococcus braunii*. *Phytochem.* 19:1043–1051.

Lee, S. J., Yoon, B.-D., and Oh, H.-M. 1998. Rapid method for the determination of lipid from the green alga *Botryococcus braunii*. *Biotech. Tech.* 12:553–556.

Leon-Banares, R., Gonzalez-Ballester, D., Galvan, A. and Fernandez, E. 2004. Transgenic microalgae as green cell-factories. *Trends Biotechnol.* 22:45–52.

Lewis, L. A., and McCourt, R. M. 2004. Green algae and the origin of land plants. *Am. J. Bot.* 9:1535-1556.

Li, B., Mao, D., Liu, Y., Li, L., and Kuang, T. 2005. Characterization of the cytochrome b(6)f complex from marine green alga, *Bryopsis corticulans*. *Photosynth. Res.* 83:297–305.

Lichtenthaler, H. K. 2010. The Non-mevalonate DOXP/MEP (Deoxyxylulose 5-Phosphate/Methylerythritol 4-Phosphate) Pathway of Chloroplast Isoprenoid and Pigment Biosynthesis. In Rebeiz, C. A., Benning, C., Bohnert, H. J., Daniell, H., Hoober, J. K., Lichtenthaler, H.K., et al. (Ed.), The Chloroplast: Basics and Applications. Springer, Dordrecht, Netherlands 31:95-114.

Lohr, M., Schwender, J., and Polle, J. E. W. 2012. Isoprenoid biosynthesis in eukaryotic phototrophs: A spotlight on algae. *Plant Sci.* 185-186:9-22.

López-Gómez, R. and Gómez-Lim, M. A. 1992. A method for extracting intact RNA from fruits rich in polysaccharides using ripe mango mesocarp. *Hortic. Sci.* 27:440–2.

Lupi, F. M., Fernandes, H. M. L., Sá-Correia, I., and Novais, J. M. 1991. Temperature profiles of cellular growth and exopolysaccharide synthesis by *Botryococcus braunii* Kütz. UC 58. *Appl. Phycol.* 3:35-42.

Lupi, F. M., Fernandes, H. M. L., Tomé, M. M., Sá-Correia, I., and Novais, J. M. 1994. Influence of nitrogen source and photoperiod on exopolysaccharides synthesis by the microalga *Botryococcus braunii* UC 58. *Enzyme Microb. Tech.* 16:546-550.

Mastalerz, M. and Hower, J.C. 1996. Elemental composition and molecular structure of *Botryococcus* alginite in Westphalian cannel coals from Kentucky. *Org. Geochem.* 24:301–308.

Matsushima, D., Jenke-Kodama, H., Satoa, Y., Fukunaga, Y., Sumimoto, K., Kuzuyama, T., Matsunaga, S., and Okada, S. 2012. The single cellular green microalga *Botryococcus braunii*, race B possesses three distinct 1-deoxy-d-xylulose 5-phosphate synthases. *Plant Sci.* 185–186:309–320.

Matsuzaki, M., Misumi, O., Shin, I. T., Maruyama, S., Takahara, M., Miyagishima, S. Y., Mori, T., et al. 2004. Genome sequence of the ultrasmall unicellular red alga *Cyanidioschyzon merolae* 10D. *Nature* 428:653–7.

Maxwell, J. R., Douglas, A. G., Eglinton, G. and McCornick, A. 1968. Botryococcenes-hydrocarbons of novel structure from the alga *Botryococcus braunii* Kützing. *Phytochem.* 7:2157–71.

McKirdy, D.M., Cox, R.E., Volkman, J.K., and Howell, V.J. (1986) Botryococcanes in a new class of Australian on-marine crude oils. *Nature* 320:57–59.

Meister, A. and Barow, M. 2007. DNA base composition of plant genomes. *In* Dolezel, J., Greilhuber, J. and Suda, J. [Eds.] *Flow Cytometry with Plant Cells.* Wiley-VCH Verlag GmBH & Co. KGaA, Weinheim, Germany, pp. 177–215.

Merchant, S. S., Prochnik, S. E., Vallon, O., Harris, E. H., Karpowicz, S. J., Witman, G. B., Terry, A., et al. 2007. The *Chlamydomonas* genome reveals the evolution of key animal and plant functions. *Science* 318:245–50.

Metzger, P., Berkaloff, C., Casadevall, E., and Coute, A. 1985a. Alkadiene producing and botryococcene-producing races of wild strains of *Botryococcus braunii*. *Phytochem.* 24:2305–2312.

Metzger, P., Casadevall, E., Pouet, M.J., and Pouet, Y. 1985b. Structures of some botryococcenes: branched hydrocarbons from the B-race of the green alga *Botryococcus braunii*. *Phytochem.* 24:2995–3002.

Metzger P, Templier J, Largeau C, Casadevall E 1986. An n-alkatriene and some n-alkadienes from the A race of the green alga *Botryococcus braunii*. *Phytochem.* 25:1869–1872.

Metzger, P. and Casadevall, E. 1987a. Lycopadiene, a tetraterpenoid hydrocarbon from new strains of the green alga *Botryococcus braunii*. *Tetrahedron Lett.* 28:3911–3934.

Metzger, P., David, M., and Casadevall, E. 1987b. Biosynthesis of triterpenoid hydrocarbons in the B-race of the green alga *Botryococcus braunii*. Sites of production and nature of the methylating agent. *Phytochem.* 26:129–134.

Metzger, P., Casadevall, E., and Couté, A. 1988. Botryococcene distribution in strains of the green alga *Botryococcus braunii*. *Phytochem.* 27:1383–1388.

Metzger, P., Allard, B., Casadevall, E., Berkaloff, C., and Coute, A. 1990. Structure and chemistry of a new chemical race of *Botryococcus braunii*. *J. Phycol.* 26:258–266.

Metzger, P., Pouet, Y., Bischoff, R., and Casadevall, E. 1993. An aliphatic polyaldehyde from *Botryococcus braunii* (A race). *Phytochem.* 32:875–883.

Metzger, P. and Largeau, C. 1999.Chemicals of *Botryococcus braunii*. In Cohen, Z. (Ed.), *Chemicals from Microalgae*. Taylor and Francis Ltd., London, pp. 205-260.

Metzger, P. and Largeau, C. 2005. *Botryococcus braunii*: a rich source for hydrocarbons and related ether lipids. *Appl. Microbiol. Biotechnol.* 66:486–96.

Metzger, P., Rager, M. N., and Largeau, C. 2007. Polyacetals based on polymethylsqualene diols, precursors of algaenan in *Botryococcus braunii* race B. *Org. Geochem.* 38:566–581.

Metzger, P., Rager, M. N., and Fosse, C. 2008. Braunicetals: acetals from condensation of macrocyclic aldehydes and terpene diols in *Botryococcus braunii*. *Phytochem.* 69:2380–2386.

Misumi, O., Yoshida, Y., Nishida, K., Fujiwara, T., Sakajiri, T., Hirooka, S., et al. 2008. Genome analysis and its significance in four unicellular algae, *Cyanidioshyzon merolae,*

Ostreococcus tauri, *Chlamydomonas reinhardtii*, and *Thalassiosira pseudonana*. *J. Plant. Res.* 121:3–17.

Miziorko, H. M. 2011. Enzymes of the mevalonate pathway of isoprenoid biosynthesis. *Arch. Biochem. Biophys.* 505:131-143.

Moldowan, J. M. and Seifert, W. K. 1980. First discovery of botryococcene in petroleum. *J.Chem. Soc. Chem. Commun.* 19:912–4.

Moreno, N., Bougourd, S., Haseloff, J., and Feijó, J. A. 2006. *Imaging Plant Cells*. In J. B. Pawley (ed.), Handbook of Biological Confocal Microscopy, 3rd ed. Springer Science and Business Media, New York. pp. 769-787.

Morita, N., Shibahara, A., Yamamoto, K., Shinkai, K, Kajimoto, G., and Okuyama, H. 1993. Evidence for cis-trans Isomerization of a Double Bond in the Fatty Acids of the Psychrophilic Bacterium *Vibrio sp.* Strain ABE-1. *J. Bacteriol.* 175:916-918.

Niehaus, T. D., Okada, S., Devarenne, T. P., Watt, D. S., Sviripa, V., and Chappell, J. 2011. Identification of unique mechanisms for triterpene biosynthesis in *Botryococcus braunii*. *Proc. Natl. Acad. Sci.* 108:12260–12265.

Niehaus, T. D., Kinison, S., Okada, S., Yeo, Y., Bell, S. A., Cui, P., Devarenne, T. P., and Chappell, J. 2012. Functional Identification of Triterpene Methyltransferases from *Botryococcus braunii* Race B. *JBC* 287:8163–8173.

Nonomura, A. M. 1988. *Botryococcus braunii* var. Showa (Chlorophyceae) from Berkeley, California, United States of America. *Jpn. J. Phycol.* 36:285–91.

Okada, S., Murakamis M., and Yamaguchi, K. 1995. Hydrocarbon composition of newly isolated strains of the green microalga *Botryococcus braunii*. *J. Appl. Phycol.* 7:555–559.

Okada, S., Matsuda, H., Murakami, M., and Yamaguchi, K. 1996. Hydrocarbon composition of newly isolated strains of the green microalga *Botryococcus braunii*. *Tetrahedron Lett.* 37:1065–1068.

Okada, S., Murakami, M., and Yamaguchi, K. 1997. Characterization of hydrocarbons from the Yayoi strain of the green microalga *Botryococcus braunii*. *Phytochem. Anal.* 8:198–203.

Okada, S., Tonegawa, I., Matsuda, H., Murakami, M., and Yamaguchi, K. 1998. Botryoxanthin B and α-botryoxanthin a from the green microalga *Botryococcus braunii* kawaguchi-1. *Phytochem.* 47:1111–1115.

Okada, S., Devarenne, T. P. and Chappell, J. 2000. Molecular characterization of squalene synthase from the green microalga *Botryococcus braunii*, race B. *Arch. Biochem. Biophys.* 373:307–17.

Okada, S., Devarenne, T. P., Murakami, M., Abe, H., and Chappell, J. 2004. Characterization of botryococcene synthase enzyme activity, a squalene synthase-like activity from the green microalga *Botryococcus braunii*, Race B. *Arch. Biochem. Biophys.* 422:110–118.

Page, R. D. 1996. TreeView: an application to display phylogenetic trees on personal computers. *Comput. Appl. Biosci.* 12:357–8.

Pandit, J., Danley, D.E., Schulte, G.K, Mazzalupo, S., Pauly, T. A., Hayward, C. M. et al. 2000. Crystal structure of Human Squalene Synthase A Key Enzyme in Cholesterol Biosynthesis. *J. Biol. Chem.* 275:30610-30617.

Phillips, M. A., León, P., Boronat, A., and Rodríguez-Concepción, M. 2008. The plastidial MEP pathway: unified nomenclature and resources. *Trends Plant Sci.* 13:619-623.

Pollingher, U. 1986. Non-siliceous algae in a five meter core from Lake Kinneret (Israel). *Hydrobiologia* 143:213-216.

Poulton, E. M. 1930. Further Studies on the Heterokontae: Some Heterokontae of New England, U.S.A. *New Phytologist* 29:1-26.

Prochnik, S.E., Umen, J., Nedelcu A.M., Hallmann, A., Miller, S.M., Nishii I., et al. 2010. Genomic analysis of organismal complexity in the multicellular green alga *Volvox carteri*. *Science* 329:223–226.

Provasoli, L., McLaughlin, J. J. A., and Droop, M. R. 1957. The development of artificial media for marine algae. *Arch. Mikrobiol.* 25:392-428.

Radakovits, R., Jinkerson, R. E., Darzins, A., and Posewitz, M. C. 2010. Genetic Engineering of Algae for Enhanced Biofuel Production. *Euk. Cell* 9:486-501.

Robinson, G. W., Tsay, Y. H., Kienzle, B.K., Smithmonroy, C.A., and Bishop, R. W. 1993. Conservation between human and fungal squalene synthetases—similarities in structure, function, and regulation. *Mol. Cell Biol.* 13:2706–2717.

Rohdich, F., Hecht, S., Gartner, K., Adam, P., Krieger, C., Amslinger, S., et al. 2002. Studies on the non-mevalonate terpene biosynthetic pathway: metabolic role of IspH (LytB) protein. *Proc. Natl. Acad. Sci.* 99:1158-1163.

Rohdich, F., Zepeck, F., Adam, P., Hecht, S., Kaiser, J., Laupitz, R., et al. 2003. The deoxyxylulose phosphate pathway of isoprenoid biosynthesis: studies on the mechanisms of the reactions catalyzed by IspG and IspH protein. *Proc. Natl. Acad. Sci.* 100:1586-1591.

Rodríguez-Concepción, M. and Boronat, A. 2002. Elucidation of the Methylerythritol Phosphate Pathway for Isoprenoid Biosynthesis in Bacteria and Plastids. A Metabolic Milestone Achieved through Genomics. *Plant Physiol.* 130:1079–1089.

Sato, Y., Ito, Y., Okada, S., Murakami, M., and Abe, H. 2003. Biosynthesis of the triterpenoids, botryococcenes and tetramethylsqualene in the B race of *Botryococcus braunii* via the non-mevalonate pathway. *Tetrahedron Lett.* 44, 7035–7037.

Sawayama, S., Inoue, S. and Yokoyama, S. 1995. Phylogenetic position of *Botryococcus braunii* (Chlorophyceae) based on small subunit ribosomal RNA sequence data. *J. Phycol.* 31:419–20.

Seidman, C. E., Struhl, K., Sheen, J., and Jessen, T. 1997. Introduction of plasmid DNA into cells. *Curr. Protoc. Mol. Biol.* 37:1.8.1-1.8.10.

Senousy, H. H., Beakes, G. W. and Hack, E. 2004. Phylogenetic placement of *Botryococcus braunii* (Trebouxiophyceae) and *Botryococcus sudeticus* isolate UTEX 2629 (Chlorophyceae). *J. Phycol.* 40:412–23.

Smittenberg, R. H., Baas, M. Schouten, S., and Sinninghe Damsté, J.S. 2005. The demise of the alga *Botryococcus braunii* from a Norwegian fjord was due to early eutrophication. *The Holocene* 15:133-140.

Stasiuk, L.D. 1999. Confocal laser scanning fluorescence microscopy of *Botryococcus* alginite from boghead oil shale, Boltysk, Ukraine: selective preservation of various micro-algal components. *Org. Geochem.* 30:1021–1026.

Summons, R.E., Metzger, P., Largeau, C., Murray, A. P., and Hope, J.M. 2002. Polymethylsqualanes from *Botryococcus braunii* in lacustrine sediments and crude oils. *Org. Geochem.* 33:99–109.

Schwender, J., Gemünden, C. and Lichtenthaler, H. K. 2001. Chlorophyta exclusively use the 1-deoxyxylulose 5-phosphate/2- C -methylerythritol 4-phosphate pathway for the biosynthesis of isoprenoids. *Planta* 212:416-423.

Stamellos, K. D., Schelford, J. E., Shechter, I., Jiang, G., Conrad, D., et al. 1993. Subcellular Localization of Squalene Synthase in Rat Hepatic Cells. *J. Biol. Chem.* 268:12825-12836.

Tamura, K., Dudley, J., Nei, M. and Kumar, S. 2007. MEGA4: Molecular Evolutionary Genetics Analysis (MEGA) software version 4.0. *Mol. Biol. Evol.* 24:1596–9.

Templier, J., Largeau, C., and Casadevall, E. 1984. Hydrocarbon formation in the green-alga *Botryococcus braunii*. 4. Mechanism of nonisoprenoid hydrocarbon biosynthesis in *Botryococcus braunii*. *Phytochem.* 23:1017–1028.

Templier, J., Largeau, C., and Casadevall, E. 1991. Biosynthesis of normal alkatrienes in *Botryococcus braunii*. *Phytochem.* 30:2209–2215.

Testa, M., Gerbaudo, S., and Andri, E. 2001. *Botryococcus* Colonies in Miocene Sediments in the Western Woodlark Basin, Southwest Pacific (ODP Leg 180). *Proc. Ocean Drill Program Sci. Results* 180:1–6.

Thompson, J. F., Danley, D. E., Mazzalupo, S., Milos, P. M., Lira, M. E., and Harwood, H. J. 1998. Truncation of Human Squalene Synthase Yields Active, Crystallizable Protein. *Archv. Biochem. Biophys.* 350:283-290.

Traverse, A. 1955. Occurrence of the oil-forming alga *Botryococcus* in lignites and other Tertiary sediments. *Micropaleontology* 1:343–8.

Vieira, C., Nardon, C., Arpin, C., Lepetit, D. and Biemont, C. 2002. Evolution of genome size in *Drosophila*. Is the invader's genome being invaded by transposable elements? *Mol. Biol. Evol.* 19:1154–61.

Vinogradov, A. E. 1994. Measurement by flow cytometry of genomic AT⁄GC ratio and genome size. *Cytometry* 16:34–40.

Vinogradov, A. E. 1998. Genome size and GC-percent in vertebrates as determined by flow cytometry: the triangular relationship. *Cytometry* 31:100–9.

von Wallbrunn, A., Richnow, H. H., Beumann, G., Meinhardt, F., and Heipieper, H. J. 2003. Mechanism of cis-trans Isomerization of Unsaturated Fatty Acids in *Pseudomonas putida*. *J. Bacteriol.* 185:1730-1733.

Wagner, W. D., and Waidelich, W. 1986. Selective Observation of Chlorophyll *c* in Whole Cells of Diatoms by Resonant Raman Spectroscopy. *Appl. Spectrosc.* 40:191–196.

Wake, L. V. and Hillen, L. W. 1980. Study of a ''bloom'' of the oil-rich alga *Botryococcus braunii* in the Darwin River reservoir. *Biotechnol. Bioeng.* 22:1637–56.

Wake, L. V. and Hillen, L. W. 1981. Nature and hydrocarbon content of blooms of the alga *Botryococcus braunii* occurring in Australian freshwater lakes. *Aust. J. Mar. Freshw. Res.* 32:353–67.

Weiss, T. L., Chun, H. J., Okada, S., Vitha, S., Holzenburg, A., Laane, J., and Devarenne, T. P. 2010a. Raman spectroscopy analysis of botryococcene hydrocarbons from the green microalga *Botryococcus braunii*. *J. Biol. Chem.* 285:32458-66.

Weiss, T. L., Johnston, J. S., Fujisawa, K., Sumimoto, K., Okada, S., Chappell, J., and Devarenne, T. P. 2010b. Phylogenetic placement, genome size, and GC content of the liquid-hydrocarbon-producing green microalgae *Botryococcus braunii* strain Berkeley (Showa) (Chlorophyta). *J. Phycol.* 46:534–540.

Weiss, T. L., Johnston, J. S., Fujisawa, K., Okada, S., and Devarenne, T. P. 2011. Genome size and phylogenetic analysis of the A and L races of *Botryococcus braunii*. *J. Appl. Phycol.* 23:833–839.

Wolf, F. R. and Cox, E. R. 1981. Ultrastructure of Active and Resting Colonies of *Botryococcus braunii* (Chlorophyceae). *J. Phycol.* 17:395-405.

Wolf, F.R. 1983. *Botryococcus braunii*: An Unusual Hydrocarbon Producing Alga. *Appl. Biochem. Biotech.* 8:249-260.

Wolf, F. R., Nemethy, E. K., Blanding, J. H., and Bassham, J. A. 1985a. Biosynthesis of unusual acyclic isoprenoids in the Alga *Botryococcus braunii*. *Phytochem.* 24:733–737.

Wolf, F. R., Nonomura, A. M., and Bassham, J. A. 1985b. Growth and Branched Hydrocarbon Production in a Strain of *Botryococcus braunii* (Chlorophyta). *J. Phycol.* 21:388–396.

Wood, B. R., Heraud, P., Stojkovic, S., Morrison, D., Beardall, J., and McNaughton, D. 2005. A portable Raman acoustic levitation spectroscopic system for the identification and environmental monitoring of algal cells. *Anal. Chem.* 77:4955–4961.

Wood, P. J. 1980. Specificity in the interaction of direct dyes with polysaccharides. *Carb. Res.* 85:271-287.

Worden, A. Z., Lee, J.-H., Mock, T., Rouzé, P., Simmons, M. P., Aerts, A. L. et al. 2009. Green Evolution and Dynamic Adaptations Revealed by Genomes of the Marine Picoeukaryotes *Micromonas*. *Science* 324: 268-272.

Wu, Q., Nelson, W. H., Hargraves, P., Zhang, J., Brown, C. W., and Seelenbinder, J. A. 1998. Differentiation of algae clones on the basis of resonance Raman spectra exited by visible light. *Anal. Chem.* 70:1782–1787.

Yoo, C., Jun, S.-Y., Lee, J.-Y., Ahn, C. –Y., and Oh, H.-M. 2010. Selection of microalgae for lipid production under high levels carbon dioxide. *Bioresource Tech.* 101:S71-S74.

York, W.S., Darvill, A. G., McNeil, M., Stevenson, T.T., and Albersheim, P. 1986. Isolation and Characterization of Plant-Cell Walls and Cell-Wall Components. *Methods Enzymol.* 118:3-40.

Zhang, Z., Metzger, P., and Sachs, J. P. 2007. Biomarker evidence for the co-occurrence of three races (A, B and L) of *Botryococcus braunii* in El Junco Lake, Galápagos. *Org. Geochem.* 38:1459–1478.

Zohary, T. 2004. Changes to the phytoplankton assemblage of Lake Kinneret after decades of a predictable, repetitive pattern. *Freshw. Biol.* 49:1355-1371.

VITA

Taylor Leigh Weiss

Born: May 2, 1984, Traverse City, MI

Address: Texas A&M University
Biochemistry and Biophysics Building
MS 2128
College Station, TX 77843-2128

Email: tweiss@tamu.edu

Education: B.S., Biochemistry, University of Rochester, New York, 2006

Professional Experience:

Texas A&M University, Department of Biochemistry/Biophysics, College Station, Texas, August 2006 to present, Graduate Student

University of Rochester, **Department of Biochemistry/Biophysics** Rochester, New York, June 2004 to June 2006, Technical Assistant

Publications:

Weiss, T. L., Chun, H. J., Okada, S., Vitha, S., Holzenburg, A., Laane, J., and Devarenne, T. P. 2010. Raman spectroscopy analysis of botryococcene hydrocarbons from the green microalga *Botryococcus braunii*. *J. Biol. Chem.* 285:32458-66.

Weiss, T. L., Johnston, J. S., Fujisawa, K., Okada, S., and Devarenne, T. P. 2010. Genome size and phylogenetic analysis of the A and L races of *Botryococcus braunii*. *J. Appl. Phycol.* 23:833-839.

Weiss, T.L., Johnston, J.S., Fujisawa, K., Sumimoto, K., Okada, S., Chappell, J., and Devarenne, T.P. 2010. Phylogenetic placement, genome size, and GC content of the liquid-hydrocarbo*n*-producing green microalgae *Botryococcus braunii* strain Berkeley (Showa) (Chlorophyta). *J. Phycol.* 46:534-540.

Deng, L., Senseman, S. A., Gentry, T. J., Zuberer, D. A., **Weiss, T. L.**, Devarenne, T. P., and Camargo, E. R. 2012. Effect of selected herbicides on growth and hydrocarbon content of *Botryococcus braunii* (Race B). *Ind. Crop Prod.* 39:154-161.